

ABSTRACT

Title of Document: IMPROVED QUANTIFICATION OF FOREST COVER CHANGE AND IMPLICATIONS FOR THE CARBON CYCLE

Xiaopeng Song, Doctor of Philosophy, 2015

Directed By: Professor John R. Townshend
Department of Geographical Sciences

Changes in forest cover significantly affect the global carbon cycle, the hydrological cycle and biodiversity richness. This dissertation explores the potential of satellite-derived land cover datasets in quantifying changes in global forest cover and carbon stock. The research involved the following three components: 1) improving forest cover characterization, 2) developing advanced methods for detecting forest cover change (FCC) and 3) estimating the amount and trend of forest carbon change.

The first component sought to improve global forest cover characterization through data fusion. Multiple global land cover maps have been generated, which collectively represent our current best knowledge of global land cover, but substantial discrepancies were found in their depiction of forest. I demonstrated that the extent and density of forest cover could be much better characterized by integrating existing datasets. However, these independent map products cannot be directly compared to quantify FCC, because post-classification change detection requires significant

consistency in land cover definition, satellite data source and classification procedure. The yearly vegetation continuous field (VCF) product derived from the Moderate Resolution Imaging Spectroradiometer (MODIS) provides a prototype that fulfills such requirement. The second component was intended to explore the features of this time series dataset in change analysis. A new algorithm called VCF-based Change Analysis was developed that can explicitly characterize the timing and intensity of FCC. The efficiency and robustness of this algorithm stem from two realistic assumptions—the spatial rarity and the temporal continuity of land cover change/modification. The developed method was applied to continental scales for mapping forest disturbance hotspots.

The third component of the research combined MODIS-based deforestation indicators, a Landsat sample and a biomass dataset to estimate annual carbon emissions from deforestation with a regional focus on the Amazon basin. I found that deforestation emissions varied considerably not only across regions but also from year to year. Moreover, deforestation has been progressively encroaching into higher biomass lands in the Amazon interior. These observed deforestation and emission dynamics are expected to provide scientific support to policies on reducing emissions from deforestation and forest degradation (REDD+). The generated panel data are also of great value for evaluating forest protection policies.

IMPROVED QUANTIFICATION OF FOREST COVER CHANGE AND
IMPLICATIONS FOR THE CARBON CYCLE

By

Xiaopeng Song

Dissertation submitted to the Faculty of the Graduate School of the
University of Maryland, College Park, in partial fulfillment
of the requirements for the degree of
Doctor of Philosophy
2015

Advisory Committee:
Professor John R. Townshend, Chair
Dr. Chengquan Huang (co-advisor)
Professor Matthew C. Hansen
Dr. Jeffrey G. Masek
Professor Maureen L. Cropper

© Copyright by
Xiaopeng Song
2015

Foreword

Materials presented in Chapters 2, 3 and 4 of this dissertation have been published as peer-reviewed journal articles. The research in these chapters, as well as the remainder of the thesis, was carried out in its entirety by Xiaopeng Song. The following articles have appeared in the literature.

- Song, X.P., Huang, C. Feng, M., Sexton, J.O., Channan, S. & Townshend, J.R. (2014) Integrating global land cover products for improved forest cover characterization: An application in North America. *International Journal of Digital Earth*, 7(9), 709-724.
- Song, X.P. Huang, C. Sexton, J.O., Channan, S. & Townshend, J.R. (2014) Annual Detection of Forest Cover Loss Using Time Series Satellite Measurements of Percent Tree Cover. *Remote Sensing*, 6(9), 8878-8903.
- Song, X.P., Huang, C., Saatchi, S.S., Hansen, M.C. & Townshend, J.R. (2015) Annual carbon emissions from deforestation in the Amazon basin between 2000 and 2010. *PLOS ONE*, 10(5): e0126754.

During the course of my Ph.D. study, I also participated in several projects funded by NASA, USGS and the University of Maryland. These projects were highly relevant to the research topic of this dissertation. The following co-authored papers have been published, accepted or submitted for publication in peer-reviewed journals or conference proceedings.

- Song, X.P., Sexton, J.O., Huang, C., Channan, S. & Townshend, J.R. (in review) Characterizing the magnitude, timing and duration of urban growth from time series of Landsat-based records of impervious cover. *Remote Sensing of Environment*.
- Sexton J.O., Noojipady, P., Song, X.P., Feng, M., Song, D.X., Kim, D.H., Anand, A., Huang, C., Channan, S., Pimm, S.L. & Townshend, J.R. (in review) How much forest is there? *Nature Climate Change*.
- Channan, S., Feng, M., Kim, D.H., Sexton, J.O., Song, X.P., Song, D.X., Noojipady, P., Collins, K., Anand, A., & Townshend, J.R. (in press) The GLS+: an

enhancement of the global land survey datasets. *Photogrammetric Engineering and Remote Sensing*.

Sexton, J.O., Noojipady, P., Anand, A., Song, X.P., McMahon, S., Huang, C., Feng, M., Channan, S. & Townshend, J.R. (2015) A model for the propagation of uncertainty from continuous estimates of tree cover to categorical forest cover and change. *Remote Sensing of Environment*, 156, 418-425.

Song, X.P., Huang, C. and Townshend, J.R. (2014) An integrated framework for evaluating the effects of deforestation on ecosystem services. *The 35th International Symposium on Remote Sensing of Environment (ISRSE35), IOP Conference Series: Earth and Environmental Science 17*, 012061, 22-26 April, Beijing, China.

Sexton, J.O., Song, X.P., Feng, M., Noojipady, P., Anand, A., Huang, C., Kim, D.H., Collins, K.M., Channan, S. & Townshend, J.R. (2013) Global, 30-m resolution continuous fields of tree cover: Landsat-based rescaling of MODIS continuous fields and Lidar-based estimates of error. *International Journal of Digital Earth*, 6(5), 427-448.

Sexton, J.O., Song, X.P., Huang, C., Channan, S., Baker, M.E. & Townshend, J.R. (2013) Urban growth of the Washington, D.C - Baltimore, MD metropolitan region from 1984-2010 by annual, Landsat-based estimates of impervious cover. *Remote Sensing of Environment*, 129, 42-53.

Maher, J. & Song, X.P. (2013) Linking remote sensing and economics: evaluating the effectiveness of protected areas in reducing tropical deforestation. *Agricultural and Applied Economics Association & Canadian Agricultural Economics Society Joint Annual Meeting*, 4-6 August, Washington, DC.

Townshend, J.R., Masek, J.G., Huang, C., Vermote, E.F., Gao, F., Channan, S., Sexton, J.O., Feng, M., Narasimhan, R., Kim, D., Song, K., Song, D., Song, X.P., Noojipady, P., Tan, B., Hansen, M.C., Li, M. & Wolfe, R.E. (2012) Global characterization and monitoring of forest cover using Landsat data: opportunities and challenges. *International Journal of Digital Earth*, 5(5), 373-397.

Song, X.P., Huang, C., Sexton, J.O., Feng, M., Narasimhan, R., Channan, S., & Townshend, J.R. (2011) An assessment of global forest cover maps using regional higher-resolution reference data sets. *Proceedings of IEEE International Geoscience and Remote Sensing Symposium (IGARSS)*, pp.752-755, 24-29 July, Vancouver, Canada.

Dedication

To my parents

Lixian Song & Jinying Zhou

Acknowledgements

First and foremost I thank my primary advisor Dr. John Townshend for his academic guidance throughout my study. His extensive knowledge and dedication to excellence have always been a source of inspiration. I owe my understanding and appreciation of Earth system science to him. I thank my co-advisor Dr. Chengquan Huang for encouraging me to develop independent ideas and guiding me to reach this milestone. I also wish to thank other members of my advisory committee Dr. Matt Hansen, Dr. Jeff Masek and Dr. Maureen Cropper for providing their insightful questions and valuable time to improve my research.

Special thanks to friends and colleagues at the Global Land Cover Facility: Saurabh Channan, Joe Sexton, Min Feng, Do-Hyung Kim, Dan-Xia Song, Praveen Noojipady, Anupam Anand, Maosheng Zhao and Jyote Nagol. I have learnt enormously from you through 6-years of weekly meetings. This dissertation would never be completed without your help. It has been a great pleasure. Thanks must also be extended to friends, colleagues and teachers at the Department of Geographical Sciences: Mengxue Li, Hao Tang, Cheng Fu, Xin Tao, Feng (Aron) Zhao, Feng (Robin) Zhao, Wenli Huang, Qing Ying, Lei Wang, LeeAnn King, Alexander Krylov, Bernard Adusei and Peter Potapov.

This dissertation was funded by NASA's Earth and Space Science Fellowship program (NNX12AN92H), NASA's MEaSURES program (NNX08AP33A) and the University of Maryland Council on the Environment Green Fund Fellowship.

Last but not least, I would like to express my deepest gratitude to my family for their unconditional love. I simply would not get here without their support.

Table of Contents

Foreword.....	ii
Dedication.....	iv
Acknowledgements.....	v
Table of Contents.....	vi
List of Tables.....	viii
List of Figures.....	ix
Chapter 1 : Introduction.....	1
1.1 The role of forests in the global carbon cycle.....	1
1.2 Historical trend of carbon emissions from deforestation.....	2
1.3 Estimating carbon emissions from deforestation.....	4
1.3.1 Characterizing forest cover with satellite data.....	7
1.3.2 Quantification of forest cover change.....	11
1.3.3 Estimating forest carbon stock and change.....	13
1.4 Research objectives.....	16
1.5 Dissertation organization.....	16
Chapter 2 : Integrating Global Land Cover Products for an Improved Forest Cover Characterization.....	18
2.1 Introduction.....	18
2.2 Data.....	22
2.2.1 Global Land Cover Characterization.....	22
2.2.2 UMD land cover product.....	22
2.2.3 Global Land Cover 2000.....	23
2.2.4 MODIS land cover product.....	24
2.2.5 MODIS vegetation continuous fields.....	24
2.2.6 GlobCover land cover product.....	25
2.2.7 U.S. National Land Cover Database.....	26
2.3 Method.....	27
2.3.1 Standardization to a common spatial and thematic scale.....	28
2.3.2 Supervised training and prediction.....	33
2.3.3 Product evaluation.....	34
2.4 Results.....	35
2.4.1 Model fitting and assessment.....	35
2.4.2 The integrated forest cover map over North America.....	36
2.4.3 Evaluation of the integrated product versus input datasets.....	39
2.5 Discussion.....	42
2.5.1 Global patterns of land cover agreement.....	42
2.5.2 Global application of the data integration methodology.....	45
2.6 Conclusions.....	50
Chapter 3 : Annual Detection of Forest Cover Loss Using Time Series Satellite Measurements of Percent Tree Cover.....	51
3.1 Introduction.....	51
3.2 Yearly MODIS VCF data.....	54

3.3 The VCA algorithm	56
3.3.1 Algorithm overview	56
3.3.2 Identifying candidate change pixels.....	57
3.3.3 Curve fitting to model change trajectory	62
3.4 Algorithm evaluation	66
3.4.1 Deriving reference datasets.....	67
3.4.2 Balancing regional biases in disturbance area estimates from MODIS.....	69
3.4.3 Qualitative assessment	71
3.4.4 Quantitative assessment.....	73
3.5 Discussion.....	80
3.5.1 Advantages and disadvantages of the VCA algorithm	80
3.5.2 Global application of the VCA algorithm for mapping disturbance hotspots	84
3.6 Conclusions.....	89
Chapter 4 : Annual Carbon Emissions from Deforestation in the Amazon Basin between 2000 and 2010	90
4.1 Introduction.....	90
4.2 Materials and methods	94
4.2.1 Study area.....	94
4.2.2 Deriving annual deforestation rates from MODIS and Landsat datasets ..	95
4.2.3 Combining deforestation and biomass maps to estimate carbon emissions	99
4.2.4 Uncertainty estimates.....	100
4.3 Results.....	103
4.3.1 Annual deforestation rates in the Amazon basin	103
4.3.2 Annual gross carbon emissions from deforestation in the Amazon basin	109
4.4 Discussion.....	112
4.4.1 Effectiveness of MODIS VCF products for REDD+ MRV	112
4.4.2 Implications of annual emission estimates for REDD+ baseline setting.	114
4.4.3 Uncertainties in carbon emissions from deforestation.....	116
4.4.4 Risks of future deforestation in the Amazon	117
4.4 Conclusions.....	121
Chapter 5 : Conclusion.....	123
5.1 Summary of research	123
5.2 Implications for future research	125
Glossary	130
Bibliography	132

List of Tables

Table 2.1 Summary of key features of the global and regional land cover products .	27
Table 2.2 Proportional legend translation rules for different land cover legends.....	31
Table 2.3 Usage of predictor variables in the regression tree model.....	36
Table 2.4 Evaluation of the integrated percent forest cover map and the six input global land cover maps.	42
Table 3.1 Temporal accuracy of the MODIS disturbance-year layer against Landsat reference in WA, USA.....	76
Table 3.2 Temporal accuracy of the MODIS disturbance-year layer against Landsat reference in MT, Brazil.....	77

List of Figures

Figure 1.1 Carbon emissions from deforestation and forest degradation (D&FD) and fossil-fuel emissions from 1980 onwards (adapted from van der Werf et al. [2009]).	3
Figure 1.2 Disagreement among six land cover products on their representation of global forest cover.....	9
Figure 1.3 Landsat-based global tree cover products and their difference.....	11
Figure 2.1 Overall flowchart for deriving the integrated 5-km percent forest cover product.....	28
Figure 2.2 The integrated percent forest cover map over North America.....	37
Figure 2.3 Subsets of forest cover maps in the Chesapeake Bay region in eastern U.S.	38
Figure 2.4 Scatter plots of 5-km percent forest cover derived from global land cover products against reference percent forest cover.....	40
Figure 2.5 Agreement and disagreement between global land cover maps for (a) forest and (b) cropland.....	43
Figure 2.6 An equalized histogram of 1-km cross-product agreement metrics against reference forest cover.....	45
Figure 2.7 Regional reference land cover datasets collected or generated for the integration of global land cover products.....	46
Figure 2.8 The integrated percent forest cover map over South America.....	47
Figure 2.9 The integrated percent forest cover map over Africa.....	48
Figure 2.10 The integrated percent forest cover map over Eurasia.....	49
Figure 3.1 Overview of the VCF-based Change Analysis (VCA) algorithm.....	57
Figure 3.2 Detecting likely change pixels as outliers of a chi-square distribution.....	59
Figure 3.3 Flowchart of detecting outliers through approximating a chi-square distribution.....	61
Figure 3.4 Typical trajectories of percent tree cover (y-axis) from 2000 to 2010 (x-axis) for selected sites.....	64
Figure 3.5 Structural metrics to characterize a change event.....	65
Figure 3.6 Distribution of tree canopy cover in the two test sites and the globe.....	68
Figure 3.7 Under- or over-estimation of disturbance area derived from VCA as a function of the magnitude of tree cover loss (coefficient a of the logistic model, equation 3.6) against the Landsat reference for two study sites: (a) WA and (b) MT.	70
Figure 3.8 Examples of disturbance-year maps derived from MODIS compared with the Landsat reference.....	72
Figure 3.9 An illustration of pixel-level accuracy of VCA's disturbance-year layer..	73
Figure 3.10 Evaluation of VCA-derived disturbance rates in the Western U.S. at 5-km resolution against VCT disturbance rates.....	78
Figure 3.11 Evaluation of VCA-derived disturbance rates in Mato Grosso at 5-km resolution against PRODES disturbance rates.....	80
Figure 3.12 Inter-annual VCF variance versus inter-annual VCF mean in various forest biomes in Latin America.....	85
Figure 3.13 VCA-derived forest disturbance hotspots in the Americas between 2000 and 2010.....	86

Figure 3.14 Global examples of forest disturbance mapped using MODIS VCF in this study compared with the recently published Landsat results by Hansen et al. (2013).	88
Figure 4.1 Flowchart of generating annual forest cover change rates by integrating MODIS and Landsat.	96
Figure 4.2 Calibrating MODIS indicators to derive accurate deforestation rates.....	97
Figure 4.3 Estimating errors in MODIS-derived deforestation rates with Landsat-derived deforestation rates as reference.	102
Figure 4.4 Deforestation year map derived from time-series of MODIS VCF tree cover dataset.....	104
Figure 4.5 Maps of forest, deforestation, carbon stocks and carbon emissions in the Amazon basin.....	106
Figure 4.6 Trends of deforestation and associated carbon emissions from 2000 to 2010.....	107
Figure 4.7 Comparing annual deforestation maps derived from MODIS with Landsat-based maps in the Brazilian Amazon.....	108
Figure 4.8 Comparing MODIS-derived annual deforestation rates with Landsat results in the Brazilian Amazon.	109
Figure 4.9 Carbon density of lost forests between 2005 and 2010.	111
Figure 4.10 Annual deforestation and associated carbon emissions in the Brazilian and non-Brazilian Amazon.	115
Figure 4.11 Carbon density of lost forests and remaining forests in 2010.	118
Figure 4.12 Forest, deforestation and protected areas in the Amazon basin.	120

Chapter 1: Introduction

1.1 The role of forests in the global carbon cycle

Forests cover 4 billion hectares (ha) of land globally, approximately 31% of the Earth's total land surface, corresponding to an average of 0.6 ha per capita (FAO 2012). They account for 80% of the Earth's total plant biomass (carbon = 50% biomass) (Kindermann et al. 2008) and store 861 petagrams of carbon (Pg C), of which 42% is in living biomass, 8% in dead wood, 5% in litter, and 44% in soil, more than the 829 Pg C of the entire atmosphere (Mackey et al. 2013; Pan et al. 2011). Living forests sequester carbon dioxide (CO₂) from the atmosphere through photosynthesis and release carbon back to the atmosphere through autotrophic respiration. C is also transferred from plants to soil in the form of leaf, wood and root litter and is eventually released back into the atmosphere through decomposition (Malhi and Grace 2000). Growing forests accumulate photosynthetically fixed carbon in leaves, branches, stems and roots, acting as a sink for the atmospheric CO₂. When forests are damaged, carbon stored in the biomass is released as CO₂ into the atmosphere.

At the global scale, the world's forests are a large and persistent carbon sink (Pan et al. 2011). The annual gross carbon uptake by established and recovering forests was estimated to be 4.0 ± 0.7 Pg C/yr from 1990 to 2007, equivalent to 50% of fossil-fuel carbon emissions in 2009 (Le Quéré et al. 2009; Pan et al. 2011). The net forest carbon sink geographically resides in temperate and boreal regions, whereas the tropical region is nearly carbon-neutral because of a balanced sink from intact and

recovering forests and a carbon source from deforestation (Friedlingstein et al. 2010; Pan et al. 2011).

1.2 Historical trend of carbon emissions from deforestation

Tropical land cover and land use change (LCLUC), primarily deforestation, accounts for 10–20% of total anthropogenic emissions—the second largest source after fossil-fuel combustion (Houghton et al. 2012; van der Werf et al. 2009). Emissions from LCLUC are also the most uncertain component of the global carbon cycle, which requires an accurate estimate to close the global carbon budget (Canadell et al. 2007; Ciais et al. 2013; Schimel et al. 2001). While annual emissions from fossil-fuel combustion have been continually increasing since the 1960s, historical trends of deforestation and associated carbon emissions have remained poorly understood (Grainger 2008; Peters et al. 2011; van der Werf et al. 2009). Using various data and methods recent studies estimate that deforestation in the tropics accounts for 0.6 to 2.0 Pg C/yr of the carbon emitted into the atmosphere in the 1980s, 0.9 to 2.2 Pg C/yr in the 1990s, and 0.8 to 2.9 Pg C/yr in the 2000s (Achard et al. 2004; Baccini et al. 2012; DeFries et al. 2002; Harris et al. 2012b; Houghton 2005; Pan et al. 2011). The large range of uncertainty of these emission estimates arises from many factors including definitions of forest and deforestation, terrestrial carbon pools (above-ground biomass, below-ground biomass, dead wood and litter, and soil) accounted, uncertainty in deforestation rates, uncertainty in initial carbon stocks of vegetation and soil, land cover dynamics after deforestation, fate of cleared carbon, and the carbon cycle model used, for most of which current carbon cycle science lacks

standardization or consistency (Ramankutty et al. 2007). In addition, the wide ranges of these emission estimates across different periods greatly obscure our understanding of the trend and temporal variability of carbon emissions from deforestation (Figure 1.1).

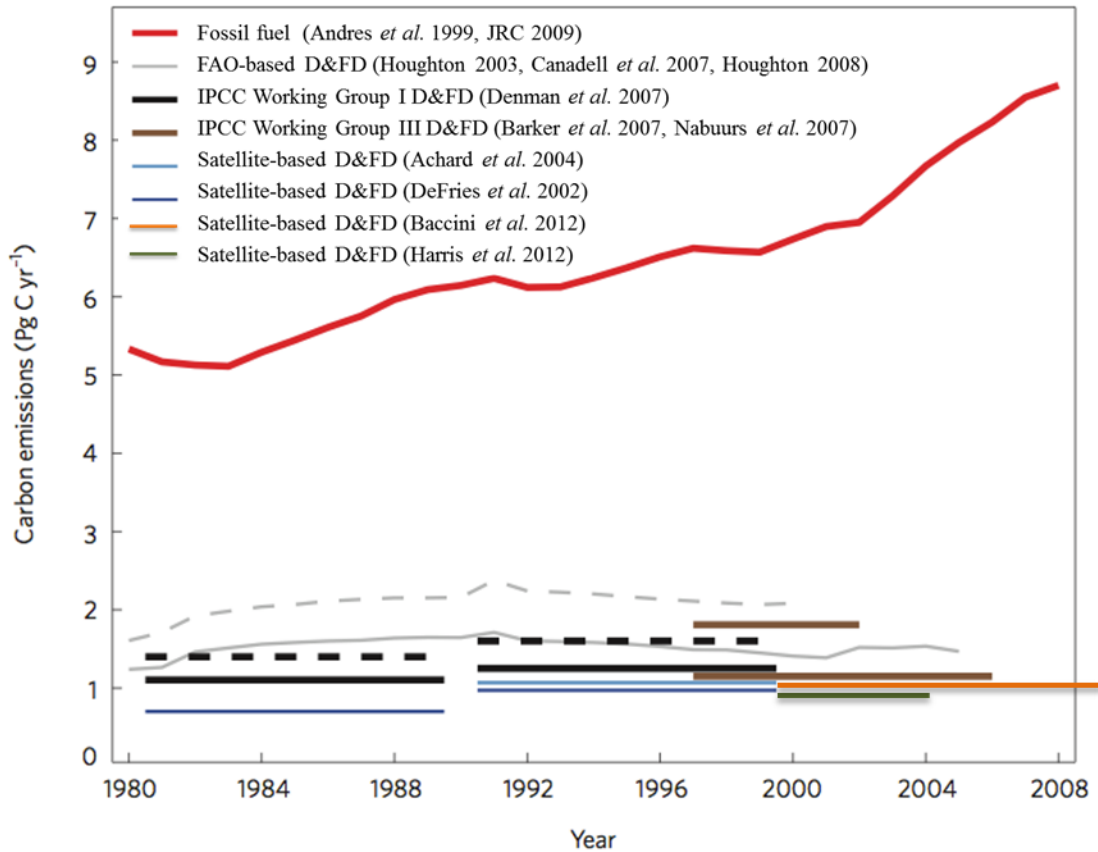


Figure 1.1 Carbon emissions from deforestation and forest degradation (D&FD) and fossil-fuel emissions from 1980 onwards (adapted from van der Werf et al. [2009])

Knowing the trend and temporal variability of carbon emissions from deforestation is significant for a number of reasons. First, it may explain some of the inter-annual variability of atmospheric CO₂ concentration (Keeling et al. 1995). Atmospheric inversion studies suggest that the inter-annual variability of global CO₂

growth rate is dominated by tropical land ecosystems, with positive anomalies related to El Niño and negative anomalies related to La Niña (Bousquet et al. 2000; Ciais et al. 2013; Rayner et al. 2008). A recent study further recognizes that semi-arid ecosystems may become a more relevant driver of the global carbon anomaly in the future (Poulter et al. 2014), but questions remain about how much of the variability can be attributed to carbon released by land cover change (Houghton 2000; Keeling et al. 1995). Second, the trend of deforestation is critical for understanding the complex and changing drivers of deforestation (Nepstad et al. 2014). For example, the increasing deforestation between 2001 and 2004 in the Brazilian Amazon is related to trends in the international soybean price and the declining deforestation after 2005 is associated with the collapse of commodity markets as well as shifting land use dynamics (Macedo et al. 2012; Morton et al. 2006). Studies also link time series of deforestation emissions with economic input-output models to attribute emissions to domestic consumption and to international trade of agricultural products (Karstensen et al. 2013). Third, knowing the trend and variability of historical emissions likely has a strong influence on policies of reducing emissions from deforestation and forest degradation (REDD+). The inter-annual variability itself is a key factor for setting the reference emission level (REL) or the baseline in some proposed REL methods (e.g., the corridor approach [Joanneum Research et al. 2006]).

1.3 Estimating carbon emissions from deforestation

Current methods of estimating carbon emissions from deforestation can be classified into three broad categories: (1) process-based terrestrial ecosystem models, (2) the

bookkeeping model and (3) direct satellite observations (Ciais et al. 2013).

Process-based ecosystem models simulate carbon, water and energy fluxes between vegetation, soil and atmosphere on a grid basis using a variety of climatological and ecological datasets. These models have the advantage of understanding the physiological mechanisms of terrestrial carbon storage and flux, such as the effect of elevated atmospheric CO₂ concentration (i.e. the CO₂ fertilization effect) (Kicklighter et al. 1999), climate variability (Kindermann et al. 1996; Tian et al. 1998), anthropogenic nitrogen deposition (Thomas et al. 2010), land use change (Jain and Yang 2005) or the combined effects (McGuire et al. 2001). However, the individual and the combined effects of these mechanisms are not completely known, leading to significant disagreement and a wide range of C flux estimates among different model simulations (Ciais et al. 2013; Le Quéré et al. 2014; McGuire et al. 2001).

The bookkeeping model tracks carbon changes in major terrestrial carbon pools assuming generic time-dependent functions for carbon losses and gains in different ecosystem types (Moore et al. 1983). Several early studies use the bookkeeping model with data from the Food and Agriculture Organization's (FAO's) country-level deforestation reports and biome-averaged carbon densities (Houghton 1999; Houghton 2003; Houghton et al. 1987). Others make improvements by either replacing deforestation data with area estimates from satellite imagery (Achard et al. 2004; DeFries et al. 2002) or replacing surveyed carbon density with satellite-derived biomass data (Baccini et al. 2012). The bookkeeping approach explicitly accounts for the fate of lost carbon (e.g. harvested wood product vs. litter decay) in estimating

actual carbon emissions (as opposed to committed emissions), but the model is not spatially explicit and the parameterization is largely subject to expert opinions.

The direct satellite-observation approach quantifies changes in forest cover and the pre-change biomass separately and integrates both datasets to estimate changes in forest carbon stocks with Geographic Information System (GIS) analysis. Deforestation data and initial biomass data are spatially matched to calculate carbon stock changes in specific locations. As such, the spatial heterogeneity of carbon emissions across ecological and/or political boundaries can be effectively revealed (Harris et al. 2012b; Tyukavina et al. 2013). This approach assumes immediate carbon release at forest clearing without considering the time-lag effect of ecological processes. The end result is the so-called “committed emissions”, which represent the total emissions that will be eventually released to the atmosphere. This approach also does not investigate the mechanisms of ecosystem carbon flux but emphasizes the role of monitoring and accurate data in reducing uncertainty.

Overall, the diverse processes and time scales captured by these different methods make a comparison of their estimations of CO₂ emissions from LCLUC difficult. However, previous studies showed that satellite observations generally revised emission estimates downward more than other approaches (Figure 1.1). This finding may provide a partial explanation for the “missing carbon sink” (Tans et al. 1990), which is derived in part on the basis of the FAO data and the bookkeeping model (Houghton et al. 1987).

Estimating deforestation emissions using satellite data is built on several key steps. First, the extent and density of forest cover must be characterized. Second,

changes in forest cover must be accurately quantified. Third, initial forest biomass must be accurately estimated. Fourth, FCC and biomass data must be matched on the same spatiotemporal scale to calculate carbon stock change.

1.3.1 Characterizing forest cover with satellite data

Optical satellite imagery is the primary data source for characterizing land cover and monitoring land cover change. Because incident solar energy is absorbed, transmitted and reflected differently by different land surfaces, a land cover type can be identified on the basis of its distinct reflective features. Key factors determining the spectral properties of vegetated land cover include the chemical content and physical structure of leaves as well as the multi-layer structure of vegetation canopy. Healthy green vegetation has low reflectance in the blue (450–520 nm) and red (630–690 nm) wavelengths because of strong absorption of sunlight by chlorophylls for photosynthesis, but has high reflectance in the near-infrared (760–900 nm) wavelength because of intra- and inter-leaf scattering of photons (Tucker 1979). Additionally, forest typically appears darker than herbaceous vegetation because of the substantial shadow cast within the canopy, most apparent in the visible and shortwave ranges, depending on the sun-target-view geometry (Colwell 1974). Furthermore, the spectral reflectance of different vegetation also has different seasonality (phenology) over time (Justice et al. 1985).

On the basis of these features, digital satellite images are converted to land cover maps using either an unsupervised or a supervised approach. In the unsupervised approach, pixels are first clustered by a computer algorithm and each cluster is subsequently labeled to a thematic type by a person. In the supervised

approach, a classifier is first trained with reference samples that have known class labels and then each pixel is categorized to its respective land cover class by the classifier (Mather and Koch 2011). Widely used unsupervised algorithms include K-means and the Iterative Self-Organizing Data Analysis Technique, and supervised classification algorithms include maximum likelihood, artificial neural networks, support vector machines, and classification and regression trees (Mather and Koch 2011).

Meta-analysis of peer-reviewed land cover classification literature, most of which focused on small areas, showed no obvious improvement in terms of classification accuracy over the past four decades (Wilkinson 2005; Yu et al. 2014). For operational land cover monitoring, an algorithm should be selected on the basis of multiple criteria, including its accuracy, the computational resources required, its stability, and its robustness to noise in training data (DeFries and Chan 2000). Beyond algorithm selection, the most significant constraint to automated land cover mapping over continental to global scales is the availability/derivation of sufficient and representative training samples.

Research on characterizing global patterns of land cover using remotely sensed data has been conducted since the mid-1990s. As a result, a number of global land cover maps have been generated, including: Global Land Cover Characterization (GLCC) (Loveland et al. 2000), the University of Maryland land cover (UMD LC) product (Hansen et al. 2000), Global Land Cover 2000 (GLC2000) (Bartholomé and Belward 2005), the Moderate Resolution Imaging Spectroradiometer land cover (MODIS LC) product (Friedl et al. 2002), the MODIS Vegetation Continuous Fields

(MODIS VCF) product (Hansen et al. 2003) and the GlobCover land cover product (Bicheron et al. 2008). Each of these data sets is derived from moderate resolution satellite imagery at spatial resolutions between 300 m and 1 km. The diversity of the data and methods used in deriving these maps has led to substantial disagreement in their representation of forest (Figure 1.2).

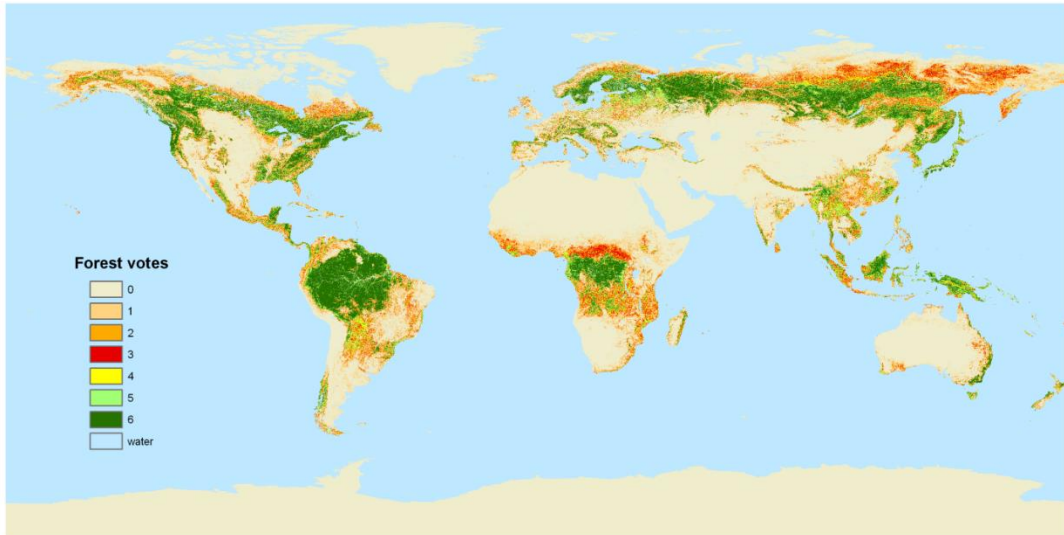
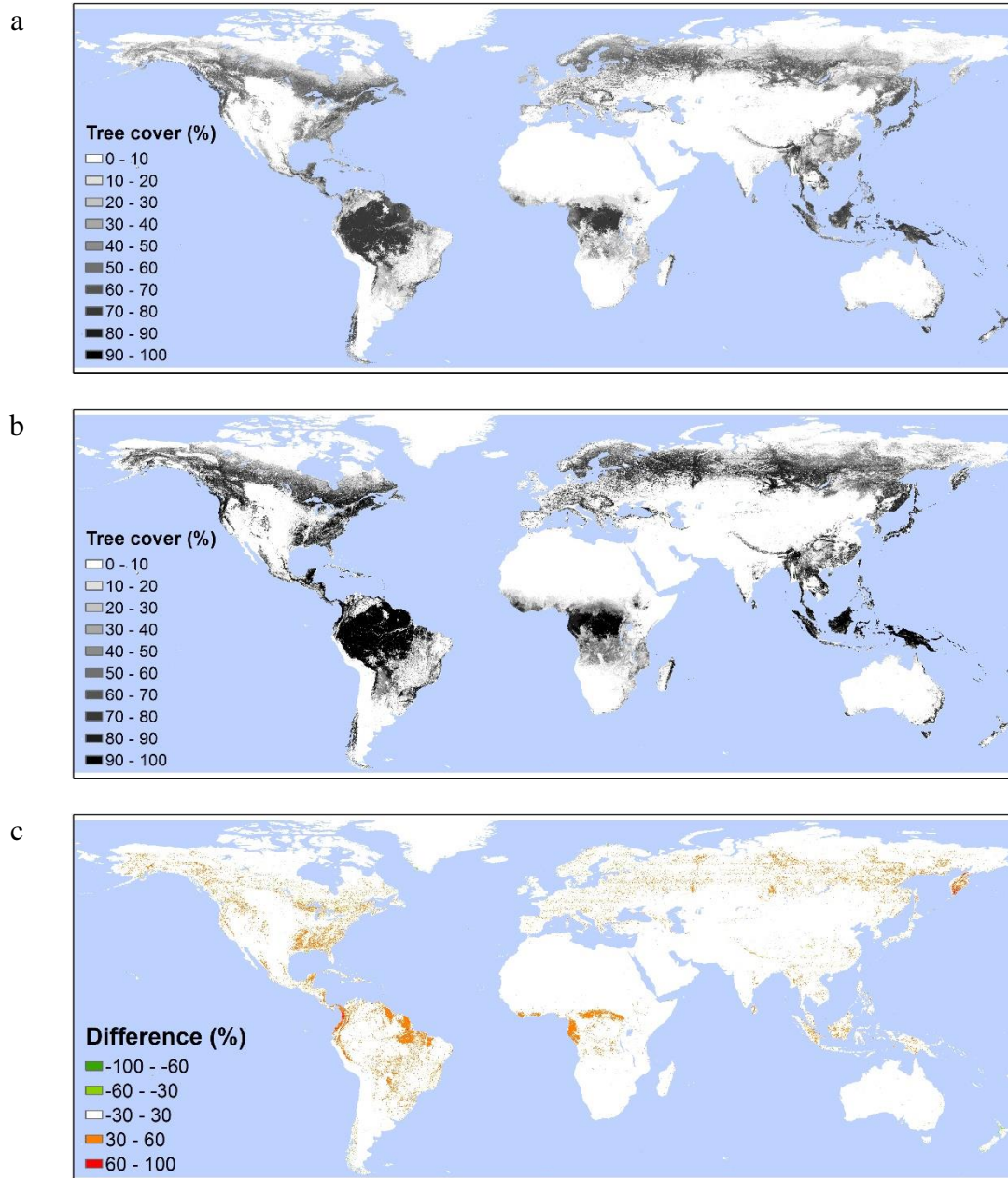


Figure 1.2 Disagreement among six land cover products on their representation of global forest cover. The six products are GLC2000, GLCC, GlobCover, MODIS LC, MODIS VCF and UMD LC.

Global-scale forest cover mapping at 30 m resolution has only become feasible in recent years, owing much to the United States Geological Survey (USGS)'s open Landsat data policy (Wulder et al. 2012) and the reduced cost of data storage and computation. So far, five 30 m global forest/tree cover maps have been generated by Gong et al. (2013), Sexton et al. (2013), Hansen et al. (2013), Kim et al. (2014), and Chen et al. (2014), and more datasets are in production (Giri et al. 2013; Townshend et al. 2012). The spatial details revealed by these Landsat-based map

products are 100-1000 times more than those coarse-resolution maps and the cross-map consistency has improved considerably because of the common data source (Figure 1.3). However, the overall global disagreement patterns resemble to a noticeable degree those coarse-resolution datasets (Figure 1.3c).



d

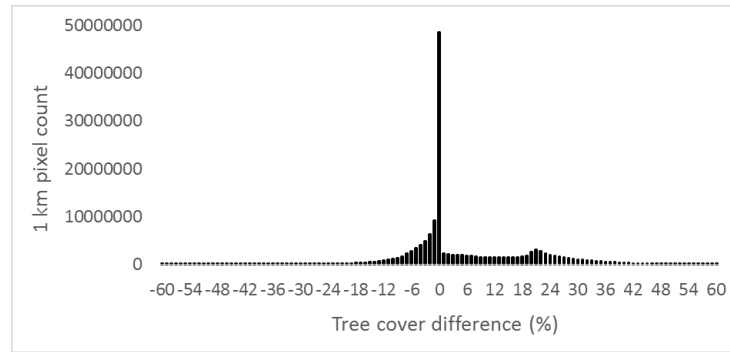


Figure 1.3 Landsat-based global tree cover products and their difference. Both datasets were aggregated to 1 km and the difference was calculated at 1 km resolution. (a) Data from Sexton et al. (2013) (b) Data from Hansen et al. (2013). (c) Difference map between b and a. Red represents higher estimates in Hansen et al. (2013) and green represents higher estimates in Sexton et al. (2013). (d) Histogram of the difference map.

Although increasing the spatial resolution of land cover maps represents a continued advancement in land cover mapping, exploratory questions can also be asked. For instance, what are the implications of the observed agreement and disagreement patterns for future forest and land cover mapping? Can these diverse datasets, each of which has its unique advantage and as a collection has a reasonable level of agreement, be synthesized to generate a more accurate forest cover map?

1.3.2 Quantification of forest cover change

Quantification of FCC with satellite data takes either a sampling approach or a wall-to-wall approach (Tucker and Townshend 2000). In the latest advancement, Landsat samples have been used to determine tropical deforestation rates between 1990 and 2010 (Achard et al. 2014); MODIS and Landsat data have been jointly used to

quantify global gross forest cover loss between 2000 and 2005 (Hansen et al. 2010; Hansen et al. 2008c); the wall-to-wall Landsat Thematic Mapper (TM) and Enhanced Thematic Mapper Plus (ETM+) surface reflectance data have been used to derive global FCC between 1990, 2000, 2005, and 2010 (Kim et al. 2015; Sexton et al. 2015; Sexton et al. 2013a) with change maps between 1975 and 1990 being generated (Townshend et al. 2012); Landsat ETM+ top-of-atmosphere (TOA) reflectance data have been composited at annual resolution to create global forest cover loss and gain maps between 2000 and 2012 (Hansen et al. 2013); and the Advanced Land Observing Satellite Phased Array L-band Synthetic Aperture Radar data have been employed to produce forest/non-forest maps over the globe, but the generation of globally consistent change product with Synthetic Aperture Radar (SAR) data is yet to be studied (Shimada et al. 2014).

Most existing studies on large-area FCC monitoring are carried out at long temporal intervals (e.g., 5 years, 10 years, or longer) (Achard et al. 2007; Hansen et al. 2010; Hansen et al. 2008c; Huang et al. 2009c; Masek et al. 2008; Mayaux et al. 2013; Sexton et al. 2014). However, the rate of FCC can vary substantially from one year to another at local to global scales (Hansen et al. 2013; Huang et al. 2009b; Masek et al. 2013). Thus, change products derived at sparse temporal intervals cannot capture such temporal dynamics. In areas where forests can re-establish within a few years after having been cleared, coarse-interval change detection may also miss significant portions of forest loss that are followed by rapid regrowth (Masek et al. 2008). Therefore, international initiatives such as the Global Observations of Forest

Cover and Land Cover Dynamics (GOFC-GOLD) have specified the need for monitoring forest dynamics at < 5-year frequency (GOFC-GOLD 2012).

Recent years have also seen a growing number of methods toward the use of biennial or annual satellite imagery for mapping forest disturbance, such as vegetation change tracker (Huang et al. 2010a) and LandTrendr (Kennedy et al. 2010). These methods typically seek a structural deviation of a pixel's spectral response or vegetation index from the nominal value to infer forest disturbance. Sophisticated thresholding is required to generalize the algorithms across different forest and disturbance types. The globally applicable approach presented in Hansen et al. (2013) first classifies forest cover loss (stand-replacing disturbance), and then attributes a specific year to the detected loss pixel based on maximum drop in the annual Normalized Difference Vegetation Index (NDVI). However, assigning one time to the detected loss may result in omission errors in places with rapid land cover turnover (e.g. tree crop rotation). More research is required to either improve these existing methods or explore new means that can explicitly detect FCC, applicable at annual or finer temporal resolutions, and can be generalized to the global scale.

1.3.3 Estimating forest carbon stock and change

Because of the saturation of spectral signals at high vegetation canopy closure, optical satellite imagery is limited in estimating plant biomass (Steininger 2000). Inventory data and active remote sensing, such as light detection and ranging (Lidar) and radio detection and ranging (Radar), are commonly used to estimate live biomass (Gibbs et al. 2007). Field-measured tree height and diameter at breast height (DBH) can yield the least uncertain estimate of tree biomass for a specific plot, but because of the

limited data availability and high economic cost, producing wall-to-wall biomass maps relying on field data alone is impractical (Goetz et al. 2009). Lidar can accurately measure forest vertical structures such as canopy height, which can then be related to biomass with allometric equations (Dubayah and Drake 2000). However, space-borne Lidar data are only available at scattered locations and in large ground footprints (tens of meters in diameter) (Harding and Carabajal 2005; Lefsky 2010). Spatially contiguous Radar backscatter data do not directly measure biomass, but Radar data are sensitive to the size and orientation of canopy elements such as leaves, branches, and stems and thus can provide a good proxy to biomass (Saatchi et al. 2012; Woodhouse et al. 2012).

Current best practice on biomass estimation often employs a combination of these data sources, optimizing their combined advantage while overcoming each respective shortcoming. The procedure first uses field-calibrated allometric equations (Brown 1997; Chave et al. 2005) to relate Lidar-derived forest structure metrics to live biomass, and then spatially extrapolates biomass estimation to a landscape using machine learning models, with input data from Radar and optical imagery. To date, two pan-tropical biomass maps have been derived at 1 km (Saatchi et al. 2011) and 500 m resolution (Baccini et al. 2012), respectively. Substantial differences were noted between these two maps in a variety of forest types, although they were both derived from similar input data and with a similar processing chain (Mitchard et al. 2014; Mitchard et al. 2013). When they were compared with a high-resolution biomass map derived from field-plot calibrated aircraft Lidar in Colombia (Asner et al. 2012), a closer match appeared to be observed between the Saatchi et al. (2011)

data and the high-resolution data. Attempts have also been made to fuse these two biomass maps for an improved biomass estimation (Ge et al. 2014). Because of the lack of validation data, conducting systematic error estimation for biomass data has yet to become a consensus, as with land cover mapping. Improving the spatial resolution of biomass maps appears to have a high priority in ongoing research.

Despite the lack of thorough error estimation, the spatially explicit forest biomass information has been combined with FCC maps to quantify forest carbon stock change. This approach is a methodological improvement in carbon emission estimation over the bookkeeping model based on FAO data, because carbon stocks clearly vary greatly within the forests of every country. For each grid cell, the area of forest change (in ha) and the corresponding biomass density (in t C/ha) are multiplied to calculate the change in carbon stock (in t C). With this approach, Harris et al. (2012b) calculated carbon emissions from deforestation for pan-tropics between 2000 and 2005. A similar study was carried out for the Congo basin for the period of 2000–2010 (Tyukavina et al. 2013). Both studies revealed the spatial heterogeneity of land-cover change emissions at national and sub-national scales. However, these studies only derived an average emission estimate over a 5-year or 10-year interval, similar to the FAO reports. Hence, they do not embrace the necessary temporal details to uncover historical trends.

Unlike fossil-fuel emissions that are known to have been increasing steadily (Peters et al. 2011), the trend and temporal variability of deforestation emissions is still largely unknown (Figure 1.1). Because of the repetitive nature of satellite

observations, the annual or seasonal variability of deforestation and associated C emissions can be studied with time-series satellite data.

1.4 Research objectives

The central research question this dissertation attempts to answer is what is the trend and inter-annual variability of carbon emissions from deforestation? To address this question, spatially consistent, time-series satellite data are used to achieve an improved quantification of deforestation and associated carbon emissions. The following specific research objectives are sequentially addressed:

1. Improve the global characterization of forest cover through map integration.
2. Develop reliable methods for monitoring forest cover change at an annual frequency.
3. Integrate annual forest cover change data and biomass data to quantify carbon emissions from deforestation.
4. Analyze trend and inter-annual variability of deforestation emissions at national and sub-national scales.

1.5 Dissertation organization

The dissertation consists of five chapters corresponding to the specific research objectives. Chapter 1 introduces the topic, reviews current data and methods for quantifying forest cover change and associated carbon stock change, and sets the research objectives. Chapter 2 compares and evaluates six global land cover maps and explores an approach to integrate them for an improved characterization of forest

cover. Chapter 3 focuses on developing a new method for detecting forest cover loss at annual time steps using the yearly MODIS Vegetation Continuous Field product and Landsat sample. In Chapter 4, the developed method is applied to the Amazon basin to map annual deforestation, which is then combined with a biomass map to quantify carbon emissions. Trends and temporal variability of emissions are subsequently analyzed. Chapter 5 summarizes the findings and draws implications for future research.

Chapter 2: Integrating Global Land Cover Products for an Improved Forest Cover Characterization

2.1 Introduction

Defining “forest” is a complex issue. There are over 800 definitions of forest viewed from the land cover, land use, ecological or administrative perspectives and these definitions vary from local to national and international scales (Lund 2014).

Considering forest as a land cover type which is directly measurable from satellite imagery, its definition also varies across different land cover schemes in terms of tree cover, tree height and land area. For example, the International Geosphere-Biosphere Programme (IGBP) defines closed forest as an area with tree cover > 60% and open forest as an area with tree cover between 30% and 60%, both with tree height > 2 meters (Belward 1996). The FAO defines forest as land of at least 0.5 hectares in size which is covered by 10% or more trees that are 5 meters or taller (FAO 2012). The United Nations Framework Convention on Climate Change (UNFCCC) defines forest as an area of > 0.05-1.0 ha with tree cover > 10-30% and with trees with the potential to reach a minimum height of 2-5 meters at maturity (UNFCCC 2002). The specific thresholds adopted by participating countries of UNFCCC vary within the ranges of the three parameters. To be consistent, forest cover in this dissertation refers to the IGBP definition (i.e. > 30% tree cover) at the Landsat pixel scale (0.09 ha).

Satellite images have been used to characterize global patterns of land cover since the mid-1990s. The first global satellite-based land cover map was produced at 1-degree resolution using data collected by National Oceanic and Atmospheric

Administration (NOAA)'s Advanced Very High Resolution Radiometer (AVHRR) (Defries and Townshend 1994b). This map product was subsequently updated to 8-km resolution (DeFries et al. 1998). Developed using different datasets and different methodologies, many global maps are now freely available at 300-m to 1-km resolutions, such as Global Land Cover Characterization (GLCC) (Loveland et al. 2000), Global Land Cover 2000 (GLC2000) (Bartholomé and Belward 2005), GlobCover land cover (GlobCover) (Bicheron et al. 2008), the Moderate Resolution Imaging Spectroradiometer land cover (MODIS LC) (Friedl et al. 2002), the University of Maryland land cover (UMD LC) (Hansen et al. 2000), and the MODIS Vegetation Continuous Fields (MODIS VCF) (Hansen et al. 2003). 30-m Landsat data have also been used to produce global tree cover or land cover maps until recently (Gong et al. 2013; Hansen et al. 2013; Sexton et al. 2013a).

The generation of global land cover product has been continually evolving with increasing spatial resolution and temporal frequency. Early products such as the UMD LC and GLCC were derived at 1-km resolution for one year. MODIS VCF was generated at 250-m resolution annually between 2000 and 2010 (DiMiceli et al. 2011). The latest Landsat maps were made at 30-m resolution with forest cover loss allocated annually between 2000 and 2012 (Hansen et al. 2013). The potential utility and downstream applications of these map products have also changed as a result of improved map quality. While early datasets are primarily designed to provide boundary conditions for Earth system models (Bonan et al. 2002b), recent maps of finer-resolution not only fulfil the need of the biogeochemical modelling community,

but also provide essential information for natural resource management (Hansen et al. 2013).

The accuracy of a land cover map is often users' primary concern. For instance, GLC2000 has an overall accuracy of 68.6% (Mayaux et al. 2006) and GlobCover has an accuracy of 73.1% (Bicheron et al. 2008). However, these accuracy numbers are often generated with diverse validation datasets and thus are not directly comparable (Fritz and See 2008; Pflugmacher et al. 2011). More importantly, the overall accuracy does not reflect the complex error structure of those maps, because errors in land cover classification are not equally distributed across thematic classes as well as across spatial regions (Strahler et al. 2006).

Per-pixel comparison of land cover products is more informative than overall accuracy as it can reveal the spatial patterns of agreement and disagreement between different maps. Many previous studies (DeFries and Townshend 1994a; Fritz and See 2008; Giri et al. 2005; Hansen and Reed 2000; Herold et al. 2008; Jung et al. 2006) have compared sets of two or three of the existing products and found substantial discrepancies among them. Pflugmacher et al. (2011) compared four global land cover datasets for Northern Eurasia and assessed them with six Landsat-based reference maps. They found positive relationships between map errors and landscape heterogeneity. High agreement tends to be located in relatively homogeneous and spectrally distinct regions, while low agreement tends to be located in heterogeneous landscapes, land cover transition zones and between spectrally similar classes. However, all previous comparison studies are limited to a subset of existing

categorical maps and none of them includes fractional land cover products such as the MODIS VCF.

Given the many available datasets and the level of agreement among them, opportunities may exist to combine these data for an improved land cover characterization. Yet few attempts have been made in this direction. Jung et al. (2006) collected multiple versions of GLC2000, GLCC and MODIS LC and merged them into a joint 1-km map by cross-walking different land cover legends. Fritz et al. (2011) created a hybrid cropland map for Africa using an approach modified from Jung et al. (2006). Similarly, Schepaschenko et al. (2011) produced a hybrid land cover dataset over Russia by combining satellite-derived land cover maps, GIS database and national statistics based on a set of knowledge rules.

The objective of this chapter is to propose a supervised, harmonization-based method for integrating multi-resolution, multi-source global datasets to improve land cover characterization. To demonstrate this approach, six global maps are used as input and one Landsat-based map is used as reference to derive an integrated percent forest cover (IPFC) map over North America. The integrated map is evaluated using Landsat reference in the same way as the six input datasets to show the improvement resulted from data integration. Additionally, the existing global maps are cross-compared with each other to understand the implications of the agreement and disagreement among different products. Although we focus on the representation of forests in North America where sufficient reference data are available for assessment of the results, the approach derived here can potentially be applied to any large area and any other land cover type.

2.2 Data

2.2.1 Global Land Cover Characterization

The GLCC database was developed at a continent-by-continent basis (Loveland et al. 2000). AVHRR 10-day NDVI composites for the period of April 1992 to March 1993 were aggregated into monthly maximum NDVI composites to minimize cloud contamination. Non-vegetated land covers such as barren land, snow and ice were identified using thresholds of the maximum NDVI and were masked prior to classification. Water bodies and urban land cover were not classified from AVHRR, but imported from the hydrography layer and populated places' data layer from the Defense Mapping Agency's Digital Chart of the World (DCW) (Danko 1992). An unsupervised algorithm was then applied to cluster the masked AVHRR monthly composites and each cluster was labeled as one of the 961 seasonal land cover regions. Each seasonal land cover region was firstly translated into Olson's Global Ecosystems Legend (Olson 1994) and then cross-walked into six different land cover legends, including the IGBP scheme and the USGS Anderson scheme.

2.2.2 UMD land cover product

The University of Maryland land cover product was also generated from AVHRR data but with a supervised classification procedure (Hansen et al. 2000). The 1-km AVHRR 10-day NDVI composites and the five optical bands were used to create a total of 41 annual metrics including the maximum, minimum and mean NDVI as well as pixel values of channels 1 to 5 associated with the eight greenest and the four warmest months. Training data were derived from a total of 156 60-m Landsat

Multispectral Scanner (MSS) images. A decision tree model was trained and applied to the annual metrics to create vegetation classifications. The urban and built-up class was taken from GLCC, which was in turn taken from DCW. The UMD product employs a classification scheme modified from IGBP for use with the Simple Biosphere (SiB) general circulation model (Sellers et al. 1986). Since the SiB scheme does not include agricultural mosaics, wetlands, snow and ice classes, these classes were not explicitly characterized. Instead, the snow and ice class is included in the bare ground class.

2.2.3 Global Land Cover 2000

The Global Land Cover 2000 (GLC2000) project was initialized by the European Union's Joint Research Center (JRC) with the objective of producing a land cover map for the International Conventions on Climate Change, the Convention to Combat Desertification, the Ramsar Convention and the Kyoto Protocol (Bartholomé and Belward 2005). Input data were based on SPOT-4 VEGETATION VEGA2000 acquired from November 1999 to December 2000. The whole globe was divided into 19 regions and the classification for each region was carried out by local experts using independent methods and legends that are most appropriate for the respective region. Subsequently, regional land cover classes were translated to a global legend according to FAO's Land Cover Classification System (LCCS) (Di Gregorio 2005). Some parts of global classification were further improved using ancillary data such as digital elevation data and night-time lights data.

2.2.4 MODIS land cover product

One of the standard MODIS products is the global land cover map (MCD12Q1) generated at Boston University. Multiple versions of this product have been generated, all of which employed a supervised decision tree algorithm (Friedl et al. 2002; Friedl et al. 2010). Input data and features included the nadir BRDF (bidirectional reflectance distribution function)-adjusted reflectance data, land surface temperature, enhanced vegetation index, and annual metrics (min, max, mean) of each band. Training data were derived from Landsat images taken from the System for Terrestrial Ecosystem Parameterization database, which included 1860 sites distributed across the globe. The final map was a result of an iterative “boosting” procedure – an ensemble classification method in which multiple classifications were carried out based on resampled training data and the final classification was determined by an accuracy-weighted vote. The product is available in multiple land cover legends, including the IGBP scheme, the UMD scheme, the MODIS leaf area index/fraction of photosynthetically active radiation class system (Myneni et al. 2002), an 8-biome classification system (Running et al. 1995) and a 12-class plant functional type classification system (Bonan et al. 2002a).

2.2.5 MODIS vegetation continuous fields

The MODIS vegetation continuous fields (VCF) product is also a standard MODIS land product (MOD44B). It estimates fractional vegetation cover at sub-pixel level, representing a theoretically advanced characterization of land cover over categorical maps. The latest version is generated at a spatial resolution of 250-m annually from

2000 to 2010 (DiMiceli et al. 2011). Following an established method described in Hansen et al. (2003), bagged regression tree models were trained using a large Landsat-based reference sample and annual phenological metrics composited from the 16-day surface reflectance including bands 1-7 and brightness temperature from bands 20, 31 and 32. The models were applied to annual phenological metrics to predict percent tree cover per MODIS pixel per year. Poor pixels which were either cloud, cloud shadow, high aerosol or had a view zenith angle $> 45^\circ$ were reduced through the composition process and the remnant were flagged in the quality assurance (QA) layer. White et al. (2005) validated the Collection 1 MODIS VCF against independent field data across the arid southwestern United States, and later Montesano et al. (2009) evaluated the Collection 4 product using reference data derived from high-resolution images across the boreal-taiga ecotone. Recently, Sexton et al. (2013a) estimated the error of Collection 5 VCF against measurements of tree cover from small-footprint Lidar data in four sites across three different forest biomes and found that the root-mean-square-error (RMSE) of Collection 5 MODIS VCF ranges from 7-21%.

2.2.6 GlobCover land cover product

The GlobCover project, conducted by the European Space Agency, was designed to generate a land cover map of the world using 300-m data from the Medium Resolution Imaging Spectrometer Instrument on-board the ENVISAT satellite (Bicheron et al. 2008). Input data were acquired for the period between December 2004 and June 2006. Cloud-free surface reflectance mosaics were generated through a series of pre-processing steps including geometric correction, cloud screening and

shadow detection, land/water classification, atmospheric correction, BRDF correction and temporal compositing. The mosaics were stratified into bioclimatically homogenous regions across the world and then converted to land cover maps region by region. The overall classification procedure consisted of a supervised step and an unsupervised step. Land cover classes that were not well represented such as urban and wetland, were classified with a supervised algorithm and the remaining pixels were clustered with an unsupervised algorithm. Clusters with similar temporal features were grouped into a manageable number of spectral-temporal classes and then labeled to land cover types following the UN LCCS. Some local land cover products were used as reference to fine-tune the global map as a post-classification step. Flooded forests which were largely underestimated were directly imported from the regional data. Delineation of water bodies was improved by incorporating the Shuttle Radar Topography Mission Water Body Data.

2.2.7 U.S. National Land Cover Database

The Landsat-based National Land Cover Database 2001 (NLCD2001) over the conterminous United States (CONUS) (Homer et al. 2004) is used as reference for training the integration model as well as evaluating the input and output products. To produce the NLCD2001, the CONUS was divided into 66 relatively homogenous zones with respect to landform, soil, vegetation, spectral reflectance, etc. AVHRR-derived NDVI was used to select Landsat 7 or 5 images acquired in early, peak and late of vegetation growing seasons. Selected Landsat images were converted to at-satellite reflectance for the six reflective bands and to at-satellite temperature for the thermal band and subsequently transformed to brightness, greenness and wetness

indices through a Tasseled Cap Transformation (Huang et al. 2002; Kauth and Thomas 1976). A decision tree classifier was used with training data obtained from aerial photographs, field-work as well as the Forest Inventory Analysis (FIA) database. As a result, 29 land cover classes were mapped. Validated against expert-interpreted 1-m Digital Orthophoto Quarter Quadrangles, the NLCD2001 was proved to have 87% user's accuracy and 88.5% producer's accuracy for the forest class (Wickham et al. 2010).

Table 2.1 Summary of key features of the global and regional land cover products

Product	Sensor	Date	Resolution	Classification approach
GLCC	AVHRR	Apr. 1992 –Mar. 1993	1-km	Clustering – labeling
GLC2000	SPOT-4	Nov. 1999 – Dec. 2000	1-km	Depends on individual region
GlobCover	MERIS	Dec. 2004 –Jun. 2006	300-m	Supervised and unsupervised
MODIS LC	MODIS	Oct. 2000 –Oct. 2001	1-km	Decision tree
MODIS VCF	MODIS	Oct. 2000 – Dec. 2001	500-m	Regression tree
UMD LC	AVHRR	Apr. 1992 –Mar. 1993	1-km	Decision tree
NLCD2001	Landsat 5 & 7	Circa 2001	30-m	Decision tree

2.3 Method

The data integration method consists of a series of steps, which are illustrated in Figure 2.1 and are described in details in each of the sub-sections bellow. As a pre-processing step, all products were reprojected to Lambert Azimuthal Equal Area projection with the WGS84 datum. They were also matched to an exactly same spatial extend using nearest neighbour resampling.

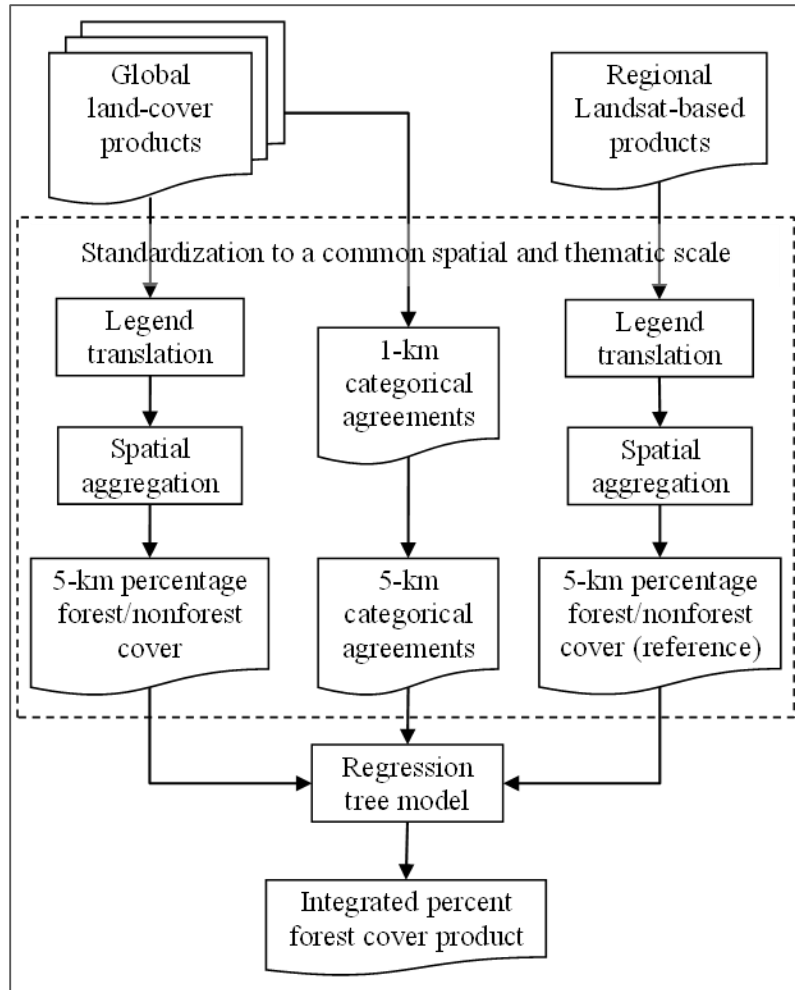


Figure 2.1 Overall flowchart for deriving the integrated 5-km percent forest cover product.

2.3.1 Standardization to a common spatial and thematic scale

These various datasets need to be standardized to the same spatial and thematic scale for integration. We first define a set of translation rules to convert each categorical land cover class into proportional forest canopy cover and proportional non-forest cover based on each specific definition and then spatially coarsen each product from its native resolution to 5-km to derive fractional canopy coverage of forest and

nonforest per 5-km grid. A 5-km spatial resolution was chosen for consistency with the Climate Modeling Grid used for MODIS and AVHRR products (Pedelty et al. 2007). Aggregating categorical cover maps from 1-km to 5-km reduces spatial misregistration between products and also yields a dynamic range sufficient for fractional cover.

2.3.1.1 Legend translation

A set of translation rules was used to convert each map's categorical "forest" class into a "forest canopy cover" percentage based on its classification scheme. All of the maps' vegetation classes are defined based on woody and herbaceous canopy closure as well as vegetation height. As discussed earlier, the IGBP defined closed forest as an area with woody cover > 60% and open forest as woody cover between 30% and 60%, both with tree height > 2 meters (Belward 1996). Aside from misclassification which is inevitable in any practical land cover map, a "correctly" classified pixel of closed forest in the IGBP scheme can still have forest canopy closure as low as 60%, with up to 40% of the remaining area being occupied by other land cover types. To approximate the actual forest cover in a coarse grid, we assigned a proportional weight to each classified pixel corresponding to the mean value of its woody canopy closure as defined in its original legend, e.g. 80% to closed forest and 45% to open forest for the IGBP legend. Classes like closed and open shrublands, croplands, grasslands, permanent wetlands, urban and built-up, snow and ice, bare, as well as water bodies, do not contain any forest cover. Therefore they were assigned a 0% forest cover and 100% non-forest cover. The mosaic classes in different land cover legends raise challenges in any legend harmonization work (Jung et al. 2006). The

cropland/natural vegetation mosaic class in the IGBP legend contains a mixture of four classes including croplands, forests, shrublands and grasslands (Belward 1996). It was therefore split into 25% forest cover and 75% non-forest cover. The complete legend translation rule set is given in Table 2.2. MODIS VCF directly gives percent canopy cover for each pixel and hence no further translation is needed.

Table 2.2 Proportional legend translation rules for different land cover legends.

Land cover legend	Categorical class	Forest canopy proportion
IGBP legend (GLCC, MODIS LC)	Forest (>60%) (evergreen needleleaf, deciduous needleleaf, everygreen broadleaf, everygreen needleleaf, mixed)	80%
	Woody savannas (30-60%)	45%
	Savannas (10-30%)	20%
	Cropland/natural vegetation mosaic	25%
	Shrublands (closed, open), grasslands, permanent wetlands, urban and built-up, snow and ice, barren or sparsely vegetated, croplands, water bodies	0%
UMD LC	Forest (>60%) (evergreen needleleaf, deciduous needleleaf, everygreen broadleaf, everygreen needleleaf, mixed)	80%
	Woodland (40-60%)	50%
	Wooded grassland (10-40%)	25%
	Shrubland(closed, open), grassland, bare ground, urban and built, cropland, water	0%
GLC2000	Tree cover, closed (>40%) (evergreen broadleaved, deciduous broadleaved)	70%
	Tree cover, open (15-40%) deciduous broadleaved)	27.5%
	Tree cover (>15%) (everygreen needleleaf, deciduous needleleaf, mixed leaf type, regularly flooded fresh or saline)	57.5%
	Mosaic: tree cover / other natural vegetation	50%
	Mosaic: cropland / tree cover / other natural vegetation	25%
	Burnt, shrub cover (evergreen, deciduous), herbaceous cover, sparse herbaceous or sparse shrub cover, regularly flooded shrub and or herbaceous cover, bare areas, artificial surfaces and associated areas, cultivated and managed areas, mosaic: cropland / shrub and/or herbaceous cover	0%
GlobCover	Closed forest (>40%) (broadleaved deciduous, needleleaved evergreen)	70%
	Closed to open forest (>15%) (broadleaved evergreen or semi-deciduous forest, mixed broadleaved and needleleaved, broadleaved forest regularly flooded)	57.5%
	Open (15-40%) broadleaved deciduous forest/woodland, open (15-40%) needleleaved deciduous or evergreen forest	27.5%
	Mosaic forest or shrubland (50-70%) / grassland (20-50%)	30%
	Mosaic grassland (50-70%) / forest or shrubland (20-50%)	17.5%
	Mosaic vegetation (grassland/shrubland/forest) (50-70%) / cropland (20-50%)	20%
	Mosaic cropland (50-70%) / vegetation (grassland/shrubland/forest) (20-50%)	11.7%
	Closed to open shrubland, closed to open herbaceous vegetation, sparse vegetation, closed broadleaved forest or shrubland permanently flooded, closed to open grassland or woody vegetation on regularly flooded or waterlogged soil, artificial surfaces and associated areas, bare areas, permanent snow and ice, post-flooding or irrigated croplands, rainfed croplands, water bodies	0%

Note: nonforest proportion = 100% - forest canopy proportion. Land cover classes in each legend are grouped in the table according to forest canopy proportion in each respective class.

2.3.1.2 Spatial aggregation

With the legend translation rules described above, each land cover product was converted to a percent forest cover map at its native resolution. Each percent forest cover map was then overlaid on the 5-km grid to calculate percent cover within each 5-km grid cell. For example, for the 1-km categorical GLCC, the aggregation was carried out by employing a 5×5 pixel window moving across the map. Within the local window, each classified pixel was first multiplied by its class-specific proportional weight defined by the legend translation rule, and then averaged to derive the proportional forest and non-forest cover within the 5-km grid. Other categorical maps were aggregated in the same way as GLCC. As MODIS VCF directly measures the percentage of forest canopy, we simply aggregated it from 500-m to 5-km with a 10×10 moving window by averaging the 100 pixel values within the window.

2.3.1.3 Deriving agreement metrics

At the pixel level, it is reasonable to believe that a given land pixel is more likely to be forest if all six products independently classify the pixel as forest than if only one product identifies it as forest and the other five products label it as non-forest. Thus, different levels of agreement reflect varying degrees of certainty regarding the true forest cover in one pixel. In order to directly incorporate this agreement information into data integration, we calculated the pixel-based agreement metrics for the forest class. This analysis is based on categorical maps in parallel with the above legend translation and spatial aggregation process. As four of the six input products (i.e.

GLCC, GLC2000, MODIS LC and UMD LC) have an original resolution of 1-km, we first align all the six products at 1-km resolution to calculate a 1-km forest “vote” map and then derive the 5-km agreement metrics based upon the 1-km vote map. The 300-m GlobCover was resampled to 1-km resolution and the 500-m fractional MODIS VCF was spatially averaged to 1-km first and converted to binary forest and non-forest by applying a 30% threshold according to the IGBP definition.

To assess the degree of correspondence between the six products at 1-km, we evaluated each pixel as the number of times it was labeled as forest by the six maps, resulting in a value between 0 and 6: the higher the value, the higher the agreement between the products for the forest class. The 5-km agreement metrics were derived by grouping the 1-km metrics using a 5×5 pixel moving window. Within the local window, the 1-km agreement pixels with values between 0 and 6 were noted and each 5-km grid was characterized by the frequencies of each of those values.

2.3.2 Supervised training and prediction

A supervised regression tree algorithm was used to model the relationship between reference cover from NLCD2001 and forest cover as well as agreement metrics from the coarse datasets. Tree-based classification and regression methods are well established in land cover characterization studies (e.g. Friedl et al. 2002; Hansen et al. 2003; Hansen et al. 2000; Homer et al. 2004; Sexton et al. 2013a; Sexton et al. 2013b; Xian and Crane 2005). Regression trees have the theoretical advantage of handling non-linear relationships by recursively splitting the sample into binary partitions until criteria of accuracy or purity are met (Breiman et al. 1984). This algorithm produces a hierarchical set of decision rules, each of which terminates in a linear regression

model. Predictor variables consist of the proportional forest and non-forest cover layers derived through legend translation and spatial aggregation. The seven agreement metrics layers are used in the conditional statements of the regression rules to parameterize the tree model. Reference data were derived by aggregating NLCD2001 from 30-m to 5-km resolution to calculate the percentage of forest pixels per 5-km grid. A total of 40713 pixels (~12% of land pixels) were systematically selected from the aggregated NLCD2001, from which half were randomly selected for model training and half for validation.

2.3.3 Product evaluation

Accuracies of the six input datasets and the output integrated percent forest cover (IPFC) dataset were evaluated against the aggregated NLCD2001 using mean bias error (MBE), root mean square error (RMSE) and r^2 :

$$MBE = \frac{\sum_{i=1}^n (P_i - R_i)}{n} \quad (2.1)$$

$$RMSE = \sqrt{\frac{\sum_{i=1}^n (P_i - R_i)^2}{n}} \quad (2.2)$$

$$r^2 = 1 - \frac{\sum_{i=1}^n (P_i - R_i)^2}{\sum_{i=1}^n (R_i - \bar{R})^2} \quad (2.3)$$

where i is the pixel index; P_i is the value of IPFC or forest cover of each input product; R_i is the reference forest cover per sample; \bar{R} is the mean of reference, and n is the sample size (Willmott 1982). The test sample was further divided according to reference values into three subsets representing low, moderate, and high forest cover

(i.e. 0-30%, 31-60%, 61-100%), respectively. Accuracy metrics were calculated using the entire test sample as well as these three subsets to report the disaggregated error by categories of percent forest cover.

2.4 Results

2.4.1 Model fitting and assessment

Evaluation of the regression tree model using 20,357 training cases yielded an average error of 6.46% with a correlation coefficient between reference and predicted cover of 0.94. Internal 10-fold cross-validation on training data estimated a slightly higher average error of 6.78% and an identical correlation coefficient. Independent evaluation of the model using a withheld sample of 20,356 test cases estimated a further slightly higher average error of 6.91% and a same correlation coefficient of 0.94 as using the training data, suggesting negligible model over-fitting with the training sample.

The most important predictor variable was forest cover derived from MODIS VCF, which was used in 65% of the conditional statements and in 69% of the terminal-node regression models (Table 2.3). All the six products were highly used in the leaf-node multivariate regression models, with forest cover from GLCC as the most frequently used variable and forest cover from MODIS LC as the least frequently used one. Relative to forest/nonforest cover variables, agreement metrics had moderate to low usage rates in the conditional statements. Agreement metric at level 0 was used in 32% of the conditional statements, while other agreement metrics had usage rates less than 10%. The low usage of other agreement metrics in the

conditional statements is probably due to high usages of forest cover variables from MODIS VCF, MODIS LC, UMD LC, GlobCover as well as agreement metric at level 0, which, collectively, provide adequate information for splitting the regression tree.

Table 2.3 Usage of predictor variables in the regression tree model

Predictor variable	Conditional use rate	Terminal-node regression use rate
MODIS VCF forest cover	0.65	0.69
MODIS LC forest cover	0.48	0.22
UMD LC forest cover	0.36	0.56
GLC2000 forest cover	0.36	0.83
Agreement level 0	0.32	0.00
GlobCover forest cover	0.24	0.49
MODIS LC nonforest cover	0.13	0.42
GLCC forest cover	0.10	0.90
GlobCover nonforest cover	0.07	0.30
Agreement level 6	0.05	0.00
Agreement level 1	0.05	0.00
UMD nonforest cover	0.04	0.26
Agreement level 5	0.03	0.00
Agreement level 2	0.03	0.00
Agreement level 4	0.03	0.00
Agreement level 3	0.02	0.00
GLCC nonforest cover	0.01	0.85
GLC2000 nonforest cover	0.00	0.49

2.4.2 The integrated forest cover map over North America

The integrated product depicts well-known patterns of forest cover over North America, including contiguous forests in the eastern and Pacific north-western United States and boreal Canada (Figure 2.2). The IPFC also shows the climatological fragmentation of forests in the southern Rocky Mountains as well as the longitudinal gradients in ecotones between boreal forests and tundra. Tropical and subtropical dry forests in Southern Mexico are represented by moderate to high forest cover.

Agricultural fields in the Great Plains are depicted with very low forest cover.

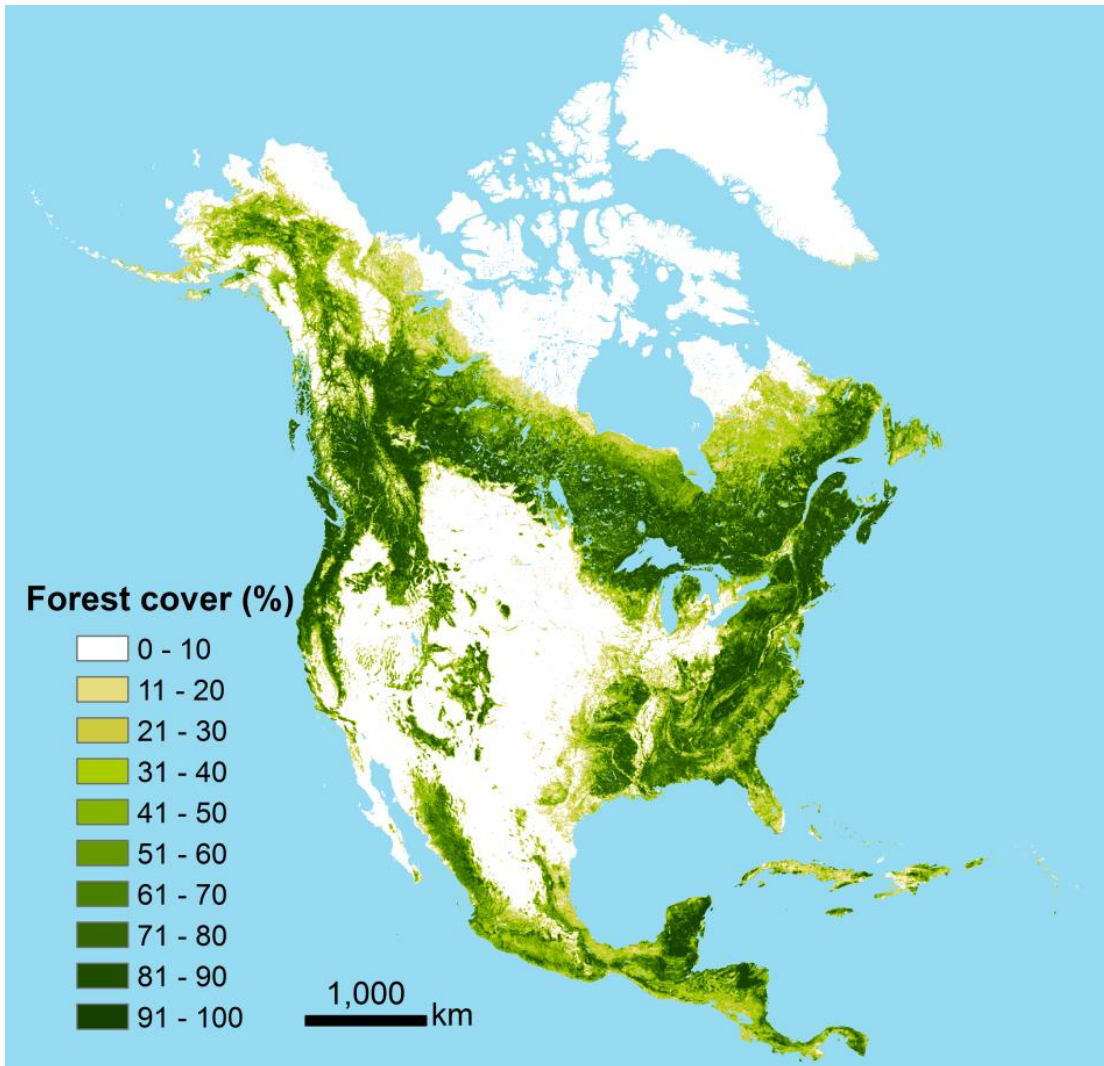


Figure 2.2 The integrated percent forest cover map over North America.

A comparison of the six input datasets and IPFC over the Chesapeake Bay region in Eastern United States highlights differences in fragmented areas (Figure 2.3). This region is covered by a complex landscape including forested national parks, high density urban lands of the Washington DC-Baltimore metropolitan, suburban low-density residential lands, as well as agriculture fields in Maryland, Delaware, and

Virginia. The fragmented and heterogeneous landscape raises great difficulties in land cover classifications with coarse resolution satellite data and can lead to substantial disagreement between the existing products (Figure 2.3 (a)). Each of the six products shows a varying degree of over- or under-estimation of forest cover as compared with NLCD2001, while the integrated product shows the closest visual similarity with the reference.

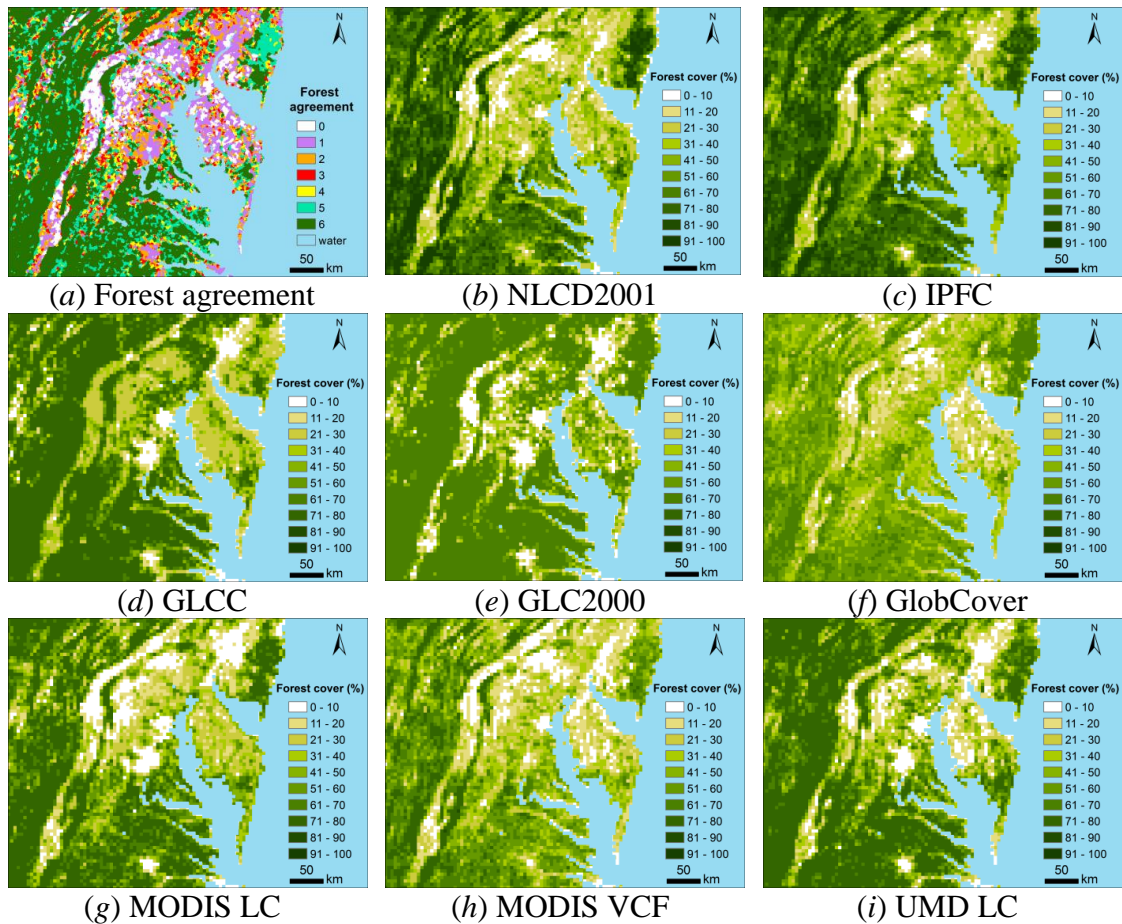


Figure 2.3 Subsets of forest cover maps in the Chesapeake Bay region in eastern U.S. (a) Forest agreement of the six input products at 1-km spatial resolution. (b) NLCD2001 reference at 5-km spatial resolution. (c) The integrated product at 5-km spatial resolution. (d–i) Forest cover derived from the six existing products at 5-km resolution.

2.4.3 Evaluation of the integrated product versus input datasets

Figure 2.4 shows the density scatter plots of 5-km forest cover derived from the six input datasets as well as the newly integrated product against reference forest cover derived from NLCD2001. General patterns of agreement and disagreement between coarse-resolution products and reference were revealed across the conterminous United States. The highest values of fractional forest cover derived from categorical maps (i.e. GLCC, GLC2000, GlobCover, MODIS LC and UMD LC) all saturated at around 80% due to semantic uncertainty in discrete classifications. Since the actual forest cover within a coarse pixel grid was unknown, a mean 80% cover value was assigned to the closed forest class. MODIS VCF also saturated at 80% – a consistent conclusion with previous VCF validation studies (Montesano et al. (2009); Sexton et al. (2013a); White et al. (2005)). However, the density scatter plots of MODIS VCF against reference presented a narrower diagonal line than other products, suggesting a less overall bias. As such, MODIS VCF was the most frequently used variables in constructing the regression tree model. Combining of the six products and calibrated by NLCD2001, the newly integrated product has substantially improved forest cover estimate as revealed by the scatter plots – a highest value of 100% forest cover and a concentrated and nearly symmetric 1:1 line.

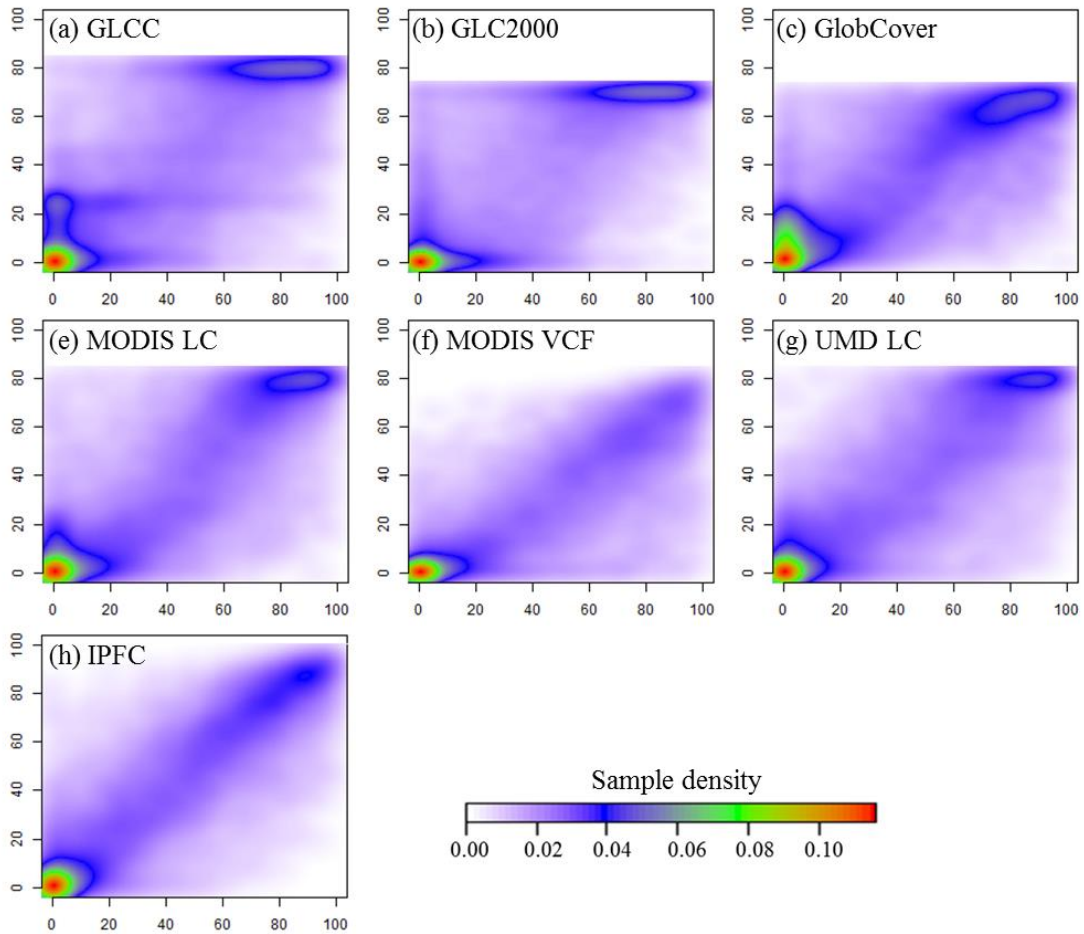


Figure 2.4 Scatter plots of 5-km percent forest cover derived from global land cover products against reference percent forest cover. The x axis in each scatter plot represents reference forest cover derived from NLCD2001 and the y axis represents each individual global product as well as the integrated product. The data are based on 20,356 systematically selected samples from conterminous United States.

Statistically, the IPFC estimates showed greater consistency with the reference data than all of the input datasets, which varied in their accuracy relative to NLCD2001 (Table 2.4). All six input datasets showed fairly high r^2 globally (between 0.7 and 0.8) against the reference data, but IPFC achieved a considerably higher r^2 of 0.87. MODIS VCF consistently underestimates forest cover in every stratum, whereas GLCC, GLC2000, GlobCover, MODIS LC and UMD LC consistently overestimate forest cover in the lowest stratum but underestimate in moderate and high strata. IPFC has a slightly greater bias than MODIS LC and UMD LC in the lowest stratum but has the lowest bias among all the products in moderate and high strata. The RMSE was twice as great in the moderate (31-60%) and high (61-100%) ranges than in the low (0-30%) stratum for every product, implying great uncertainties in characterizing medium- to high-density forests using coarse-resolution satellite data. At the low end of forest cover, the integrated dataset was slightly less accurate than MODIS VCF, but at moderate to high cover range, IPFC was considerably more accurate than any of the six input datasets. The overall RMSE of the integrated product against reference was 11.75%, significantly lower than a 17.37% of GLCC, 17.61% of GLC2000, 17.96% of GlobCover, 15.23% of MODIS LC, 19.25% of MODIS VCF, and 15.15% of UMD LC, respectively.

Table 2.4 Evaluation of the integrated percent forest cover map and the six input global land cover maps.

Product	MBE (%)				RMSE (%)				r ²
	0-30	31-60	61-100	0-100	0-30	31-60	61-100	0-100	0-100
GLCC	3.56	-2.92	-9.64	-0.59	13.45	24.28	20.34	17.37	0.72
GLC2000	1.74	-5.98	-14.75	-3.38	14.41	23.57	20.10	17.61	0.72
GlobCover	3.95	-8.51	-23.13	-4.42	11.81	18.98	27.70	17.96	0.72
MODIS LC	0.32	-8.92	-12.59	-4.20	10.28	21.00	20.32	15.23	0.79
MODIS VCF	-1.76	-16.88	-27.88	-10.33	7.55	22.82	32.77	19.25	0.77
UMD LC	0.55	-6.73	-13.92	-4.02	8.97	20.22	22.12	15.15	0.79
IPFC	1.26	-0.73	-5.53	-0.66	8.78	16.10	14.53	11.75	0.87

Note: Test sample is stratified into three subsets representing low moderate and high forest cover (i.e. 0-30%, 31-60%, 61-100%), respectively. While r² is calculated using the entire test sample (0-100%), MBE and RMSE are calculated using these subsets as well as the entire sample.

2.5 Discussion

2.5.1 Global patterns of land cover agreement

Figure 2.5 shows the spatial patterns of agreement and disagreement for forest and cropland classes between the six global maps used in the integration analysis. For the forest class, strong agreement is found in tropical humid, temperate and boreal forest biomes in all continents, but transitional zones between forest and other biomes are poorly characterized, most evident in Alaska, northern Canada and eastern Siberia. Arid, semi-arid and sparsely vegetated biomes generally have poor agreement on forest cover such as southern Mexico, the Brazilian Cerrado, the Gran Chaco, the Sahel belt and savannas in southern Africa. For the cropland class, the hotspots of global agricultural lands are well depicted, but substantial disagreement is found,

particularly in Africa.

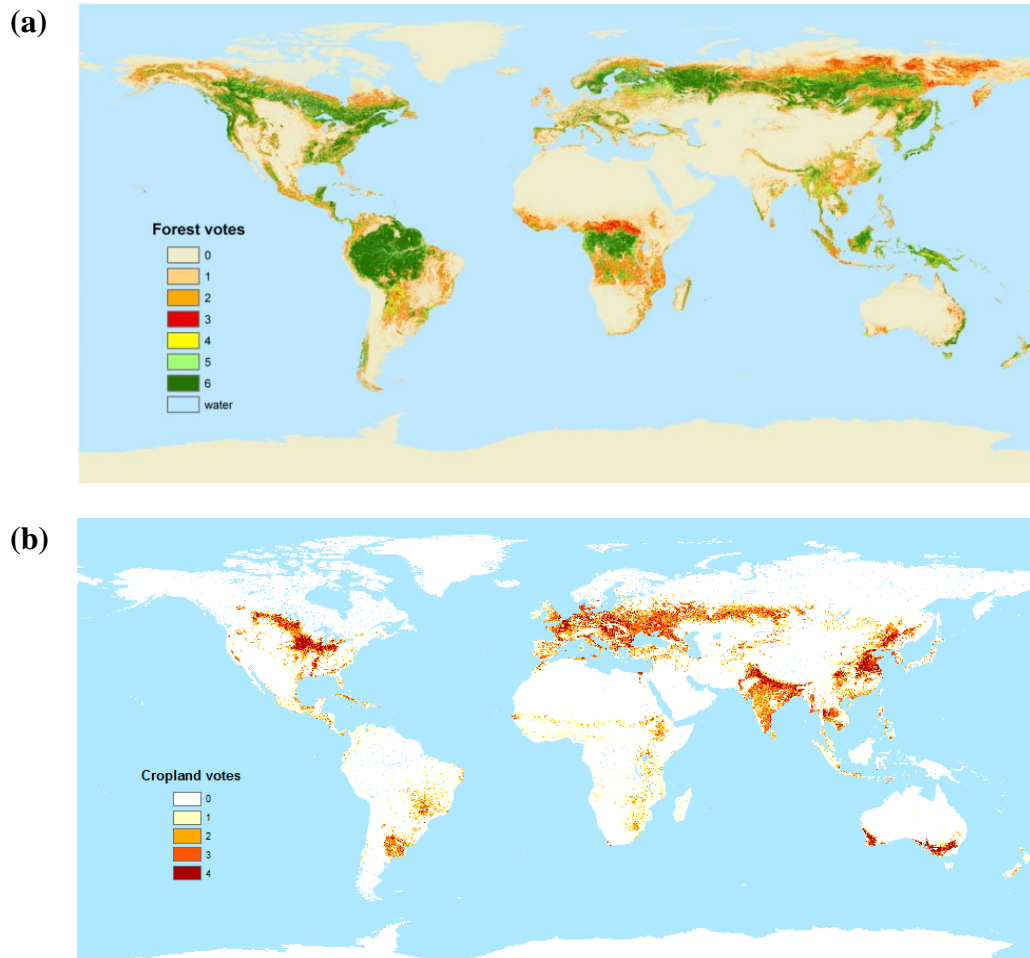


Figure 2.5 Agreement and disagreement between global land cover maps for (a) forest and (b) cropland. Each value in the legend indicates the number of products that agree on forest or cropland classification. Six products GLCC, UMD LC, GLC2000, MODIS LC, MODIS VCF and GlobCover are overlaid to calculate per pixel agreement for the forest class. Four products GLCC, UMD LC, GLC2000 and MODIS LC are used to derive agreement for the cropland class.

Differences in these global datasets can stem from multiple sources including different land cover definitions, satellite sensor systems, acquisition dates, classification algorithms, as well as image misregistration, etc (DeFries and Townshend 1994a; Fritz and See 2008; Giri et al. 2005; Hansen and Reed 2000; Herold et al. 2008; Jung et al. 2006; Pflugmacher et al. 2011; Song et al. 2014a; Townshend et al. 1992). The discussion here is not to investigate reasons of their disagreement as has been done, but to focus on the implications of such agreement and disagreement for generating or refining future land cover mapping. We find a positive relationship between the level of agreement and forest cover density (Figure 2.6). For example, at 1-km resolution, for pixels where forest cover > 60% according to NLCD reference, most of the pixels are characterized as forest by at least 4 of the 6 global maps. This finding may shed light on future global land cover mapping. Specifically, one of the key requirements in producing a global map is to collect sufficient and representative training sample (Townshend et al. 2012). The agreement map may provide useful information to guide training selection. Pixels that have high agreement may be directly used as training data. A similar idea has been successfully implemented by (Sexton et al. 2013a), in which reliable MODIS VCF pixels are employed as training to derive VCF products at the Landsat resolution. More analysis is needed to demonstrate the applicability of this idea for other classes (e.g. cropland).

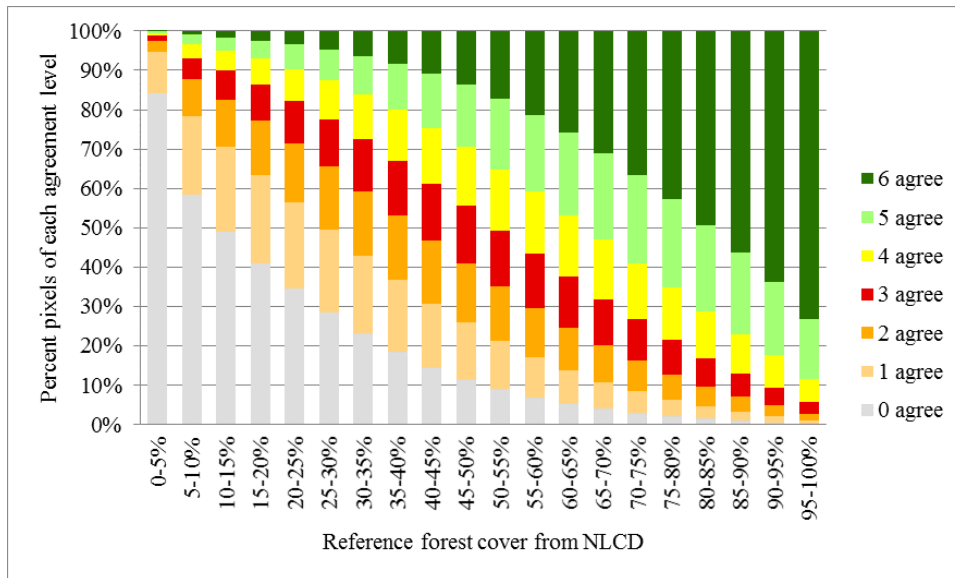


Figure 2.6 An equalized histogram of 1-km cross-product agreement metrics against reference forest cover. Strong agreements between six independent land cover products occur at the high forest cover strata, while weak agreements are concentrated around moderate forest cover strata.

2.5.2 Global application of the data integration methodology

The developed data integration methodology was applied to the global scale except Oceania and Antarctica. Regional land cover maps at sub-100 meter resolution were collected or derived as reference for map integration. Specifically, we added the Earth Observation for Sustainable Development of Forests (EOSD) forest cover map (Wulder et al. 2008) to augment the NLCD training for North America. PRODES deforestation maps over the Brazilian Amazon (<http://www.obt.inpe.br/prodes/index.php>) and the Paraguay forest cover change (FCC) dataset (Huang et al. 2009c) were used in South America. To achieve a comprehensive geographical distribution of the training data, we also classified 10 Landsat images to forest/nonforest maps in South America. They are located in a

variety of ecosystems including the Brazilian Cerrado, agricultural areas in Uruguay, and temperate mountain forests in southern Chile as well as desert in northern Chile. Similarly, the vector-based Africover database, the 60-m resolution FCC product over Democratic Republic of the Congo (Potapov et al. 2012), the South African National Land Cover product (Fairbanks et al. 2000) were used in Africa; the CORINE Land Cover database over Europe, the 60-m FCC product over European Russia (Potapov et al. 2011), China’s National Land Cover (Liu et al. 2002), and the FCC datasets generated by the Northern Eurasia Earth Science Partnership Initiative were employed in Eurasia (Pflugmacher et al. 2011). The geographical distribution of the training datasets is shown in Figure 2.7 and the derived forest cover maps are shown in Figure 2.8 (South America), Figure 2.9 (Africa) and Figure 2.10 (Eurasia), respectively.

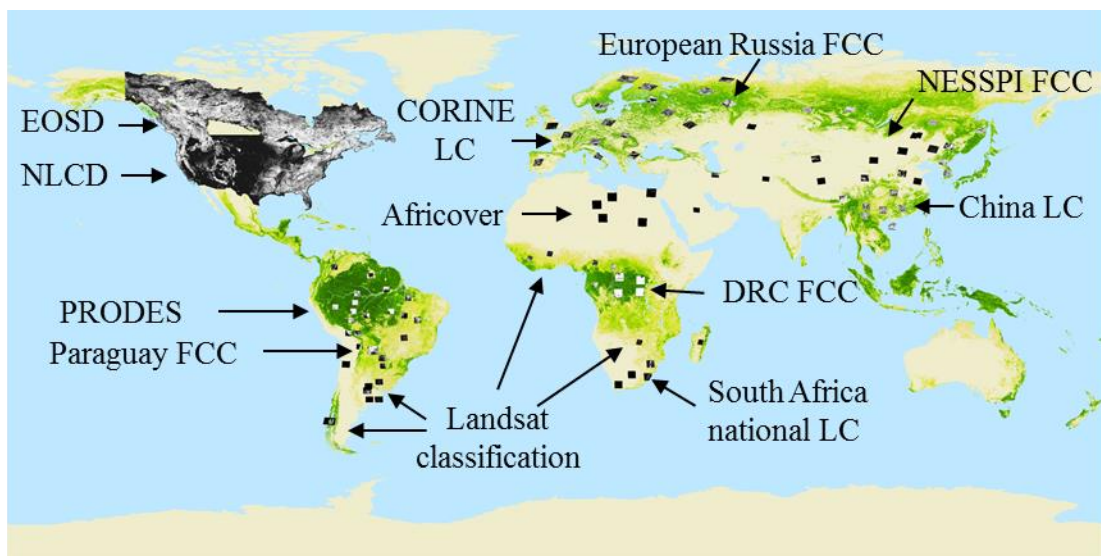


Figure 2.7 Regional reference land cover datasets collected or generated for the integration of global land cover products.

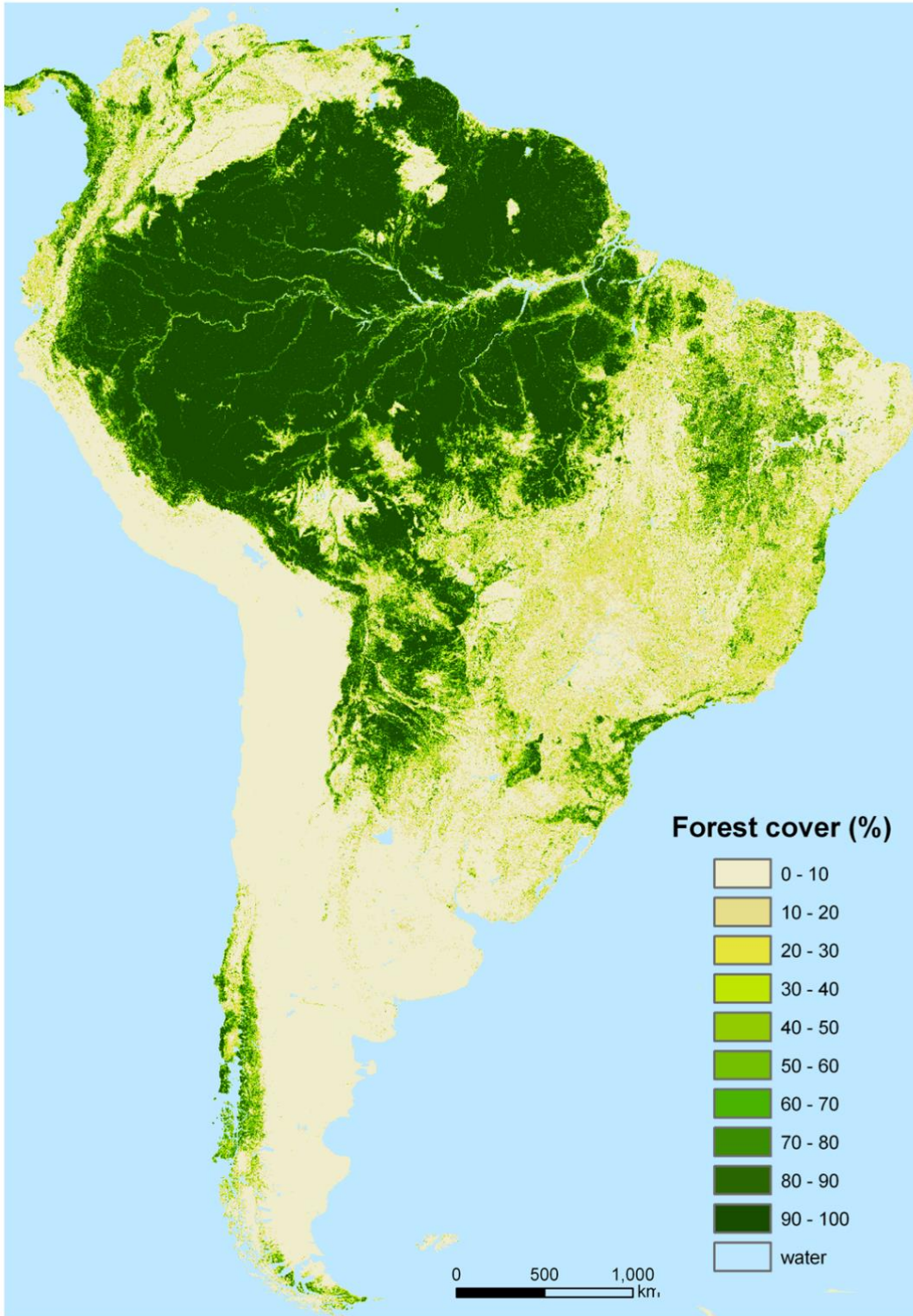


Figure 2.8 The integrated percent forest cover map over South America.

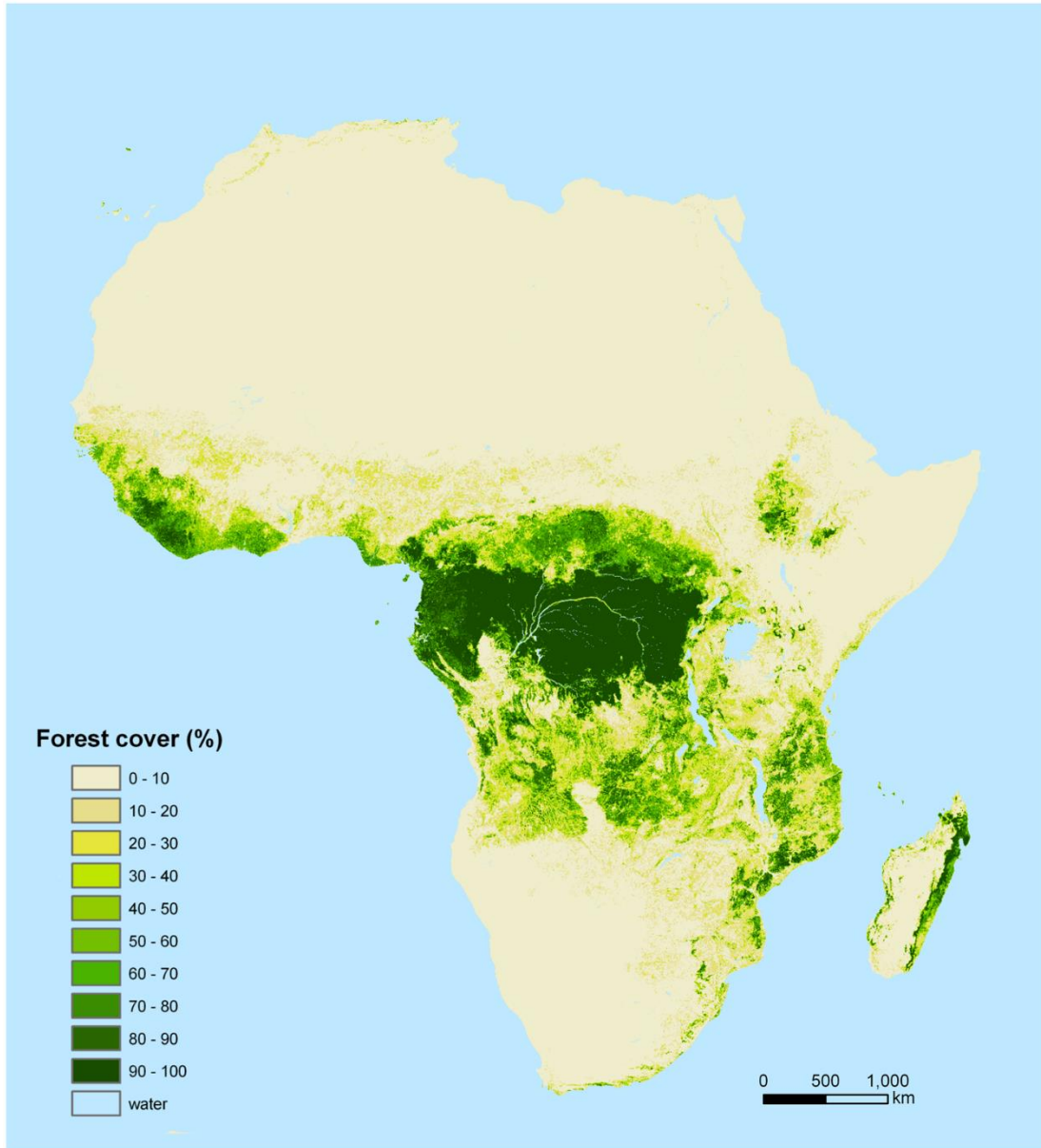


Figure 2.9 The integrated percent forest cover map over Africa.

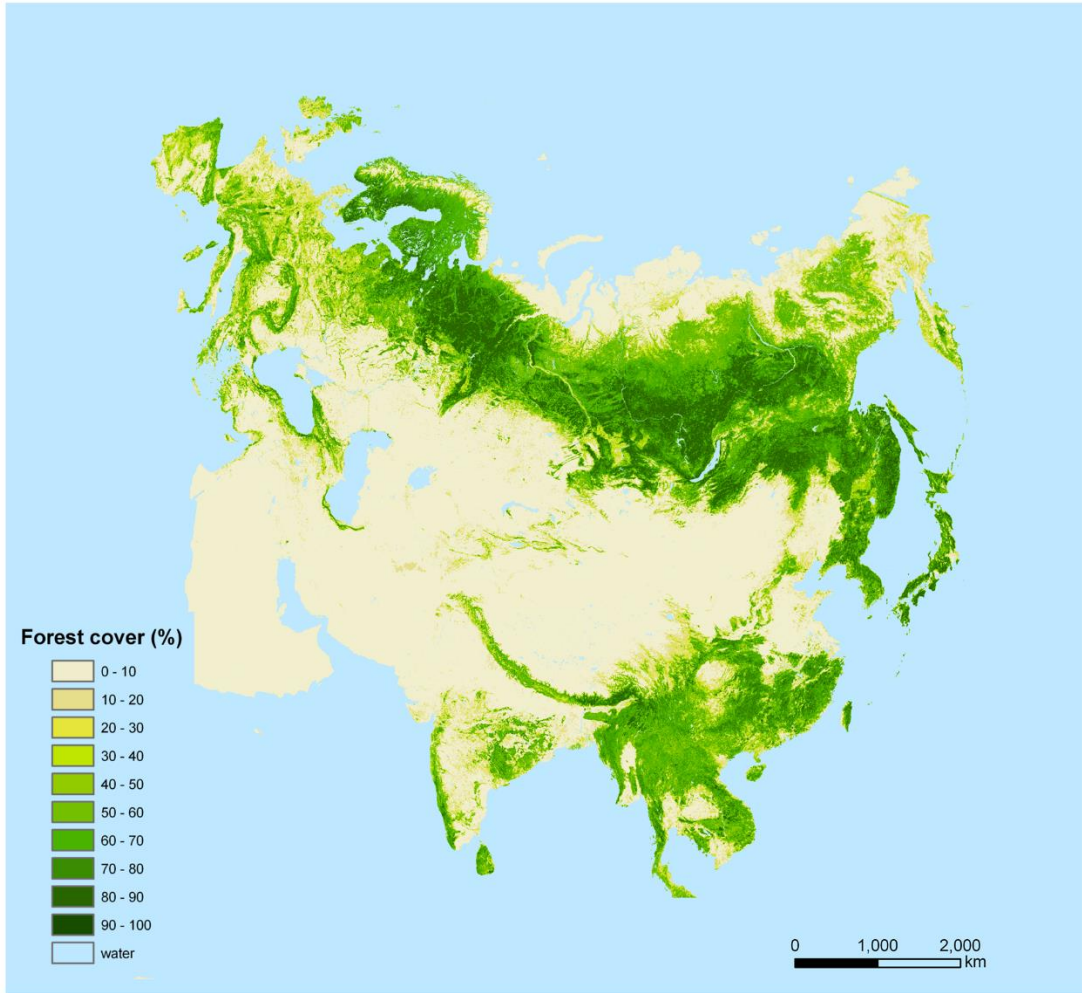


Figure 2.10 The integrated percent forest cover map over Eurasia.

2.6 Conclusions

Global land cover products show substantial discrepancies in their representation of land surface type, including forests. This chapter presents a data fusion method to integrate multi-source, multi-resolution (300-m to 1-km) global land cover maps to derive a new hybrid forest cover product. Different from previous data fusion methodology by Jung et al. (2006) and Fritz et al. (2011), which mainly relies on the agreement between different land cover products, this approach also uses a large sample of Landsat-based land cover dataset as reference to generate the integrated product with a supervised learning algorithm. Compatible with previous work, however, land cover characterization is greatly improved by combining various sources of existing datasets. Assessment of errors relative to a withheld test sample suggests that the integrated forest map has an overestimation in low forest cover stratum (i.e. 0-30%) and a slight underestimation in moderate (i.e. 31-60%) to high forest cover strata (i.e. 61-100%). Nevertheless, compared to the existing maps of forest cover, a considerable improvement is achieved through data integration with an overall RMSE of 11.75% against Landsat reference. The greatest improvements are achieved in moderate to high forest cover regions.

Research on synthesizing existing land cover datasets for improved cropland mapping is being actively conducted (Fritz et al. 2015; Fritz et al. 2010; See et al. 2014; Yu et al. 2013). Although demonstrated with forest cover here, the developed methodology may be applied to cropland and other classes.

Chapter 3: Annual Detection of Forest Cover Loss Using Time Series Satellite Measurements of Percent Tree Cover

3.1 Introduction

As reviewed in Chapter 2, given the multiple factors that can contribute to the observed disagreement between different land cover datasets, simply subtracting two land cover maps of different times do not yield reliable land cover change. To characterize land cover change, a number of basic consistency requirements are needed, particularly for post-classification change detection. (i) Land cover needs to be defined consistently across a study region and over time. (ii) Satellite data should be from the same sensor or sensors of similar characteristics in terms of spectral bandwidth, spatial resolution, view geometry and location accuracy, etc. (iii) Land cover maps should be generated using an identical procedure. An existing dataset that fulfils these requirements is the MODIS VCF product.

Land cover change detection methods have been evolving for over four decades and a variety of approaches have been developed (Coppin et al. 2004; Lu et al. 2004). Most successful applications of these methods in forest cover change monitoring are carried out at long temporal intervals (*e.g.*, 5 years, 10 years or longer) (Achard et al. 2007; Hansen et al. 2010; Hansen et al. 2008c; Huang et al. 2009c; Masek et al. 2008; Mayaux et al. 2013; Sexton et al. 2014). However, several studies have shown that forest change rates can vary substantially from one year to another at various spatial scales (Hansen et al. 2013; Huang et al. 2009b; Masek et al. 2013). Hence, change products derived at long temporal intervals cannot capture such

temporal dynamics, especially when forest cover change is caused by harvest and other land management practices (Jin and Sader 2005). In areas where forests can re-establish within a few years after having been cleared, coarse-interval change detection may also miss significant portions of forest loss that are followed by rapid regrowth (Masek et al. 2008).

To overcome these limitations, a growing number of studies have exploited dense time series of satellite observations for monitoring forest cover change. In particular, a number of novel techniques have recently emerged for reconstructing forest change history using dense time series of Landsat images (Huang et al. 2009a; Huang et al. 2010a; Kennedy et al. 2007; Kennedy et al. 2010). Consisting of “clear-view” Landsat observations every year or every two years (Huang et al. 2009b), such image stacks allow forest change mapping at annual or biennial time steps. Although Landsat provides one of the longest and most consistent satellite records of the land surface with a spatial resolution suitable for monitoring many types of anthropogenic land cover change (Townshend and Justice 1988), dense time series of Landsat observations do not exist in many areas outside the U.S. (Goward et al. 2006). So far, optimized global collections of Landsat images are available only for a few selected epochs centered at 1975, 1990, 2000, 2005 and 2010 (Gutman et al. 2013; Townshend et al. 2012; Tucker et al. 2004), although global wall-to-wall coverage has been constructed using all available Landsat 7 Enhanced Thematic Mapper Plus (ETM+) images between 2000 and 2012 (Hansen et al. 2013). In the tropics, where most carbon emissions from deforestation are located, cloud and shadow contamination is another limiting factor for large-area land cover change mapping

with Landsat (Asner 2001). Coarse-resolution sensors, such as MODIS, with a daily revisit frequency, have a greater probability of obtaining cloud-free observations annually (Asner 2001; Broich et al. 2011).

Methods for mapping forest disturbance using time series satellite data mainly rely on detecting structural changes in the spectral responses of a pixel over time (Kennedy et al. 2007; Kennedy et al. 2010; Zhu et al. 2012) or changes in spectral-based indices, such as the Normalized Difference Vegetation Index (NDVI) (Kleynhans et al. 2011; Lunetta et al. 2006; Verbesselt et al. 2010), Enhanced Vegetation Index (EVI) (Clark et al. 2010), disturbance index (Healey et al. 2005; Masek et al. 2008), MODIS global disturbance index (Mildrexler et al. 2009), the integrated forest z-score (Huang et al. 2010a), *etc.* Spectral index-based methods (*e.g.*, NDVI) typically seek a drop in inter-annual signals to infer forest loss or an increase for forest gain. Whereas NDVI is a robust indicator of vegetation cover, even a strong drop in NDVI may not be unambiguously related to forest loss, as other vegetation changes, such as crop rotation, may result in similar patterns of NDVI change. Moreover, time series of vegetation indices are often sensitive to fluctuations in primary productivity and/or climatic fluctuations at intra-annual scales, causing difficulties for land cover change detection (Lambin 1999). As an alternative, explicitly converting intra-annual satellite signals to annual continuous tree cover and then tracking year-to-year changes in tree cover provides another useful way for disturbance mapping (Hansen and DeFries 2004; Lambin 1999).

The objective of this chapter is to develop and test a novel procedure to quantify annual forest cover loss using time series MODIS Vegetation Continuous

Fields (VCF) tree cover dataset. The MODIS VCF product (MOD44B), currently in Collection 5, has a spatial resolution of 250-m and a temporal resolution of one year from 2000 to 2010 (DiMiceli et al. 2011). More details of this dataset are described in Section 3.2 of the chapter. In Section 3.3, an algorithm, called VCF-based Change Analysis (VCA), is presented with an overview followed by detailed descriptions. The algorithm is then tested in two distinctive biomes of various patterns of forest cover loss—the southern Amazon and the Western U.S.—and evaluated using reference data derived from Landsat. The qualitative and quantitative evaluation results are presented in Section 3.4. We then discuss the study using global examples of the algorithm implementation in Section 3.5 and draw general conclusions in Section 3.6.

3.2 Yearly MODIS VCF data

The MODIS VCF tree cover data have been used in a wide range of Earth system studies such as simulating climate (Lawrence and Chase 2007), quantifying gross forest cover loss (Hansen et al. 2010), mapping forest canopy height (Simard et al. 2011), mapping forest biomass (Saatchi et al. 2011), analyzing the conservation status of tropical dry forests (Miles et al. 2006), estimating carbon emissions from deforestation (Harris et al. 2012b), and as a source of training for a Landsat-based global tree cover dataset (Sexton et al. 2013a). The current version is generated at a spatial resolution of 250-m annually from 2000 to 2010 (DiMiceli et al. 2011). To make the product, bagged regression tree models are trained on a large Landsat-based reference sample and annual phenological metrics composited from the MODIS 16-

day surface reflectance including Bands 1-7 and brightness temperature from Bands 20, 31 and 32 (Hansen et al. 2003). The models are then applied to annual phenological metrics to predict percent tree cover in each MODIS pixel in each year. Here tree cover refers to percent canopy cover, which measures the proportion of skylight obstructed by tree canopies equal to or greater than 5 m in height (Hansen et al. 2003). Poor-quality pixels due to either cloud, cloud shadow, high aerosol or $>45^\circ$ view zenith angle are reduced through the composition process, and the remnants are flagged in the quality assurance (QA) layer as a per pixel quality indicator. It is important to note that the yearly VCF product is generated based on atmospherically-corrected surface reflectance (a uniform physical value that enhances spatial consistency for the global characterization of tree cover, as well as temporal consistency for change analysis).

An early version of VCF was validated using high-resolution IKONOS images and field data in Zambia (Hansen et al. 2002). The Collection 1 global VCF product was validated against independent field data across the arid Southwestern United States (White et al. 2005), and later, the Collection 4 product was evaluated using reference data derived from high-resolution images across the boreal-taiga ecotone (Montesano et al. 2009). Recently, the error of the Collection 5 VCF was estimated against measurements of tree cover from small-footprint Light Detection and Ranging (Lidar) data in four sites across three different forest biomes (Sexton et al. 2013a). Additionally, many studies have cross-compared the MODIS VCF to other remotely-sensed global land cover datasets (Heiskanen 2008; Schepaschenko et al. 2011; Song et al. 2014a; Song et al. 2011). These independent assessments found that

saturation of the optical signal, phenological noise and confusion with dense herbaceous vegetation led to errors in the earlier MODIS VCF, varying between 10-31% in terms of root-mean-square error (RMSE) and 7-21% in the latest version (Montesano et al. 2009; Sexton et al. 2013a; White et al. 2005). The latest Collection 5 MODIS VCF product is used in this study.

3.3 The VCA algorithm

3.3.1 Algorithm overview

Our algorithm explicitly tracks changes in tree cover over time, as opposed to existing time series approaches of forest cover change detection (e.g., VCT (Huang et al. 2010a), LandTrendr (Kennedy et al. 2010)), which rely on spectral indexes to infer forest cover change. This new method, which also improves upon existing empirical approaches, is developed based on the theoretical basis that land cover disturbances are rare phenomena for a relatively large area within a short time period. For example, ~1.1% of forests in the U.S. were disturbed annually between 1985 and 2005 (Masek et al. 2013), and globally, ~0.2% of the land surface experienced stand-clearing forest disturbances (gross forest cover loss) annually between 2000 and 2012 (Hansen et al. 2013). Repeated measures of land cover over the entire area therefore contain a majority of numerically-stable data points and a small set of outliers. Assuming that errors in the repeated measurements follow a normal distribution, well-established parametric statistical theories (Lancaster and Seneta 2005) provide proof that land cover changes are outliers of an underlying chi-square distribution. The first step of the algorithm is to separate these outliers from the majority of

unchanged pixels (Figure 3.1). Then, for each identified change pixel, the algorithm tracks continuous changes in tree cover over time by fitting one or more nonlinear curves. Specifically, we intend to capture the sigmoid or “S” shape of forest cover change using logistic models, a close compliance with the actual physical process of land cover change on the ground. Quantitative metrics, such as the magnitude, rate and time of forest cover change in each pixel, are then derived from the parameters of the fitted logistic equations.

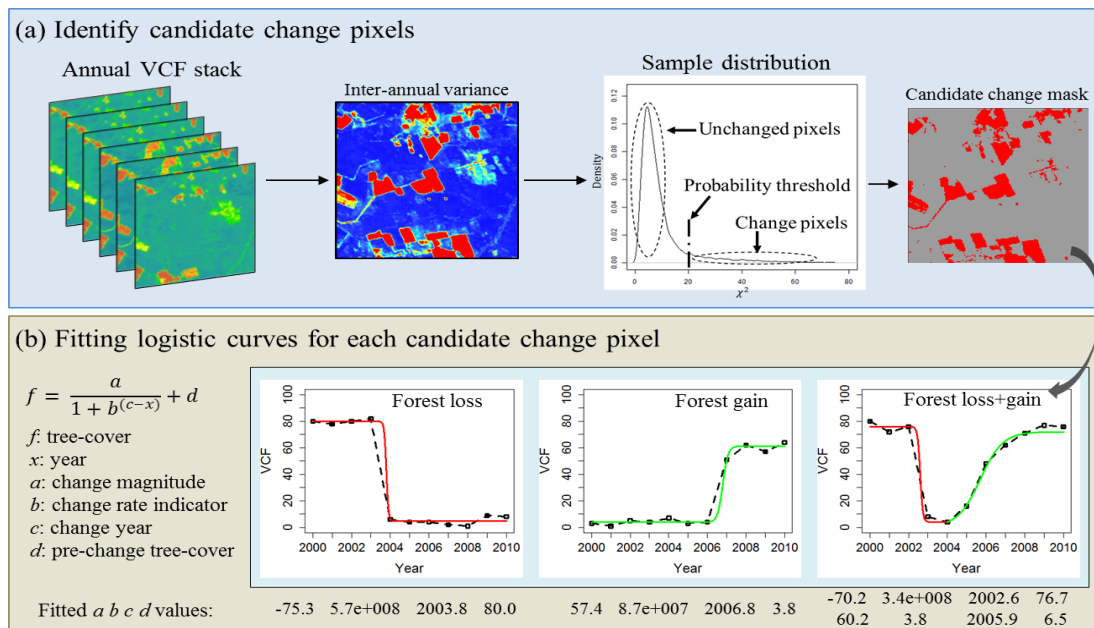


Figure 3.1 Overview of the VCF-based Change Analysis (VCA) algorithm.

3.3.2 Identifying candidate change pixels

3.3.2.1 Theoretical basis

Assuming errors in the repeated estimates of tree cover are independent and identically follow a normal distribution (I.I.D.), the idea to separate changes from unchanged pixels lies in that repeated estimates over stable locations over time follow

a normal distribution, while estimates over disturbed locations are outliers of the distribution. Mathematically, let $x_{(i,t)}$ denote the estimated percent tree cover in pixel i at time t , $\mu_{(i,t)}$ denote the true tree cover, and $\varepsilon_{(i,t)}$ be the associated error, then:

$$x_{(i,t)} = \mu_{(i,t)} + \varepsilon_{(i,t)}. \quad (3.1)$$

For any i and t , $\varepsilon_{(i,t)}$ is assumed to be independent and identically distributed. Following this assumption, the pixel value $x_{(i,t)}$ is considered as a random variable drawn from a normal distribution. For any i , the sample variance S_i^2 of the pixel vector over N years ($x_{(i,1)}, x_{(i,2)}, \dots, x_{(i,N)}$) follows a scaled chi-square distribution, with a mean of σ^2 and a variance of $2\sigma^2$:

$$S_i^2 \sim \frac{\sigma^2}{N-1} \chi_{N-1}^2, \quad (3.2)$$

where σ^2 is the population variance, $(N-1)$ is the number of degrees of freedom and the chi-square statistic (χ^2) is the sum of the squares of $(N-1)$ standard normal estimates (Lancaster and Seneta 2005); N equals 11 in this case.

Given a sample dataset consisting of a majority of stable observations (i.e. μ_i constant over time) and a small proportion of outliers (i.e. μ_i changes), the I.I.D. normality of the dataset is violated by the inclusion of change outliers. Because change pixels typically have greater variances than those of stable pixels, stable pixels are concentrated around the peak, while change pixels are located in the tail of the distribution; the greater the variance, the more likely the pixel is an outlier (Figure 3.2(a)). Because the distribution of S_i^2 has a mean value of σ^2 and a variance of $2\sigma^2$

for unchanged pixels, the unknown population variance (*i.e.*, σ^2) of random errors can then be estimated by the mean value of S_i^2 after removing change outliers.

For a dataset with a total of M pixels, let:

$$Y_i = S_i^2. \quad (3.3)$$

The scaling equations to convert Y to a standard chi-square distribution are given by:

$$\begin{cases} Y_i' = Y_i \frac{(N-1)}{\bar{Y}} \\ \bar{Y} = \frac{\sum_{i=1}^M Y_i}{M} \end{cases} \quad (3.4)$$

Compared to a standard chi-square distribution, the density curve of Y_i' is supposed to have a fatter tail and a systematic shift towards the left when the sample includes outliers (Figure 3.2(b)). The objective of detecting outliers is now to search for a threshold such that by removing likely outliers on the tail, the residual dataset has a maximum proximity to a chi-square distribution (Figure 3.2(c)).

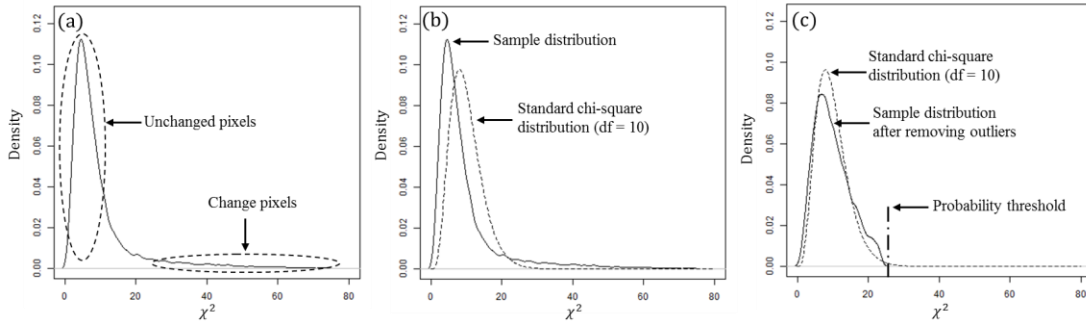


Figure 3.2 Detecting likely change pixels as outliers of a chi-square distribution. (a) The location of change and unchanged pixels in the density distribution of inter-annual variance of a data sample. (b) The density distribution of a data sample compared to a standard chi-square distribution with 10 degrees of freedom (df). (c) The density distribution of the sample after removing outliers.

3.3.2.2 Deriving parameters of the chi-square distribution

An iterative procedure was used to progressively remove the rightmost tail pixels to achieve an optimal match between the density distribution of the residual data sample and a standard chi-square distribution (Figure 3.3). The idea of adaptively trimming the distribution tail to approximate a theoretical chi-square distribution for outlier recognition has been applied in exploratory data analysis in many other disciplines, e.g., geochemistry (Filzmoser et al. 2005; Garrett 1989). Here, we employ the maximum likelihood estimation (MLE) framework to find the optimal threshold. The objective function in the MLE is to maximize the Quantile-Quantile (Q-Q) correlation coefficient (the most commonly used and effective tool for a distribution test (Garson 2012)) between the residual sample and a theoretical chi-square distribution. Iteratively, the Q-Q correlation coefficient is calculated between a standard chi-square distribution and the residual sample after removing the highest variance pixel. The iteration breaks when the residual sample reaches a maximum Q-Q correlation. The mean value of this residual dataset is then an unbiased estimate of the population variance ($\hat{\sigma}^2$) of random errors (unchanged pixels).

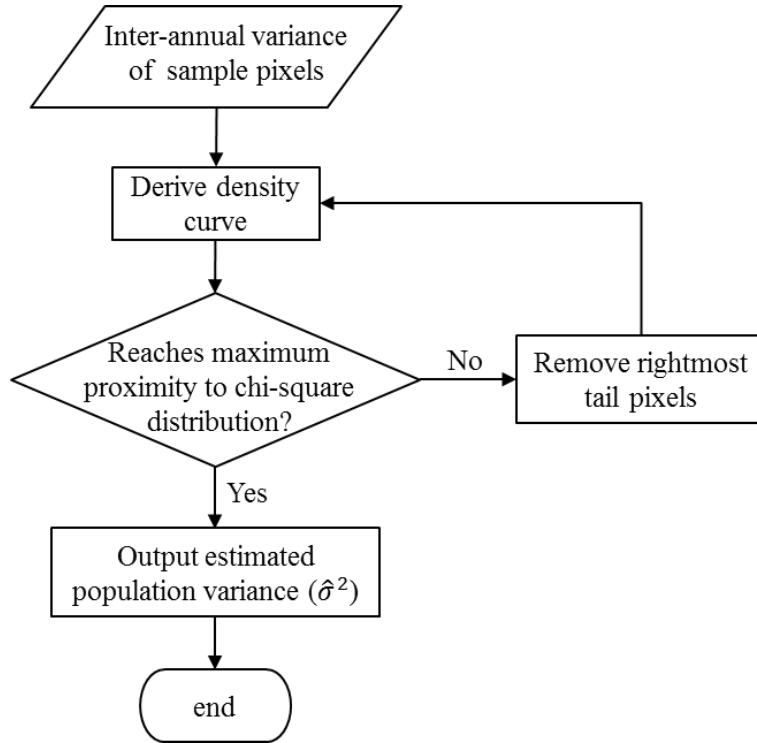


Figure 3.3 Flowchart of detecting outliers through approximating a chi-square distribution.

3.3.2.3 Create a change mask based on probabilistic threshold

The chi-square values corresponding to different probability levels of the simulated distribution are used as the threshold to separate likely change pixels from unchanged pixels. For example, the threshold corresponding to 0.9 probability is calculated as:

$$Threshold_{p=0.9} = \frac{\hat{\sigma}^2}{N-1} \chi^2_{(df=N-1, p=0.9)}. \quad (3.5)$$

We calculated the inter-annual mean and variance of the 11-year VCF vector for each pixel and found that the strong I.I.D. assumption of the error distribution is a plausible explanation for the empirical data, but not perfectly confirmed, in part due to regional differences in measurement errors. Specifically, pixels with VCF values at

the low end (0-20) and high end (60-100) tend to have relatively small variances, whereas pixels at the middle range (20-60) tend to have relatively large variances.

Therefore, we stratified the dataset into a number of strata based on the inter-annual mean tree cover, subsequently applying the outlier detection on each stratum.

It should also be noted that the purpose of this outlier detection is not to detect change with 100% accuracy, but to estimate the inter-annual variance of stable pixels ($\hat{\sigma}^2$) in order to derive the probabilistic threshold and mask out the majority of unchanged pixels. We set a conservative threshold (Figure 3.2(c)) corresponding to a probability of 0.9 to capture all of the true changes without introducing significant false positives. Temporal dynamics in each pixel of this inclusive set of candidate change pixels were then modeled using logistic equations, of which the goodness-of-fit test would further discriminate true change *versus* false detection.

3.3.3 Curve fitting to model change trajectory

3.3.3.1 Logistic model of loss or gain

Forest cover change is reflected by the increase or decrease of the continuous tree cover values over time, which can be either abrupt (e.g., clear-cutting) or gradual (e.g., forest regrowth), and show different patterns of temporal trajectory (Figure 3.4). Whereas a persistent forest or non-forest pixel has a much flatter curve over time with small anomalies, a change pixel exhibits large, structural fluctuations in time series tree cover. Further, multiple successive change events could occur within the 11-year span. These structural segments are basic elements used to characterize the complete temporal trajectory for a change pixel. Capturing change events is therefore to

decompose a pixel's temporal profile into meaningful segments with distinctive structures.

Each individual change event (forest loss or gain) typically involves three distinct stages: a pre-change stage when the VCF value is stable, a change stage when the VCF value increases or declines and a post-change stage when the VCF value stays stable until the next change event occurs. This three-stage dynamic process is modeled using a logistic function:

$$f = \frac{a}{1 + b^{(c-x)}} + d, \quad (3.6)$$

where f is tree cover in year x , parameter a defines the direction (with negative values representing loss and positive values representing gain) and the magnitude of change, b describes the change rate (where large values indicate abrupt change and small values represent gradual change), c denotes the inflection point in time when the change occurs, and d represents the pre-change value (Figure 3.5). The post-change VCF value is thus given by $(a + d)$. A logistic model of similar form was previously used to model vegetation phenology with daily MODIS data (Zhang et al. 2003). Here, we demonstrate that this simple model also performs well in detecting land cover change.

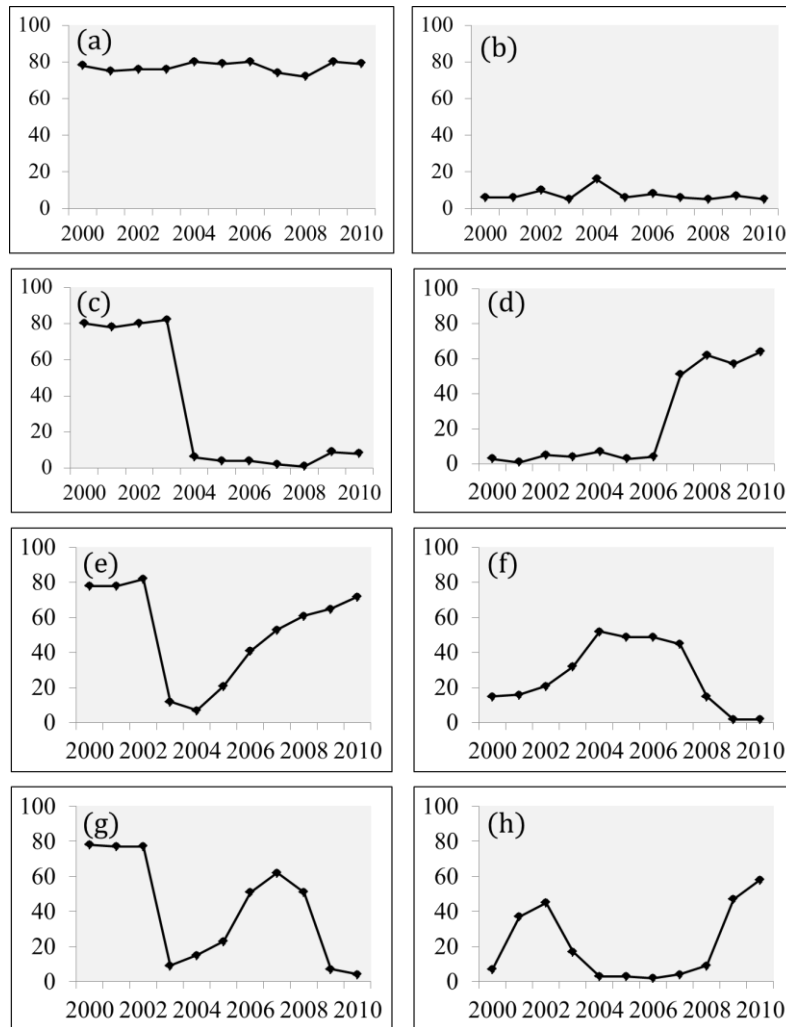


Figure 3.4 Typical trajectories of percent tree cover (y-axis) from 2000 to 2010 (x-axis) for selected sites: (a) persistent forest ($10^{\circ}56'29.997''\text{S}$, $54^{\circ}0'47.3682''\text{W}$); (b) persistent non-forest ($13^{\circ}56'15''\text{S}$, $53^{\circ}41'28.086''\text{W}$); (c) forest loss ($11^{\circ}56'7.4976''\text{S}$, $54^{\circ}43'59.736''\text{W}$); (d) forest gain ($19^{\circ}25'45.0006''\text{S}$, $53^{\circ}12'25.347''\text{W}$); (e) forest loss followed by gain ($11^{\circ}59'15''\text{S}$, $52^{\circ}42'43.1778''\text{W}$); (f) forest gain followed by loss ($13^{\circ}0'0''\text{S}$, $52^{\circ}54'6.1194''\text{W}$); (g) forest loss followed by gain and then by loss ($12^{\circ}58'52.4994''\text{S}$, $56^{\circ}37'19.3938''\text{W}$); and (h) forest gain followed by loss and then by gain ($13^{\circ}12'7.4988''\text{S}$, $57^{\circ}41'5.985''\text{W}$). The only patterns representing forest change are (c–h). A pixel is decided to be a true change if and only if its temporal profile can be fitted to one of these patterns. For cases (e–h), multiple logistic models are fitted to segments of the curves (Section 3.3.2).

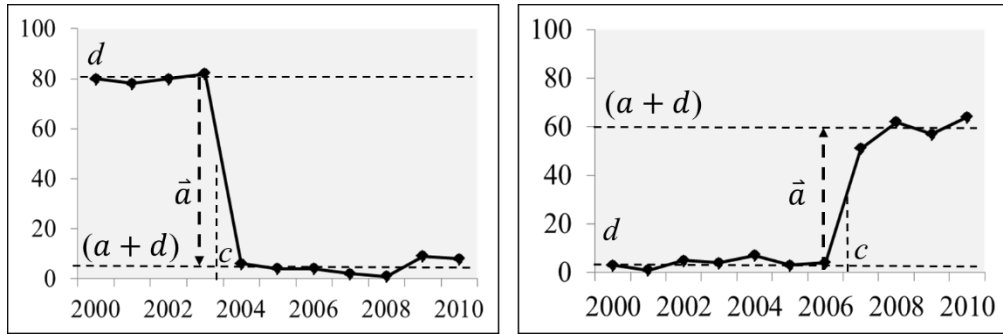


Figure 3.5 Structural metrics to characterize a change event. The y-axis is tree cover.

3.3.3.2 Modeling Multiple Loss-gain Processes

As multiple successive change events could occur within the 11-year span and as the exact number of change events within the temporal profile is unknown prior to analysis, an exhaustive moving-window curve fitting is employed to capture all possible change events in the study period. Modeling multiple changes is performed in three iterations. In the first iteration, a five-year moving window is used to model a single change segment for the window focal year from 2002 to 2008. The window size of five years is chosen because (1) this ensures the minimum number of observations required to estimate four parameters and because (2) multiple forest cover changes are highly unlikely to happen within five years. It is well understood that five years may not be long enough to capture natural forest regrowth. However, since the primary objective is to detect abrupt forest loss, a shorter window size is preferred to avoid omitting forest loss signals. Goodness-of-fit for each individual curve fit is evaluated using the chi-square value of the least-squares fit. In the second iteration, the locally best fit with the smallest chi-square value is selected as the logistic model for the expected change event. Lastly, the modeled successive change

events are crosschecked with each other based on a set of pre-defined neighborhood rules. For example, a clearing-cutting can be followed by an immediate plantation and, later on, by a second clearing, but cannot be followed by another immediate clearing. A maximum of two forest loss events or a maximum of two forest gain events are allowed within the 11-year period. The temporal neighborhood rules are defined such that only four specific patterns of change trajectories are detected: forest loss followed by gain, forest gain followed by loss, forest loss followed by gain and then by loss and forest gain followed by loss and then by gain (Figure 3.4 (e-h)).

3.3.3.3 Estimating Parameters of the Logistic Model

Parameters of the logistic model are estimated as the solution to a nonlinear least-squares problem. We use MPFIT, an implementation of the iterative Levenberg–Marquardt algorithm, to perform curve fitting (Markwardt 2009; Moré 1978). Goodness-of-fit is determined using a standard F-test ($p < 0.01$) based on the chi-square value of the least-squares fit. Only the statistically significant curves are saved in the final results.

3.4 Algorithm evaluation

The VCA algorithm generates four output layers representing change magnitude (*a*), change time (*c*), abrupt/gradual type (*b*) and pre-change tree cover (*d*). Here we focus our accuracy assessment on the change time layer, with an overarching objective of evaluating the method’s performance of retrieving the disturbance area at annual resolution. Validating forest disturbance products at annual resolution remains a challenge, mainly due to a lack of reference data (Cohen et al. 2010; Hansen et al.

2013; Huang et al. 2010a; Masek et al. 2008). Here we assess the VCA disturbance map in two distinct forest biomes, where we have dense time series disturbance products derived from Landsat images as the reference. Hence, all accuracy numbers generated are relative to Landsat. We carried out the evaluation at different spatial resolutions, which is described as follows.

3.4.1 Deriving reference datasets

The first site is located in the Brazilian state of Mato Grosso within the spatial extent of MODIS tile h12v10 (hereafter referred to as the MT site). The northern part of this test area is in the tropical humid broadleaf forest biome with high-density tree canopy cover, and the southern part is in the tropical dry broadleaf forest biome with low-density canopy cover (Figure 3.6). This site is in the so-called “arc of deforestation” region, where large patches of primary forests were cleared for mechanized agricultural production (Macedo et al. 2012). We collected year-to-year Landsat deforestation maps derived from the PRODES (Deforestation Monitoring in the Brazilian Amazon) project by the Brazilian National Institute for Space Research (INPE, <http://www.obt.inpe.br/prodes/index.php>). In PRODES, Landsat data are selected at the peak of the dry season in each year to minimize cloud contamination. This reference dataset consists of 36 Landsat path/rows. The PRODES project maps deforestation in the Brazilian Amazon using Landsat images since 1988, but we only used a subset that coincides with our study period.

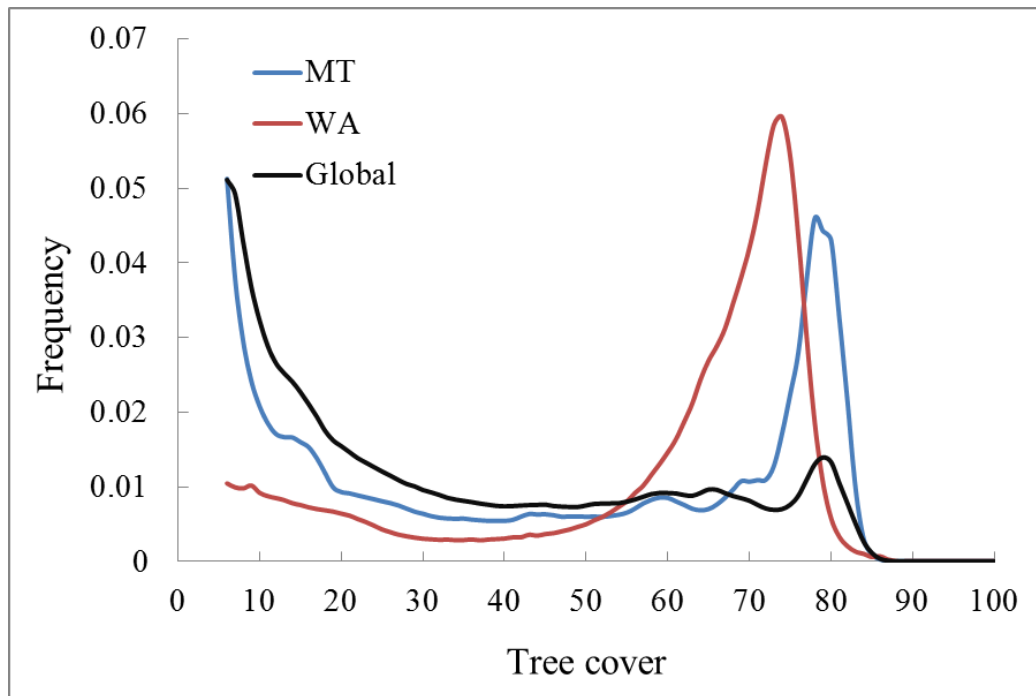


Figure 3.6 Distribution of tree canopy cover in the two test sites and the globe. Data are based on MODIS VCF in the year 2000 with pixels with greater than 5% tree cover included. MT, Mato Grosso site; WA, Washington site.

The second site is located in the U.S. state of Washington, near Olympic National Park (hereafter referred to as the WA site). It is within the temperate conifer forests biome with moderate to high density tree canopy cover (Figure 3.6). Harvesting trees for timber is the primary driver of forest cover change in this region. We collected annual growing-season Landsat images of Path 47 and Row 27 from 1984 to 2011. These Landsat images were first converted to surface reflectance through the Landsat Ecosystem Disturbance Adaptive Processing System (LEDAPS) (Masek et al. 2006) to construct a dense time series image stack (Huang et al. 2009a). This image stack was then analyzed using the vegetation change tracker (VCT) algorithm to produce an annual disturbance product (Huang et al. 2010a). The product

had an overall accuracy of 93.8%, while its average user's and producer's accuracies for the disturbance year classes were 91.5% and 91.8%, respectively (Huang et al. 2011). Only changes occurring between 2000 and 2010 were considered in evaluating the VCA disturbance products.

3.4.2 Balancing regional biases in disturbance area estimates from MODIS

Logistic parameters (a , b , c and d) were derived for every candidate change pixel in the two test sites. Parameter a describes the magnitude of tree cover change and, therefore, is a strong indicator of forest disturbance. Obviously, varying area statistics could be generated depending on the threshold chosen to label the indicator pixels as disturbance. We first evaluated the effect of varying a as a change-detection threshold on disturbance-area estimation from MODIS against the Landsat reference. An optimal threshold was then determined such that the overall area estimated from MODIS matched that derived from Landsat. This was achieved by balancing the deviations of the MODIS estimation from the reference, which were characterized using two metrics—underestimation and overestimation—calculated using the following equations. To do so, we resampled the MODIS pixel to 30-m resolution using the nearest neighbour resampling method with the `gdalwarp` utility (<http://www.gdal.org>).

Underestimation

$$= \frac{\text{Disturbance pixels mapped by reference but not by MODIS}}{\text{All disturbance pixels mapped by reference}} \times 100\%. \quad (3.7)$$

Overestimation

$$= \frac{\text{Disturbance pixels mapped by MODIS but not by reference}}{\text{All disturbance pixels mapped by reference}} \times 100\%. \quad (3.8)$$

A larger threshold (in absolute value) leads to more underestimation and less overestimation, whereas a smaller threshold leads to more overestimation and less underestimation (Figure 3.7). The optimal threshold that cancelled out underestimation and overestimation was determined to be -39 for the MT site and -15 for the WA site.

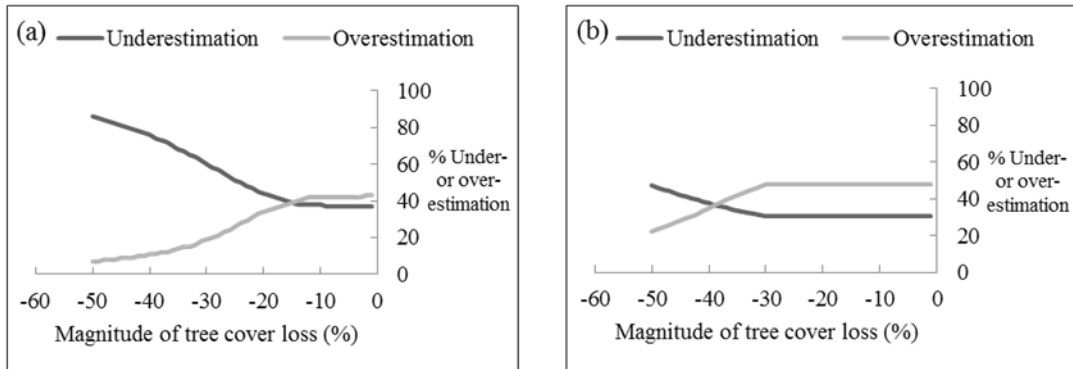


Figure 3.7 Under- or over-estimation of disturbance area derived from VCA as a function of the magnitude of tree cover loss (coefficient a of the logistic model, equation 3.6) against the Landsat reference for two study sites: (a) WA and (b) MT.

3.4.3 Qualitative assessment

The threshold derived above was applied to obtain the final disturbance-year product from MODIS (Figure 3.8). Spatial and temporal patterns of disturbed land patches mapped from MODIS closely resemble those from Landsat for both test sites. The pixel-level differences observed in the Western U.S. were mainly due to the smaller size of land patches (which is comparable to a MODIS pixel) as well as the distortion of MODIS pixels at middle to high latitude. Hence, it is not surprising that smaller change patches suffer more omission and/or commission errors than relatively larger patches (Lechner et al. 2009), a conclusion consistent with previous land cover change studies using MODIS data (Xin et al. 2013).

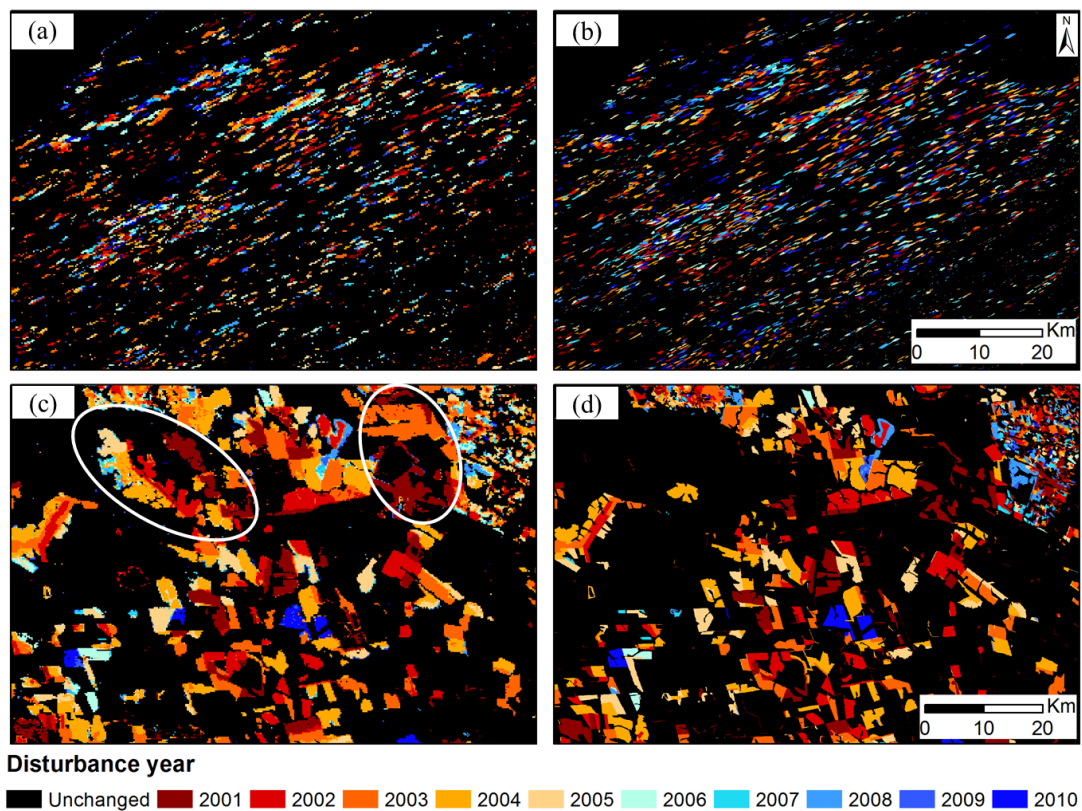


Figure 3.8 Examples of disturbance-year maps derived from MODIS compared with the Landsat reference. (a) The MODIS disturbance map in WA, USA. This subset is centered at (123° 41' 24.678"W, 47° 16' 11.104"N). (b) Landsat disturbance map derived through vegetation change tracker (VCT). (c) MODIS disturbance map in MT, Brazil. This subset is centered at (56° 3' 25.596"W, 11° 39' 20.073"S). (d) PRODES disturbance map. Notice some large disturbance patches mapped by the VCA (circled, upper left and upper right of (c)), but not by the PRODES; the lack of disturbance patches is due to omission errors in the PRODES.

Pixel-level errors are mostly distributed on the edge of land parcels, especially when the edge is between two or more disturbed patches where the disturbances occurred in different years (see Figure 3.9 for an illustration). Pixels located in the middle of the patches (*i.e.*, Pixels 1, 2, 3 and 6) show patterns of abrupt decline in tree cover in a particular year, a sign of rapid forest clearing on the ground. However, pixels located on the edge (*i.e.*, Pixels 4 and 5) have gradual change patterns over time, which causes errors in allocating a disturbance year to the pixel. These edge pixels are either mixtures of sub-pixel disturbances occurring during different times or artifacts resulting from varying footprints of MODIS observations and the geolocation mismatch between time series MODIS layers (Townshend et al. 1992; Wolfe et al. 2002; Xin et al. 2013). Moreover, we observed that spatially adjacent patches are often disturbed in successive years in the Amazon site, whereas the clearing time for adjacent patches in the Western U.S. can be several years apart, reflecting different land management practices in these two places.

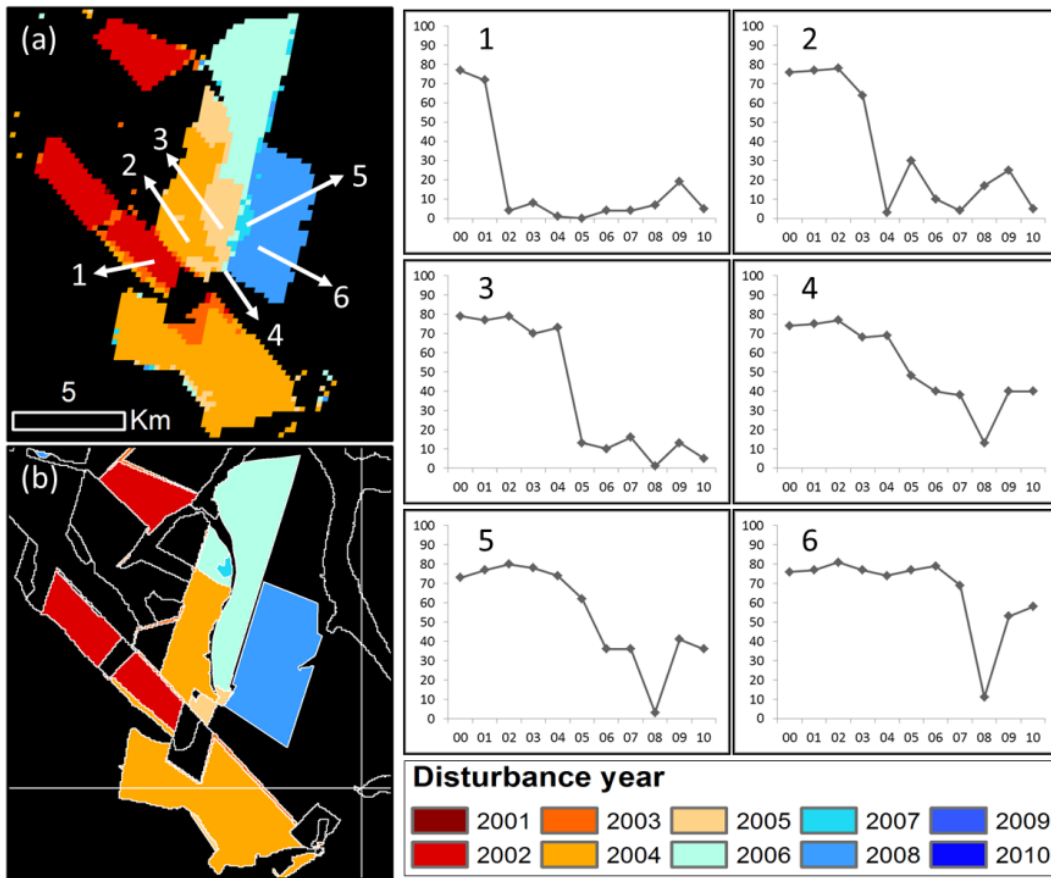


Figure 3.9 An illustration of pixel-level accuracy of VCA's disturbance-year layer. (a) Land patches depicted using colors representing the year of forest disturbance obtained from MODIS. (b) Reference map acquired from PRODES. The VCF values (y-axis) for Pixels 11 through 6 between years 2000 and 2010 (x-axis) are shown on the right. Pixels 1, 2, 3 and 6 are located in the middle of disturbed parcels, whereas Pixels 4 and 5 are on the edge; these pixels are less accurately characterized than pixels inside disturbed patches.

3.4.4 Quantitative assessment

Applying the optimal threshold matches the 11-year total disturbance estimate from MODIS to that from Landsat at the scale of the study area. However, the accuracy of the year allocation, as well as the accuracy and precision of annual disturbance rates

remain to be investigated. In this section, we first evaluate the accuracy of year allocation using a traditional error matrix at 250-m resolution and then assess the bias and precision of annual disturbance area estimates at an aggregated spatial resolution.

3.4.4.1 Temporal accuracy at 250-m resolution

To quantitatively evaluate VCA's accuracy of determining the year of disturbance in change pixels, we applied a majority filter to the Landsat disturbance-year map, resampled it to MODIS resolution, and constructed a per-pixel confusion matrix. The majority filter works as follows. Landsat pixels whose centroid falls in the MODIS grid footprint are ranked based on the frequency of their pixel value and the most frequent value was chosen to represent the value of the aggregated grid. This was performed for each evaluation site. A strict comparison between VCA disturbance-year and the reference yielded an overall accuracy of 68.7% at the WA, USA site and 59.8% at the MT, Brazil site, although the accuracy for each year varied from one time to another (Table 3.1 and Table 3.2). A close examination of the confusion matrices revealed that the majority of misclassifications were between neighboring years. Relaxing the allocated year to ± 1 year substantially increased the accuracy for each individual year, as well as the overall accuracy. As a result, the overall accuracy achieved was 86.7% for the WA site and 84.6% for the MT site.

3.4.4.2 Area accuracy at 5-km resolution

One of the practical applications of disturbance mapping is to derive the forest change rate at regional or national scales. A demonstrated way of generating such results from MODIS data is to compare and calibrate the MODIS-based estimates using temporally coincident and spatially collocated Landsat samples at a coarser resolution

(Hansen et al. 2010; Hansen et al. 2008c). This method has been applied to quantify global forest cover loss for 2000-2005 at 20-km resolution. Here we explore the potential of this approach in disturbance-area retrieval at an annual interval and at much finer spatial resolutions. As an example, both MODIS and Landsat disturbance products were aggregated to 5 km to calculate percent forest loss per coarse grid. We then calculated the root mean square error (RMSE), mean absolute error (MAE), mean bias error (MBE) and r^2 between aggregated VCA forest loss and the reference over all 10 years, as well as for each individual year.

$$\text{RMSE} = \sqrt{\sum_{i=1}^n (P_i - R_i)^2 / n}, \quad (3.9)$$

$$\text{MBE} = \sum_{i=1}^n (P_i - R_i) / n, \quad (3.10)$$

$$\text{MAE} = \sum_{i=1}^n |P_i - R_i| / n, \quad (3.11)$$

$$r^2 = 1 - \frac{\sum_{i=1}^n (P_i - R_i)^2}{\sum_{i=1}^n (R_i - \bar{R})^2}, \quad (3.12)$$

where i is the pixel index, P_i is the VCA disturbance rate per grid sample, R_i is the reference disturbance rate per sample, \bar{R} is the mean reference rate and n is the sample size (Willmott 1982).

Table 3.1 Temporal accuracy of the MODIS disturbance-year layer against Landsat reference in WA, USA.

		Reference Disturbance Year											User's Accuracy	User's Accuracy (± 1 year)
		2001	2002	2003	2004	2005	2006	2007	2008	2009	2010	Total		
MODIS Disturbance Year	2001	2062	258	66	31	52	99	63	72	31	51	2785	74.0	83.3
	2002	199	2032	134	43	52	62	53	72	43	56	2746	74.0	86.1
	2003	91	633	2619	281	90	71	76	133	52	151	4197	62.4	84.2
	2004	21	25	192	1930	300	51	34	49	28	78	2708	71.3	89.4
	2005	40	31	80	422	2342	279	75	110	39	85	3503	66.9	86.9
	2006	40	20	58	209	621	2416	168	113	52	86	3783	63.9	84.7
	2007	28	12	18	35	123	453	1754	275	41	30	2769	63.3	89.6
	2008	19	18	21	17	37	84	139	1999	99	38	2471	80.9	90.5
	2009	12	9	8	9	11	18	15	293	877	127	1379	63.6	94.1
	2010	16	17	20	12	36	34	38	119	181	1232	1705	72.3	82.9
	Total		2528	3055	3216	2989	3664	3567	2415	3235	1443	1934	28,046	
Producer's Accuracy		81.6	66.5	81.4	64.6	63.9	67.7	72.6	61.8	60.8	63.7	<i>overall:</i>	68.7	
Producer's Accuracy (± 1 year)		89.4	95.7	91.6	88.1	89.1	88.3	85.3	79.4	80.2	70.3	<i>overall:</i>	86.7	

Table 3.2 Temporal accuracy of the MODIS disturbance-year layer against Landsat reference in MT, Brazil.

		Reference Disturbance Year											User's Accuracy	User's Accuracy (±1 year)
		2001	2002	2003	2004	2005	2006	2007	2008	2009	2010	Total		
	2001	29,614	6292	1662	758	662	179	126	158	36	37	39,524	74.9	90.9
	2002	8483	45,350	7006	2614	2025	398	350	572	122	120	67,040	67.7	90.8
	2003	5705	28,727	82,677	11,611	6741	1073	1083	1782	355	313	140,067	59.0	87.8
	2004	2707	7286	18,452	83,728	17,128	2423	1883	2620	445	426	137,098	61.1	87.0
MODIS	2005	1199	3162	4626	9942	53,700	5540	2906	3674	550	341	85,640	62.7	80.8
Disturbance	2006	607	1450	2014	2999	7813	14,062	4921	4422	823	426	39,537	35.6	67.8
Year	2007	352	683	779	1147	1969	2386	9485	4873	998	456	23,128	41.0	72.4
	2008	219	402	444	555	1080	561	1903	11,361	1406	749	18,680	60.8	78.5
	2009	107	103	183	162	337	156	288	617	1985	944	4882	40.7	72.6
	2010	50	50	69	54	88	26	39	78	96	2122	2672	79.4	83.0
	Total	49,043	93,505	117,912	113,570	91,543	26,804	22,984	30,157	6816	5934	558,268		
Producer's Accuracy		60.4	48.5	70.1	73.7	58.7	52.5	41.3	37.7	29.1	35.8	<i>overall:</i>	59.8	
Producer's Accuracy (±1 year)		77.7	86.0	91.7	92.7	85.9	82.0	71.0	55.9	51.2	51.7	<i>overall:</i>	84.6	

The comparison between VCA and Landsat at 5-km resolution in the Western U.S. had an overall r^2 of 0.91 over the 10-year period. Breaking the total disturbance into individual years, the lowest r^2 was in year 2010, with a value of 0.64, while all of the other years had r^2 ranging between 0.77 and 0.92. The annual RMSE between VCA and Landsat disturbance ranges between 0.34% and 0.65% (Figure 3.10). Both high r^2 and low RMSE suggest that MODIS data can be used to retrieve area estimates that approximate Landsat estimates on an annual basis. In terms of bias, the years of 2001, 2003, 2005, 2006 and 2007 had positive MBE values, indicating that MODIS overestimates forest loss in these years; conversely, the years of 2002, 2004, 2008, 2009 and 2010 had negative MBE values, indicating an underestimation by MODIS in these years. This bias pattern (i.e., overestimation in earlier years and underestimation in later years) is probably because pixels located on the edges of land patches are mislabeled and because the algorithm favors assigning an earlier year to the edge pixels.

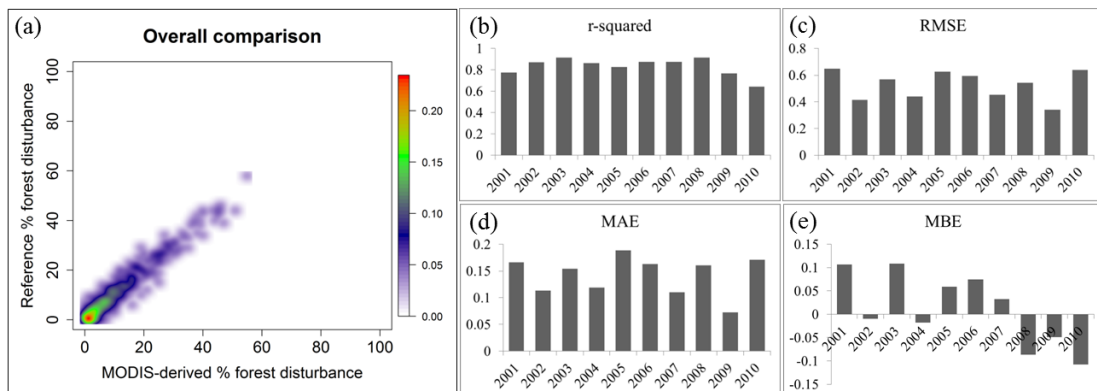


Figure 3.10 Evaluation of VCA-derived disturbance rates in the Western U.S. at 5-km resolution against VCT disturbance rates. (a) Scatter plots of 10 years of total disturbance per 5-km grid. Temporal accuracy is shown by the quantitative evaluation metrics of (b) r^2 , (c) RMSE (unit: %), (d) MAE (unit: %) and (e) MBE (unit: %). The

color bar indicates plot density ($n = 805$). The mean annual disturbance rate is 0.85% based on the reference.

The comparison between VCA and PRODES in Mato Grosso yielded an overall r^2 of 0.74 over the 10-year period. The annual RMSE between these two estimates ranged between 0.45% and 2.58% (Figure 3.11). We also found that these two products had a closer match after the year 2005, but a relatively weak relationship before the year 2005. Specifically, the VCA product identified less deforestation than PRODES in the years 2001 and 2002, but more deforestation in the years 2003 and 2004 in this region. These discrepancies were reflected in the MBE values, as well as by the scatter of observations around the 1:1 line (Figure 3.11 (a)). An example of missing patches in PRODES in the years 2003 and 2004 was previously shown in Figure 3.8 (c) and (d), where two large deforestation patches in the upper left and upper right portion of the map were missing in PRODES. Because 36 Landsat WRS (Worldwide Reference System) tiles were used in this evaluation, cloud contamination in this Landsat dataset was unavoidable, which explained some of these omission errors in PRODES. Plus, PRODES does not capture the loss of regrowth forests on previously deforested land (Hansen et al. 2008a), while our VCA product detects those events successfully.

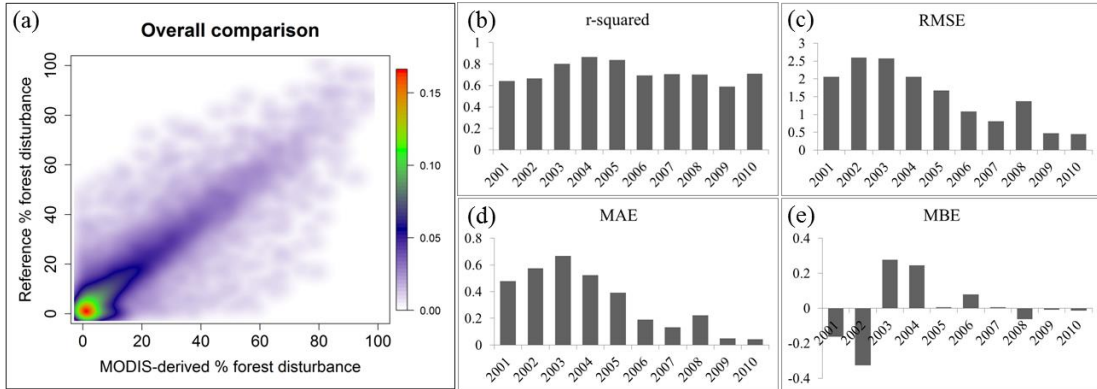


Figure 3.11 Evaluation of VCA-derived disturbance rates in Mato Grosso at 5-km resolution against PRODES disturbance rates. (a) Scatter plots of 10 years of total disturbance per 5-km grid. Temporal accuracy is shown by the quantitative evaluation metrics of (b) r^2 , (c) RMSE (unit: %), (d) MAE (unit: %) and (e) MBE (unit: %). The color bar indicates plot density ($n=14,322$). The mean annual disturbance rate is 1.25% based on the reference.

3.5 Discussion

3.5.1 Advantages and disadvantages of the VCA algorithm

The algorithm developed here provides a means to map forest disturbance at annual resolution using time series of percent tree cover estimates. The Collection 5 MODIS VCF product was used as an illustration of the algorithm. Like other time series methods for detecting change (e.g., VCT (Huang et al. 2010a), BFAST (Breaks for Additive Season and Trend) (Verbesselt et al. 2010), LandTrendr (Kennedy et al. 2010)), our method has the statistical advantage of increased degrees of freedom over bi-temporal change detection. A candidate change event must be confirmed by a sequence (as opposed to a pair) of observations before, during, and after the change in

order to be detected and identified. Moreover, although primarily designed for change detection, the idea could also be applied to remove random noise in time series of continuous field land cover product. Except for disturbance events that cause abrupt changes in tree cover, VCF values for undisturbed pixels should remain relatively stable or change gradually (e.g., resulting from natural growth) over time. Therefore, VCF values fitted to the logistic curves for those pixels likely are more realistic than the original values.

The method's foundation in well-characterized, parametric statistical models gives it the advantage of computational simplicity. Large-area land cover mapping or change detection often requires intensive human involvement (e.g., the PRODES project) or automation, which requires either sophisticated algorithm parameterization, substantial computing facilities (e.g., (Hansen et al. 2013)) or both. The method demonstrated here follows established statistical theory with little parameter fine-tuning. Although the time needed to complete a change analysis is a function of data volume, masking out the majority of stable pixels before characterizing disturbance greatly improves the method's efficiency. As such, a global application could be completed on a single PC within a reasonable amount of time.

Another unique advantage of the method is that it characterizes continuous changes in land cover at sub-pixel resolution and has the potential to capture subtle and long-term changes, such as forest degradation. Land cover conversion often exhibits a strong contrast between remotely-sensed images at two or more time points. However, stress-induced changes within the same cover type (e.g., forest

degradation) do not necessarily have apparent signatures in the short-term, but may show trends over a long time span (Neigh et al. 2014). Hence, it has been suggested that to detect forest degradation, land cover should be characterized as continuous biophysical variables and the method should be flexible to capture trends at the inter-annual scales (Hansen and DeFries 2004; Lambin 1999).

This approach is not limited to tree cover, nor to the MODIS resolutions, nor to the annual time step. Although we used percent tree cover layers from MODIS as an illustration of the algorithm, the general method had no specific requirement on the thematic type or spatial or temporal resolution. Therefore, it may be applicable to continuous fields of other land cover types generated using satellite data from different sensors. Coarse-resolution sensors provide rich data at high temporal frequencies. At the Landsat resolution, global VCF tree cover products have been generated for 2000 and 2005 (Sexton et al. 2013a). Recent advances in remote sensing demonstrated that Landsat images could be used to create near cloud-free composites by exhaustively mining the Landsat archive (Hansen et al. 2013; Roy et al. 2010), and the annually composited Landsat images could also be used to characterize land cover and change (Hansen et al. 2014; Hansen et al. 2013). This may create an opportunity to produce continuous fields of land cover at annual time steps using Landsat data. The approach developed here also provides the potential for such applications.

There are several limitations of the current algorithm. First, for each pixel, the sample size in the temporal domain is small (i.e., eleven data values from eleven years). The inter-annual variance calculated using eleven data samples may not well

represent the actual variance of the population. A practical solution adopted here is setting conservative probabilistic thresholds for detecting change. This, however, introduces commission errors in the first step and creates redundant cases for curve fitting in the second step. Should data of longer time series be available, more precise thresholds could be located following the statistical inference and a more accurate change mask could be generated. As such, we expect the algorithm to work better as the VCF record becomes longer. Second, the I.I.D. assumption obviously simplifies the actual error structure of percent tree cover estimates. We may expect spatial correlation between different pixels and serial correlation between observations of a given pixel taken over time. The effect of spatiotemporal correlation on change detection needs to be investigated in the future. Moreover, the current algorithm is optimized for detecting single or multiple abrupt forest disturbances (e.g. clear cutting). One area of future work will be to extend the method for characterizing gradual forest changes such as degradation or natural regrowth. One technical aspect that needs to be improved is the moving window size for detecting successive disturbances. While a fixed five-year window may be enough to capture clearing cutting and fast tree plantations, a longer window is likely needed to reliably characterize natural regrowth. An adaptive window size seems to be a useful technique to address the varying temporal length of different types of forest losses and gains. Lastly, our current algorithm evaluation only includes test sites in the tropical moist broadleaf forest biome and the temperate conifer forest biome. Given the global coverage of annual MODIS VCF and increasingly available high-resolution forest cover change datasets (Hansen et al. 2013; Masek et al. 2013;

Townshend et al. 2012), there is no reason that the quantitative evaluation cannot be expanded to other forest/woodland biomes. Subsequently, global annual forest change estimates could be derived.

3.5.2 Global application of the VCA algorithm for mapping disturbance hotspots

The VCA algorithm was applied to the global scale for mapping forest disturbance hotspots. The implementation was carried out on a biome-by-biome basis. As discussed earlier, the Collection 5 MODIS VCF tends to have small inter-annual variance at the low and high ends of tree cover but have large variance at moderate tree cover. This error structure is consistent in different biomes but the variance values are significantly different across biomes (Figure 3.12). To address this difference, the probability thresholds (equation 3.5) were adaptively searched for each biome in addition to the inter-annual mean tree cover strata. Subsequently, a 5-year moving window curve fitting was applied to every pixel to characterize forest disturbance.

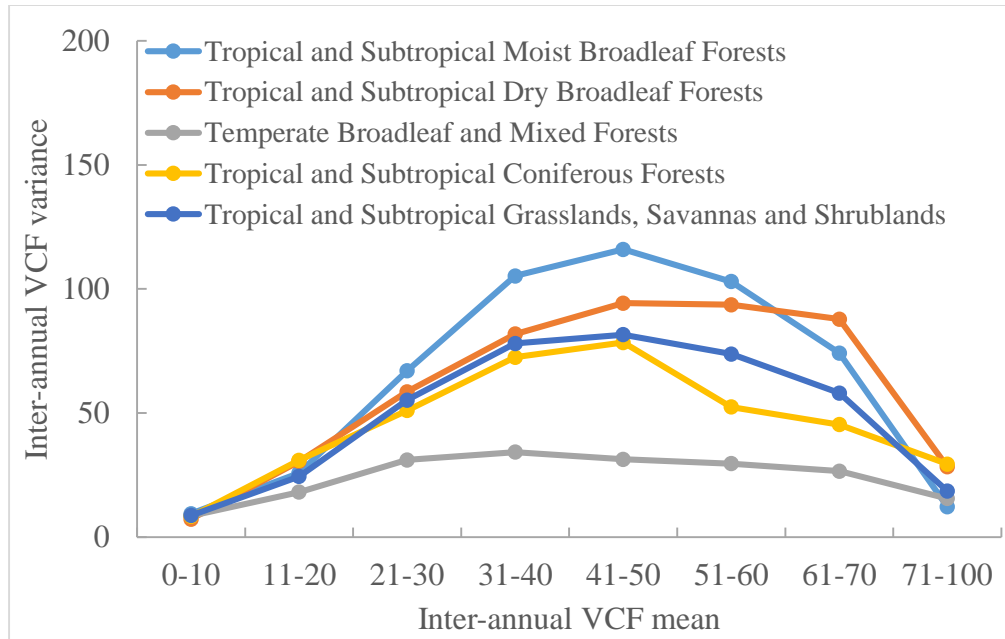


Figure 3.12 Inter-annual VCF variance versus inter-annual VCF mean in various forest biomes in Latin America.

Figure 3.13 shows the number of disturbance events (loss or gain) detected in each pixel in the Americas between 2000 and 2010. The map was resampled to 5-km resolution for visualization purposes with red representing one disturbance event over the 11-year window and green representing two or three disturbance events. Forest disturbance “hotspots” are well depicted, such as wildfires in Alaska and Canada, active logging in southeast United States, clear-cutting of primary forests in the Brazilian Amazon, loss of Chaco forests in Paraguay and Argentina, active forestry the Atlantic forests in Brazil. It is also clear that fire-caused disturbances in the boreal region and loss of primary forests in the tropics and subtropics (e.g. Amazon and Gran Chaco) have one loss or gain across the 11-year period, while rotation of tree plantations in tropical and temperate regions could have two or three land cover change events in 11 years.

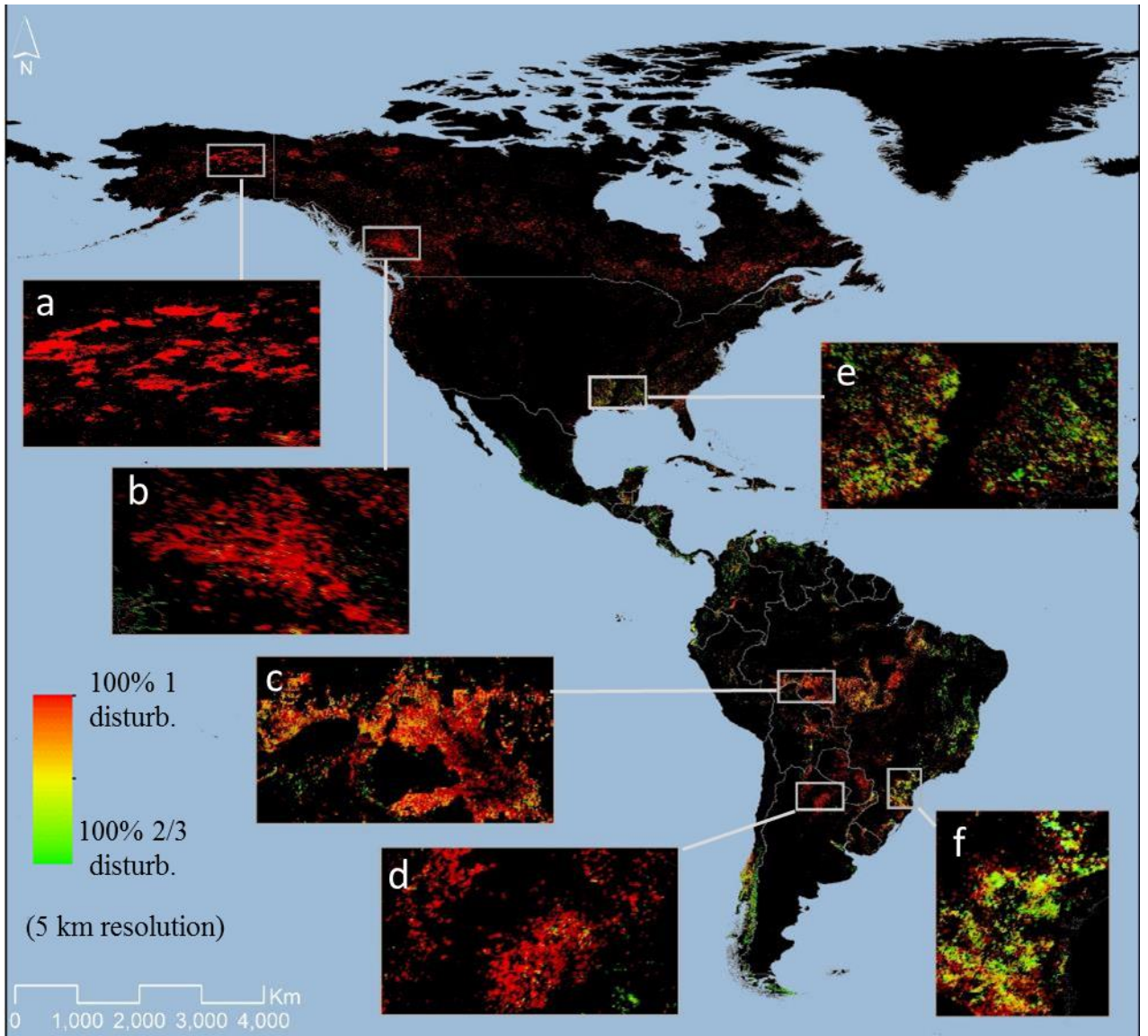


Figure 3.13 VCA-derived forest disturbance hotspots in the Americas between 2000 and 2010. The number of disturbances (maximum 3) over the 11 year period was identified for every 250 m pixel. The map was aggregated to 5 km for display purposes. Red color represents one disturbance event (loss or gain) over the 11-year window and green color represents two or three disturbance events. a: Wildfires in Alaska. b: Logging and disease in British Columbia. c: Loss of primary forests in the Brazilian Amazon. d: Loss of Chaco forests in Argentina. e: Tree crop rotation in Southeast U.S.. f: Tree crop rotation in Southeast Brazil.

It should be noted that the data displayed in Figure 3.13 at this point should be best viewed as disturbance “hotspots” or “indicators”, which include true forest cover changes as well as false positives (i.e. commission errors) where VCF values fluctuate considerably from year to year so that the change detection appears statistically significant. One of the notable places of commission error is western Mexico, where great spectral variability may be caused by the semi-arid climate and the complex terrain so that the derived tree cover estimates exhibit large year-to-year variation. A quantitative analysis of the map’s accuracy and rates of forest disturbance is subject to future research.

We visually assessed the disturbance-year estimates for selected hotspots by comparing the MODIS map with Landsat-based disturbance maps by Hansen *et al.* (2013) (Figure 3.14). The two datasets show great similarities in a number of locations. For large disturbance patches detectable at the MODIS 250-m resolution, VCA may allow for the detection of changes missed in Landsat-based results due to the lack of clear view observations (e.g., Figure 3.12 (e)). Again, like many other MODIS-based change studies, rigorous regional calibration using Landsat data is needed to derive area estimates comparable to those derived using Landsat data alone (Hansen et al. 2010; Hansen et al. 2008c).

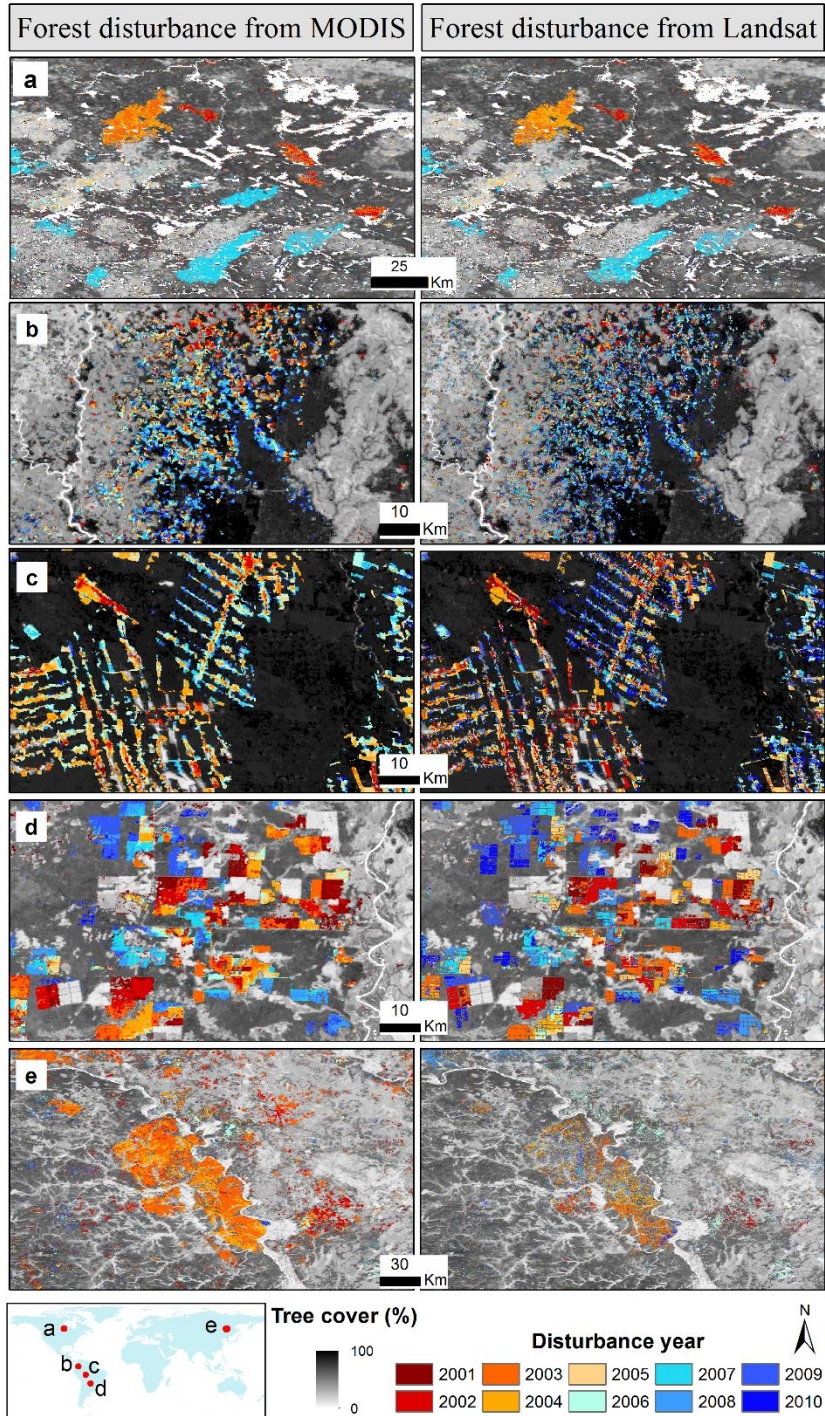


Figure 3.14 Global examples of forest disturbance mapped using MODIS VCF in this study compared with the recently published Landsat results by Hansen et al. (2013). Color pixels indicate disturbance year, and grayscale pixels represent percent tree cover in the year 2000. The center coordinates of these panels are: (a) (93°54'57"W,

52°49'12"N), (b) (74°30'26"W, 1°32'12"N), (c) (64°40'22"W, 9°56'6"S), (d) (58°19'32"W, 21°39'41"S), (e) (126°7'33"E, 52°35'40"N). Overall, the spatiotemporal patterns of forest disturbance are in close agreement in a range of different biomes. Whereas the coarse spatial resolution of MODIS is a limiting factor for detecting disturbances of small size (e.g., edges of logging roads in (c)); omission errors due to missing data in the composited Landsat ETM+ (scan line corrector -off) are also visible in some places (e.g. (e)).

3.6 Conclusions

We have developed a new method, called VCF-based Change Analysis (VCA), for characterizing forest disturbance using time series of satellite measurements of percent tree cover. The fact that land cover disturbances are rare events in a large geographic region leads to efficient change detection by employing well-established parametric statistics. Fitting nonlinear curves to time series, continuous estimates of tree cover simultaneously characterized the timing and intensity of forest cover change. Illustrated using the 250-m annual MODIS VCF product, the method requires little parameter fine-tuning to derive indicators of annual forest cover change and could generate accurate disturbance area estimates after calibration using data of a higher spatial resolution.

The major advantages of the new method presented here include: (1) reliable results, (2) computational simplicity, (3) global applicability, (4) flexibility to capture abrupt as well as gradual change, and (5) capability to apply to other satellite sensors. Because increasing the frequency of forest cover change detection to annual resolution is highly desirable for understanding the global carbon cycle, future research will investigate the inter-annual variability of global forest cover change.

Chapter 4: Annual Carbon Emissions from Deforestation in the Amazon Basin between 2000 and 2010

4.1 Introduction

Biomass is defined as the mass of live or dead organic matter in plants, about 50% of which is carbon. As the planet's largest reservoir of terrestrial biomass, forest ecosystems hold a total amount of carbon comparable to the atmosphere (Pan et al. 2011). Forests are also constantly exchanging carbon, water and energy with the atmosphere. Therefore, disturbance of the world's forests can significantly shape the global carbon cycle as well as climatic patterns (Bonan 2008).

The FAO provide periodic update on net changes in the area and biomass of the world's forests at about 5- or 10-year intervals mainly based on country reporting, with supplementary satellite sample analysis. Centralizing information through country participation is valuable in some aspects and the resulting national statistics have been widely used in a number of scientific applications (Houghton 2005; IPCC 2006; Kaimowitz and Angelsen 1998; Kindermann et al. 2008). However, limitations of FAO's Global Forest Resource Assessment are also discussed in the literature, including primarily the lack of internal consistency due to different definitions of forest among countries and time intervals (Grainger 2008; Matthews and Grainger 2002). Additionally, reporting forest area change as land-use change does not reflect the biophysical consequences of land surface transformation (Hansen et al. 2013). Furthermore, only reporting net changes in forest area, without partition to gross loss

and gain, could lead to ambiguous target (e.g. “zero deforestation”) for current and future deforestation mitigation programs (Brown and Zarin 2013).

Satellite-based observations of forest cover change provide an alternative to estimate deforestation rates consistently across space and time. At continental to global scales, maps of forest cover and change are increasingly being generated from various satellite data sources. Among the latest progresses, Landsat samples have been used to determine tropical deforestation rates between 1990 and 2010 (Achard et al. 2014); MODIS and Landsat data have been jointly used to quantify global gross forest cover loss between 2000 and 2005 (Hansen et al. 2010; Hansen et al. 2008c); wall-to-wall Landsat TM and ETM+ surface reflectance data have been used to derive global forest cover change between 1990, 2000 and 2005 (Kim et al. 2014; Sexton et al. 2015; Sexton et al. 2013a) with change maps between 1975 and 1990 being generated (Townshend et al. 2012); Landsat ETM+ TOA reflectance data have been composited at annual resolution to create global forest cover loss and gain maps between 2000 and 2012 (Hansen et al. 2013); the Advanced Land Observing Satellite Phased Array L-band Synthetic Aperture Radar data have been employed to produce forest/non-forest maps over the globe, but generating globally consistent change product with SAR data is yet to be studied (Shimada et al. 2014).

Some of these forest cover change datasets have been integrated with satellite-based forest biomass information (Baccini et al. 2012; Saatchi et al. 2011) to quantify changes in forest carbon stocks (Achard et al. 2014; Harris et al. 2012b; Tyukavina et al. 2013). These existing studies clearly reveal the spatial heterogeneity of land-cover change emissions across ecological and/or political boundaries. However, an average

emission estimate over a 5- or 10-year interval, similar to FAO reports, does not embrace the necessary temporal details to uncover historical trends. Unlike fossil-fuel emissions that are known to have been increasing steadily (Peters et al. 2011; van der Werf et al. 2009), a limited number of studies suggest that forest cover change rates can fluctuate substantially from year to year (Hansen et al. 2013; Huang et al. 2009b; Masek et al. 2013). The temporal variability of deforestation at continental to global scales has yet to be understood and linked to the global carbon cycle.

Quantifying trends and temporal variability of carbon emissions from deforestation is important for a number of reasons. First, it may explain some of the inter-annual variability of atmospheric CO₂ concentration (Keeling et al. 1995). Atmospheric inversion studies suggest that the inter-annual variability of global CO₂ growth rate is dominated by tropical land ecosystems, with positive anomalies related to El Niño and negative anomalies related to La Niña (Bousquet et al. 2000; Ciais et al. 2013; Rayner et al. 2008). A recent study further recognizes that semi-arid ecosystems may become a more relevant driver to the global carbon anomaly in the future (Poulter et al. 2014), but questions remain on how much of the variability can be attributed to carbon released from land cover change (Houghton 2000; Keeling et al. 1995). Second, the trend of deforestation is critical for understanding the complex and changing drivers of deforestation (Nepstad et al. 2014). For example, the increasing deforestation between 2001 and 2004 in the Brazilian Amazon is related to trends of the international soybean price and the declining deforestation after 2005 is associated with the collapse of commodity markets as well as shifting land use dynamics (Macedo et al. 2012; Morton et al. 2006). Studies also link time series of

deforestation emissions with economic input-output models to attribute emissions to domestic consumption as well as to international trade of agricultural products (Karstensen et al. 2013). Third, knowing the trend and variability of historical emissions likely has a strong influence on policies of reducing emissions from deforestation and forest degradation (REDD+). The inter-annual variability itself is a key variable for setting the reference emission level (REL) or baseline in some proposed REL methods (e.g. the corridor approach [Joanneum Research et al. 2006]).

In the tropics, where most carbon emissions from deforestation are located, policy instruments such as the UN-REDD programme (<http://www.un-redd.org/>) are being actively devised to combat emissions from LCLUC. This chapter turns its focus on the Amazon basin, which holds the largest rainforest of the Earth but suffered a prolonged history of deforestation. The objective is to quantify annual deforestation and related carbon emissions using time-series satellite data and to study the implications of the observed carbon dynamics for REDD+ policy.

Here forest refers to an area of at least 0.09 ha in size that is covered by 25% or more trees that are 5 m or taller. Consistent with others (Harris et al. 2012b), deforestation is defined as the reduction of tree cover to below the forest threshold. Annual deforestation rates are generated using yearly tree cover maps derived at 250 m resolution from the MODIS vegetation continuous field (VCF) product (DiMiceli et al. 2011) and then calibrated using a large sample of 30 m Landsat images, which more reliably depict change. We then combine the deforestation rates with a circa 2000 forest biomass dataset (Saatchi et al. 2011) to quantify annual carbon emissions from deforestation by applying the standard methodology described in (Harris et al.

2012b). Our estimates include deforestation due to all causes including wildfires, flooding and anthropogenic clearing. Following suggestions by Brown and Zarin (2013), we estimate carbon fluxes from gross deforestation without the inclusion of forest regrowth in order to inform ongoing policy discussions on REDD+, which is also consistent with recent studies (Harris et al. 2012b; Tyukavina et al. 2013). Our emission estimates include loss of above and below ground biomass in the deforested area. Changes in the soil carbon pool due to deforestation are not included.

4.2 Materials and methods

4.2.1 Study area

The study area is the Amazon basin, which occupies about 40% of South America. More than 60% of the basin is located in Brazil and the rest in Bolivia, Colombia, Ecuador, French Guiana, Guyana, Peru, Suriname and Venezuela. Most of the basin is covered by closed canopy rainforests, which provide habitat for a vast array of plant and animal species (Pimm et al. 2014). The leading environmental issue in this region is the pervasive loss of pristine forests, threatening terrestrial biodiversity (Ferraz et al. 2003) and altering regional and global climate (Werth and Avissar 2002). Deforestation is driven by a variety of complex socioeconomic and natural factors (Nepstad et al. 2014), including mechanized agricultural expansion (cattle ranching and soybean plantation) in the Brazilian Amazon (Macedo et al. 2012; Morton et al. 2006), illegal plantation (e.g. coca) in the Colombian Amazon (Posso 2000), gold mining in the Peruvian Amazon (Asner et al. 2013), as well as droughts, fires and floods in many different places of the basin (Brando et al. 2014; Espirito-

Santo et al. 2014; Saatchi et al. 2013).

4.2.2 Deriving annual deforestation rates from MODIS and Landsat datasets

Forest change products over the study area were derived from the yearly MODIS VCF tree cover data and calibrated using 10 km × 10 km Landsat samples. Figure 4.1 shows a flowchart of deriving annual forest cover change estimates from these two data sources. The method has three major components: a MODIS module which generates 250 m annual forest cover change indicators from 2000 to 2010, a Landsat module which generates 30 m forest cover change maps between 2000 and 2005, and a calibration module which calibrates the MODIS indicators to final change rates using a systematic sample of Landsat blocks. The MODIS module implements the newly-developed method described in Chapter 3 of this dissertation (Song et al. 2014b). The generation of the 30 m VCF product (i.e. the first part of the Landsat module) is described in detail in Sexton et al. (2013a) and the Landsat forest cover change detection method is introduced in Sexton et al. (2015). The following text briefly summarizes the Landsat module and then focuses on describing the calibration module.

The Landsat data were selected from an improved version of the Global Land Survey (GLS) collection with acquisition dates circa-2000 and -2005 (Channan et al. 2015; Gutman et al. 2013). Leaf-off images in the original GLS were replaced with leaf-on images in the USGS data archive based on MODIS phenology (Kim et al. 2011). The Landsat images were first converted to surface reflectance, filtered with cloud and shadow removal (Huang et al. 2010b), and then integrated with stable MODIS VCF pixels and nonforest samples selected by the training data automation-

support vector machine (TDA-SVM) algorithm to produce tree cover estimates using a regression tree model (Sexton et al. 2013a). Landsat VCF layers of the two epochs were then used to derive forest cover change using a probabilistic bi-temporal change detection method (Sexton et al. 2015).

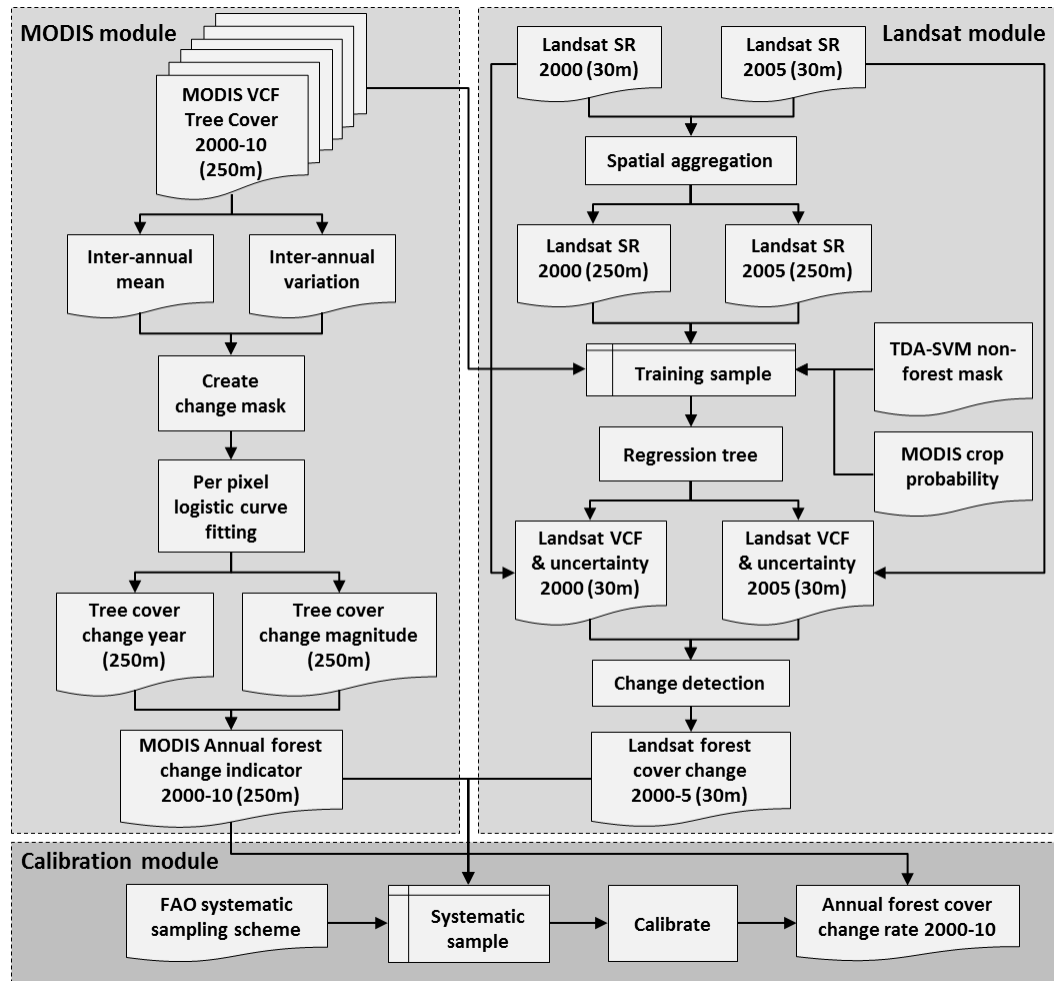


Figure 4.1 Flowchart of generating annual forest cover change rates by integrating MODIS and Landsat.

Since land cover change products derived using MODIS or coarser resolution data are typically considered indicator products, they need to be calibrated using Landsat-based products to produce more accurate change estimates (Hansen et al. 2010; Hansen et al. 2008c; Mayaux and Lambin 1995). We used the systematic

sampling scheme of FAO’s global remote sensing survey to select samples for calibration. Each sample site is 10 km × 10 km at each 1-degree intersection of latitude and longitude (Mayaux et al. 2005). For every sample polygon, both Landsat deforestation and MODIS fitted layers were clipped to the spatial extend of the polygon. Landsat samples contaminated with more than 10 % cloud and cloud shadow pixels in either date were removed. As a result, a total of 89 samples were collected in the study area (Figure 4.2(a)).

The calibration was carried out in two steps: (1) adjusting for the difference between MODIS and Landsat acquisition dates and (2) searching for optimal thresholds to match MODIS-based deforestation rate with Landsat-based rate (Figure 4.2).

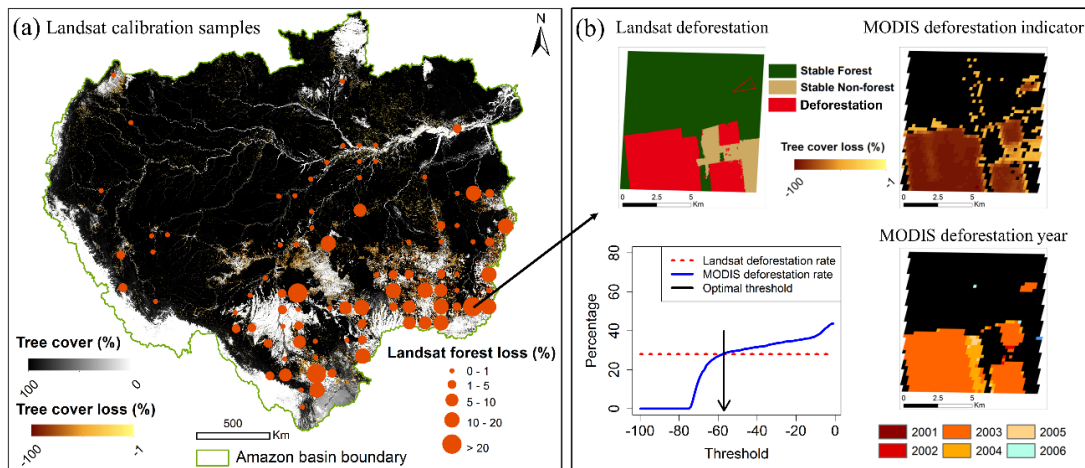


Figure 4.2 Calibrating MODIS indicators to derive accurate deforestation rates. (a) Percent tree cover in year 2000, model-fitted tree cover loss (deforestation indicator) between 2000 and 2010, and the location and deforestation rates of Landsat sample blocks. (b) An example of Landsat deforestation, MODIS deforestation indicator, the optimal threshold and the resulting MODIS deforestation year map.

The acquisition dates of the GLS images range from 2000-01-26 to 2002-11-13 for the 2000 epoch and from 2004-01-02 to 2007-10-29 for the 2005 epoch, which also vary from tile to tile. To resolve the time difference between Landsat and MODIS samples, we linearly normalized the Landsat-based deforestation rates to a common date of 30 June for the particular Landsat acquisition year. Samples contaminated by remaining cloud and cloud shadow (< 10%) were also linearly adjusted, assuming change rates in the cloudy area were the same as cloud-free area of the sample site (Achard et al. 2014; Mayaux et al. 2005; Mayaux et al. 2013). Since parameter c of the VCA algorithm (Chapter 3, equation 3.6) indicates the timing of deforestation, we used the fitted parameter c value to select MODIS pixels where deforestation likely occurred within the two Landsat dates.

The second step was to search an optimal threshold for parameter a (Chapter 3, equation 3.6), such that the MODIS-derived deforestation rate matched with the Landsat-derived deforestation rate (Figure 4.2(b)). This threshold was determined for every sample block and the mean value of a country was applied to all MODIS pixels within the country to label deforestation. Due to the much larger size of Brazil, each of its states was treated as a “country” for the purpose of this calibration. For “countries” that do not have enough samples, we applied a basin-wide average threshold. It should be noted that the use of Landsat sample here was different from previous studies (Achard et al. 2014; Mayaux et al. 2005; Mayaux et al. 2013), in which deforestation rates were determined entirely based on the Landsat sample, whereas we used the sample as representative training to derive a threshold such that our MODIS rates matched Landsat rates at the block level. In most cases, Landsat

blocks functioned mainly as a reference to clean edge pixels and salt-and-pepper noises at the MODIS resolution (Figure 4.2(b)). Our final deforestation rates were derived from the wall-to-wall MODIS data.

4.2.3 Combining deforestation and biomass maps to estimate carbon emissions

The forest carbon density map used in emissions estimate was derived from multi-sources satellite data and *in situ* forest inventory plots (Saatchi et al. 2011). Over one million laser shots were used to derive forest structure metrics, which were related to above-ground biomass, below-ground biomass and carbon density (50% of total biomass) by applying field-calibrated allometric equations. The spatially contiguous carbon density and uncertainty maps were produced by integrating Lidar data with MODIS, shuttle radar topography mission data as well as quick scatterometer data at 1 km resolution.

We followed the standard methodology described in (Achard et al. 2014; Harris et al. 2012b) and the IPCC (Intergovernmental Panel on Climate Change) guidelines (IPCC 2006) in calculating gross carbon emissions from deforestation assuming immediate carbon release at forest clearing. To resolve the resolution discrepancy and reduce the geolocation mismatch between the deforestation map and the carbon density map, we aggregated both maps to 5 km resolution and calculated the lost carbon for every 5 km grid (in Mg C). We then summarized all 5 km grids over the entire study area to calculate carbon emissions for every year between 2000 and 2010.

4.2.4 Uncertainty estimates

Uncertainties in quantifying carbon fluxes from deforestation arise from two major sources: uncertainties in deforestation estimates and uncertainties in biomass estimates (Pelletier et al. 2011; Ramankutty et al. 2007). Here we first characterize errors in the MODIS-based deforestation rates relative to those derived from Landsat data (considered as “truth”) and then combine this error with the carbon error map to analyze errors in emission estimates using an established error propagation model (GOFC-GOLD 2012; IPCC 2006).

Independent deforestation maps produced by the PRODES project were used to evaluate the overall accuracy of the MODIS deforestation. We downloaded a total of 50 Landsat tiles completely covering the Amazon portion of Mato Grosso and Rondonia as reference data. PRODES maps in these areas were chosen because (1) they were generated by local experts using Landsat images and were found highly reliable (Hansen et al. 2008a; INPE 2013; Shimabukuro et al. 2012; Souza et al. 2013); (2) Mato Grosso and Rondonia had high deforestation rates, accounting for about 50% deforestation of the study region; (3) Mato Grosso is dominated by large-scale extensive forest clearing for mechanized agriculture, which is also representative of Para, while Rondonia is famous for its small-scale “fishbone” pattern deforestation for frontier settlements, which is also found in Acre, Amazonas and Roraima (DeFries and Townshend 1994a; Macedo et al. 2012; Morton et al. 2006; Reed et al. 1994); and (4) because these two states are located on the southeastern rim of the Amazon basin, they are less affected by cloud as compared with other Brazilian states within the basin. It should be noted that PRODES has a

minimum mapping unit of 6.25 ha, close to the MODIS resolution but PRODES does not capture the clearing of secondary forests (Hansen et al. 2008a; Shimabukuro et al. 2012), which is included in our map. An annual comparison of MODIS and PRODES deforestation results over the entire Brazilian Amazon will be presented in section 4.3.1 of this chapter. Here we focus on error estimation in a spatially explicit way.

The 30 m PRODES maps with pixels labeled as deforestation between 2000 and 2010 were aggregated to 5 km resolution to derive an 11-year deforestation rates per grid. The MODIS deforestation map was also aggregated to 5 km resolution to derive an overall deforestation rate between 2000 and 2010 (Figure 4.3). We then stratified the points based on MODIS rates (bin = 5%) and calculated the standard derivations of corresponding reference rates for each deforestation level (Figure 4.3(b)). These standard errors were applied to every 5 km grid of the entire study area. Although regional variations exist, the standard errors derived using this independent, large reference sample provide a reasonable error bound for deforestation estimates from MODIS.

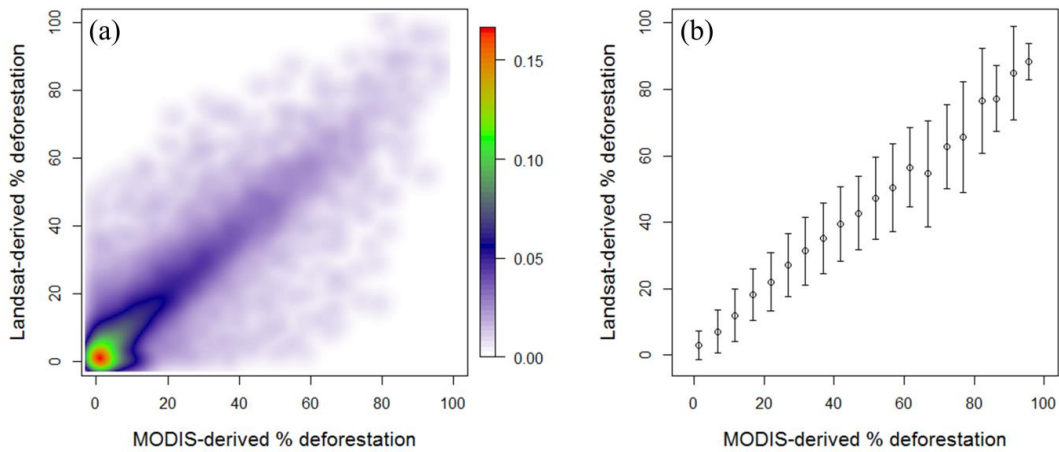


Figure 4.3 Estimating errors in MODIS-derived deforestation rates with Landsat-derived deforestation rates as reference. (a) Density scatter plot with colours representing point density (n=14,322) (b) Error bars represent \pm one standard derivation of Landsat-derived deforestation rates for each deforestation level (bin=5%).

We generated error bound for emission estimates using the error propagation model defined in the following equation. Both deforestation and carbon density error terms are expressed in terms of percentage of relative error and assuming they are independent (GOFC-GOLD 2012; IPCC 2006), the propagation model is given by:

$$\varepsilon_{carbon\ emission} = (\varepsilon_{deforestation}^2 + \varepsilon_{carbon\ density}^2)^{1/2} \quad (4.1)$$

where $\varepsilon_{carbon\ emission}$ refers to errors in emission estimates; $\varepsilon_{deforestation}$ represents errors in deforestation estimates and $\varepsilon_{carbon\ density}$ represents errors in carbon density estimates. Errors in carbon density estimates were quantified from four components including (1) measurement error associated with tree height estimation from Lidar data, (2) allometric error associated with biomass estimation from tree height, (3) sampling error associated with the representativeness of sample plots and

the spatial variation of biomass within a 1 km pixel and (4) prediction error of the machine learning model (Saatchi et al. 2011). The error propagation model was applied to every 5 km grid. We then calculated the upper bound of emission for every grid by adding this error term to the mean estimate as well as the lower bound by subtracting this error term from the mean estimate. Basin-wide upper emission estimate and lower emission estimate was then derived by summarizing all 5 km grids of upper estimate and lower estimate within the study region, respectively.

4.3 Results

4.3.1 Annual deforestation rates in the Amazon basin

The deforestation map products derived through this study identified the year of forest clearing for every MODIS pixel within the Amazon basin (Figure 4.4). Between 2000 and 2010, a total of 15.9 ± 2.5 M ha (million ha) forests were lost, which represented 2.6% of the total basin area, or 2.9% of forests in year 2000. The Brazilian Amazon and the non-Brazilian Amazon lost a total of 12.5 ± 2.0 M ha and 3.4 ± 0.5 M ha forests respectively over that decade. Brazil was the dominant country in terms of deforested area, which accounted for 79% of the total lost forests. Following Brazil, Bolivia contributed the second most deforestation in the last decade, which accounted for 12% ($1,969 \pm 212$ K ha) of the basin total, more than the sum of the Peruvian Amazon (6%, or 979 ± 123 K ha) and the Colombian Amazon (2%, or 287 ± 67 K ha).

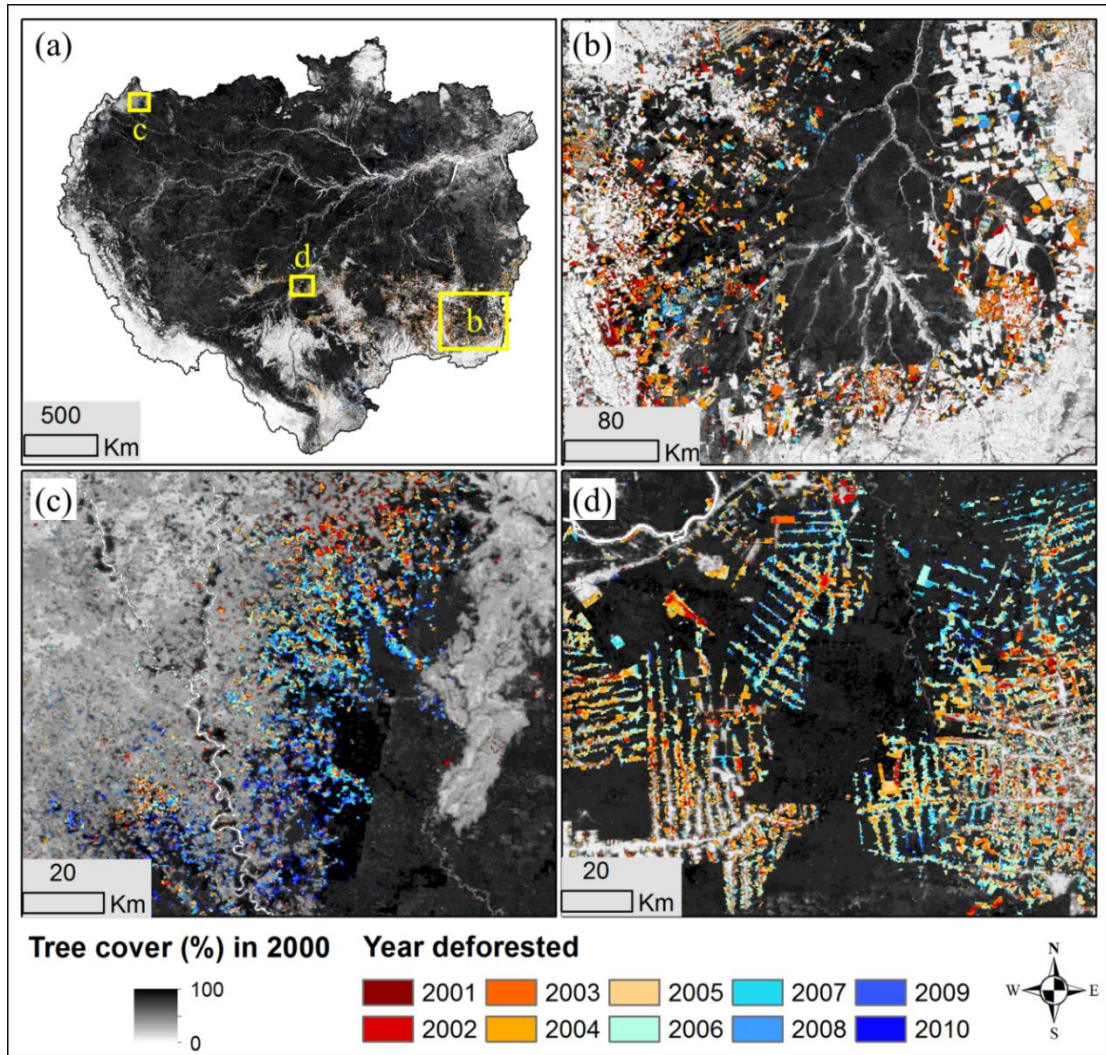


Figure 4.4 Deforestation year map derived from time-series of MODIS VCF tree cover dataset. (a) Overview of the Amazon basin with yellow boxes indicating the locations of regional close-ups. (b) Close-up over the Xingu river basin in Mato Grosso, Brazil. (c) Close-up in Colombia. (d) Close-up in Rondonia, Brazil.

The geographic locations of deforestation were largely concentrated on the southeastern edge of the basin (the so called “arc of deforestation”), with new hotspots emerging in western Amazon (Figure 4.5). Consistent with reports by the Brazilian government, the FAO and other previous studies (FAO 2012; Hansen et al. 2013; INPE 2013; Souza et al. 2013), a declining trend in the Brazilian Amazon and the entire Amazon basin after 2005 was confirmed (Figure 4.6). The annual relative share of Brazil’s deforestation changed dramatically over the study period—from the highest of 87% in the year 2004 to the lowest of 54% by the year 2010. The largest decline in deforestation rate was observed in Mato Grosso, from 1,200 K ha in 2004 to below 100 K ha in 2010. Obvious declines were also observed in Rondonia and Para, though to lesser degrees. These three states accounted for more than 80% of forest clearing in Brazil. In the western and southern parts of the basin, deforestation rates in the Peruvian Amazon and the Bolivian Amazon also decreased slightly after 2006. In the Colombian Amazon, annual rates nearly doubled from 2006 to 2009, although the total area cleared there was much lower than those in the other countries or states.

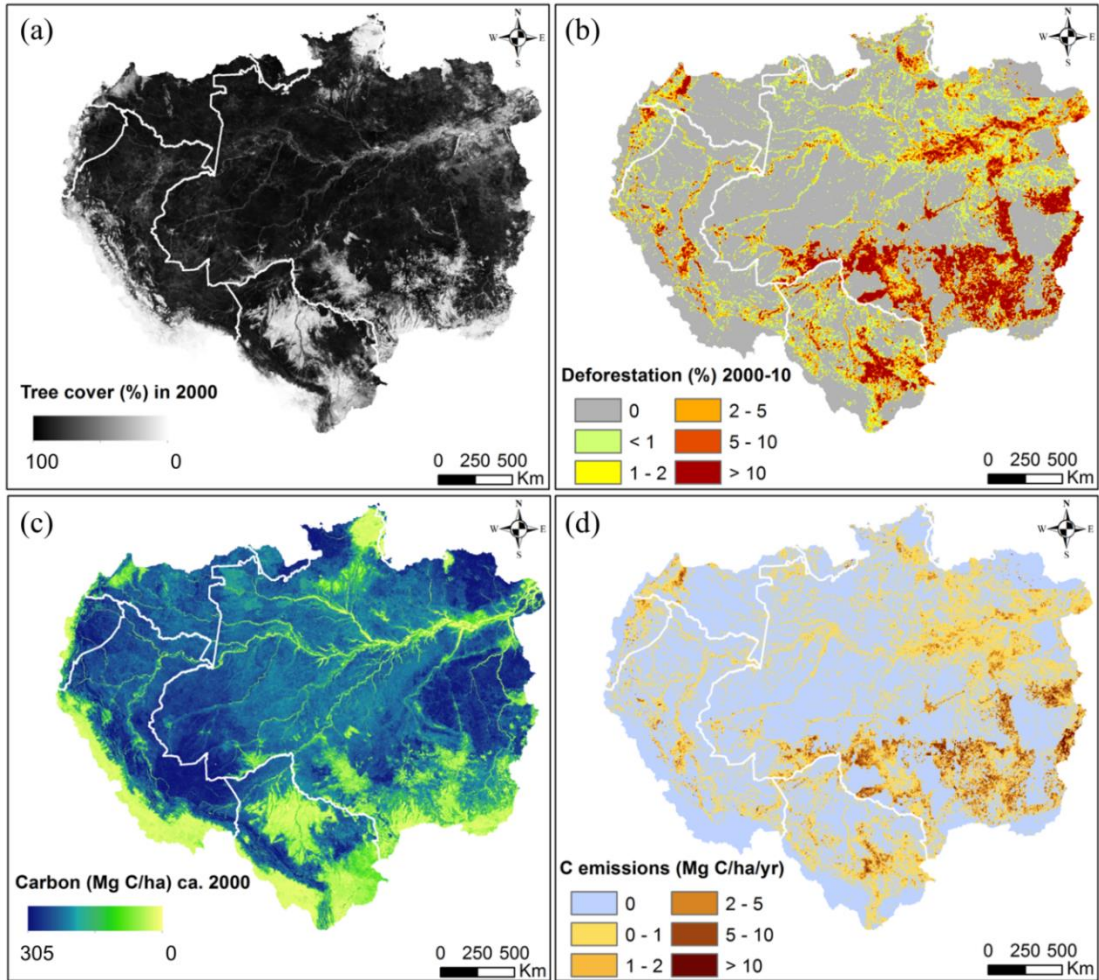


Figure 4.5 Maps of forest, deforestation, carbon stocks and carbon emissions in the Amazon basin. (a) Tree cover in year 2000 (b) Deforestation between 2000 and 2010 at 5 km spatial resolution. (c) Forest carbon density circa 2000. (d) Average C emission rate per unit deforestation at 5 km spatial resolution. White lines delineate country boundaries.

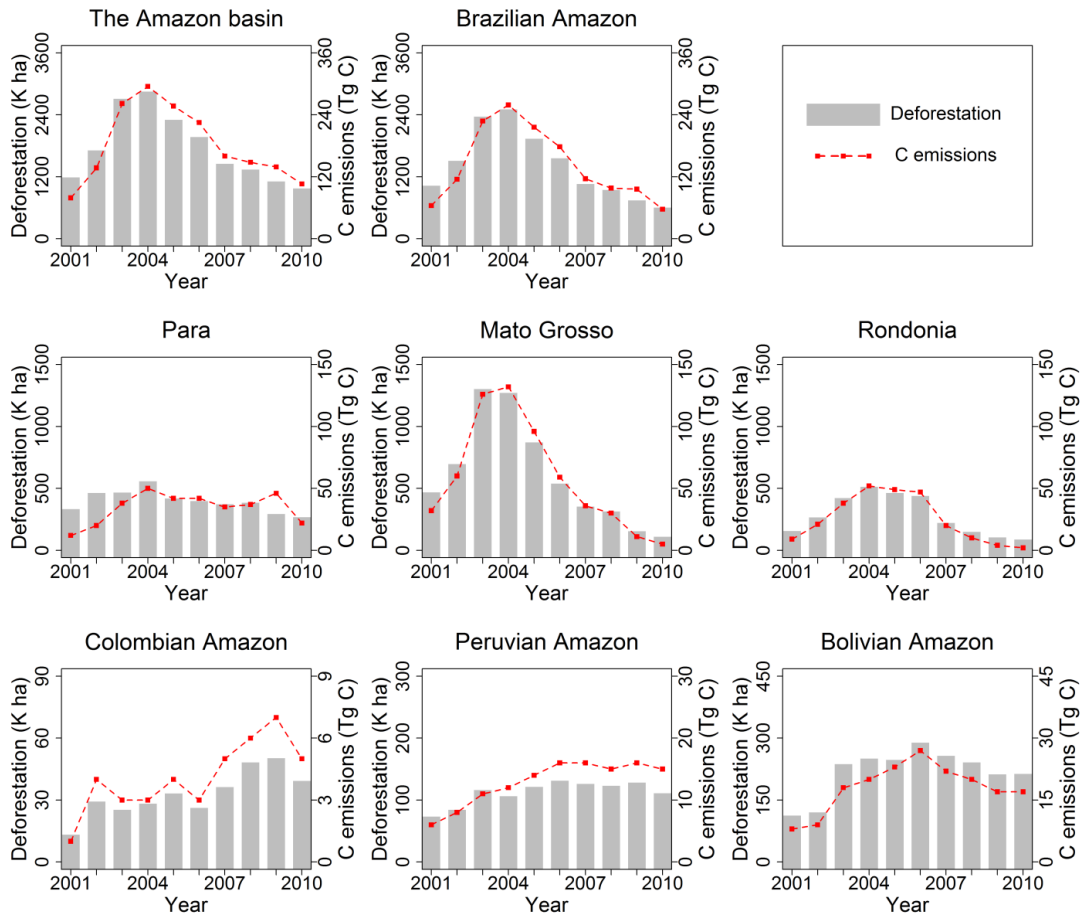


Figure 4.6 Trends of deforestation and associated carbon emissions from 2000 to 2010.

Deforestation estimates derived through this study were comparable to those derived based on Landsat data. At individual patch level, the deforestation maps derived through this study had spatiotemporal patterns similar to the PRODES product (INPE 2013) and a Landsat-based global forest cover loss (GFCL) dataset (Hansen et al. 2013) (Figure 4.7). At the state-level, annual deforestation rates derived through this study were highly correlated with those calculated based on the two Landsat-based products (Figure 4.8). Over the Brazilian Amazon basin, the total

deforestation rates over the 11-year period derived based on PRODES (12.8 M ha) and GFCL (14.6 M ha) were within or near the upper bound of our estimate.

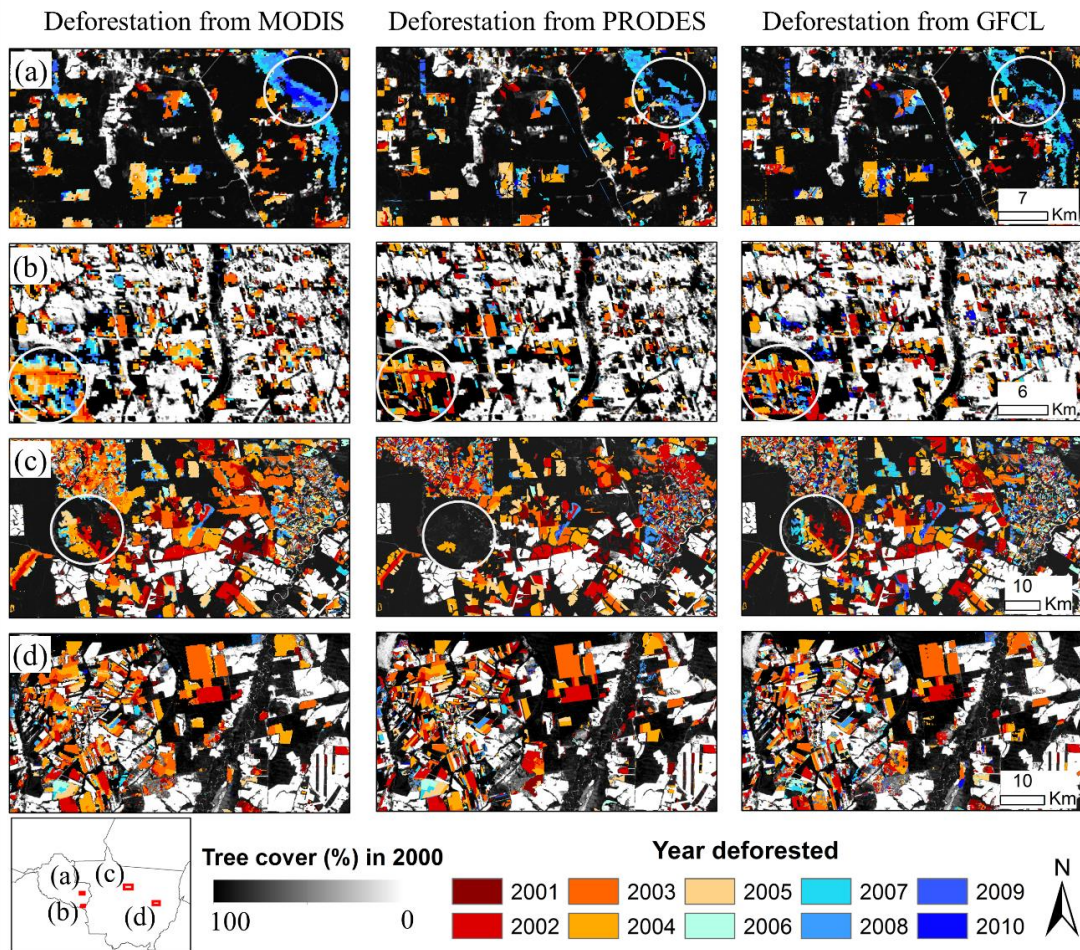


Figure 4.7 Comparing annual deforestation maps derived from MODIS with Landsat-based maps in the Brazilian Amazon. The left column is MODIS results from this study, the middle column is PRODES and the right column is GFCL. The spatiotemporal patterns of deforestation agree remarkably well in these products with some disagreement highlighted in circles. (a) Deforestation near Pimenta Bueno, Rondonia (60.821W, 12.088S); (b) Deforestation to the south of Colorado do Oeste in Rondonia (60.754W, 13.396S); (c) Forests cleared for agriculture in central Mato Grosso (55.974W, 11.466S); (d) Deforestation to the south of indigenous reserves in the lower Xingu river basin in Mato Grosso (53.033W, 13.158S). The MODIS map likely omits cleared patches below the 250 m pixel size and it also tends to

overestimate deforestation over small but inter-connected patches (b). The two Landsat-based products have an advantage to reveal small-patch clearings, but may overlook some deforestation due to missing data from e.g. cloud contamination (a and c).

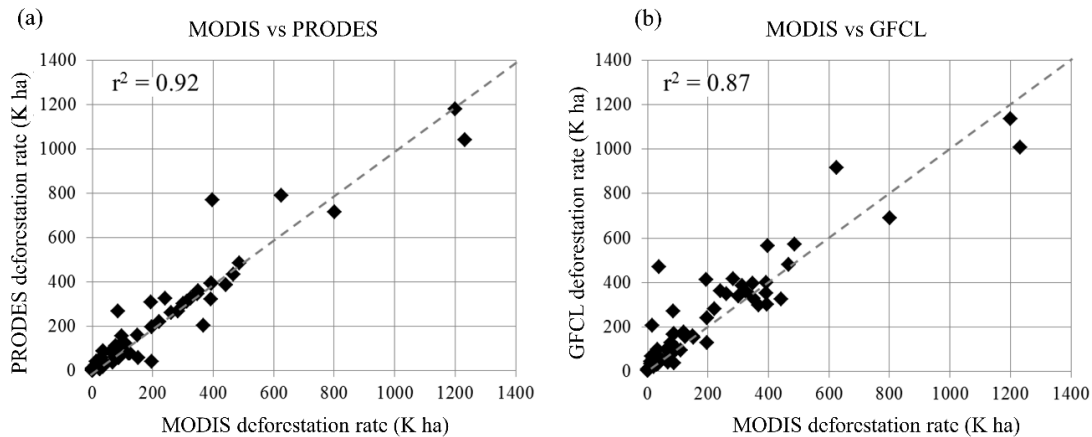


Figure 4.8 Comparing MODIS-derived annual deforestation rates with Landsat results in the Brazilian Amazon. (a) MODIS vs PRODES. (b) MODIS vs GFCL. A total of 70 data points are used in the scatter plot, which represent annual estimates between 2000 and 2010 in seven Brazilian states in the legal Amazon, including Acre, Amapa, Amazonas, Mato Grosso, Para, Rondonia and Roraima.

4.3.2 Annual gross carbon emissions from deforestation in the Amazon basin

Assuming immediate carbon release at forest clearing (Achard et al. 2014; Harris et al. 2012b), the total committed carbon emissions due to loss of above and below ground biomass within the Amazon basin were estimated to be 1.81 ± 0.68 Pg C between 2000 and 2010, or 0.18 ± 0.07 Pg C·yr⁻¹. Not surprisingly, the largest share of emissions was found in Brazil (79%, 143 ± 56 Tg C·yr⁻¹), followed by Bolivia (10%, 18 ± 8 Tg C·yr⁻¹), Peru (7%, 13 ± 3 Tg C·yr⁻¹) and Colombia (2%, 4 ± 1 Tg C·yr⁻¹).

Calculated as the ratio of emission over deforestation area, the average carbon density of cleared forests or emission factors in the IPCC terminology (IPCC 2006) also varied over time and differed substantially among different regions. Here we focus on the 2005-2010 period in discussing the emission factors, because some of the Lidar data used to derive the carbon density map were acquired in 2003-2004 (Saatchi et al. 2011), and hence may not allow accurate calculation of the emission factors for clearing occurred in or before 2004 (Mitchard et al. 2014; Mitchard et al. 2013). The Colombian Amazon and the Peruvian Amazon had the highest emission factors, averaging at $141 \text{ Mg C}\cdot\text{ha}^{-1}$ between 2005 and 2010, followed by Brazil ($129 \text{ Mg C}\cdot\text{ha}^{-1}$) and Bolivia ($94 \text{ Mg C}\cdot\text{ha}^{-1}$). The 2005-2010 basin-wide average emission factor was $130 \text{ Mg C}\cdot\text{ha}^{-1}$. When calculated annually, these emission factors had different trends in different countries (Figure 4.9). From 2005 to 2010, statistically significant increasing trends ($p < 0.05$) were found in Colombia, Peru and Brazil, which had slope values of $6 \text{ Mg C}\cdot\text{ha}^{-1}\cdot\text{yr}^{-1}$ (Colombia), $3 \text{ Mg C}\cdot\text{ha}^{-1}\cdot\text{yr}^{-1}$ (Peru), and $7 \text{ Mg C}\cdot\text{ha}^{-1}\cdot\text{yr}^{-1}$ (Brazil). Bolivia had an opposite trend ($p < 0.001$) with a slope of $-3 \text{ Mg C}\cdot\text{ha}^{-1}\cdot\text{yr}^{-1}$. The basin-wide slope was $7 \text{ Mg C}\cdot\text{ha}^{-1}\cdot\text{yr}^{-1}$ ($p < 0.001$).

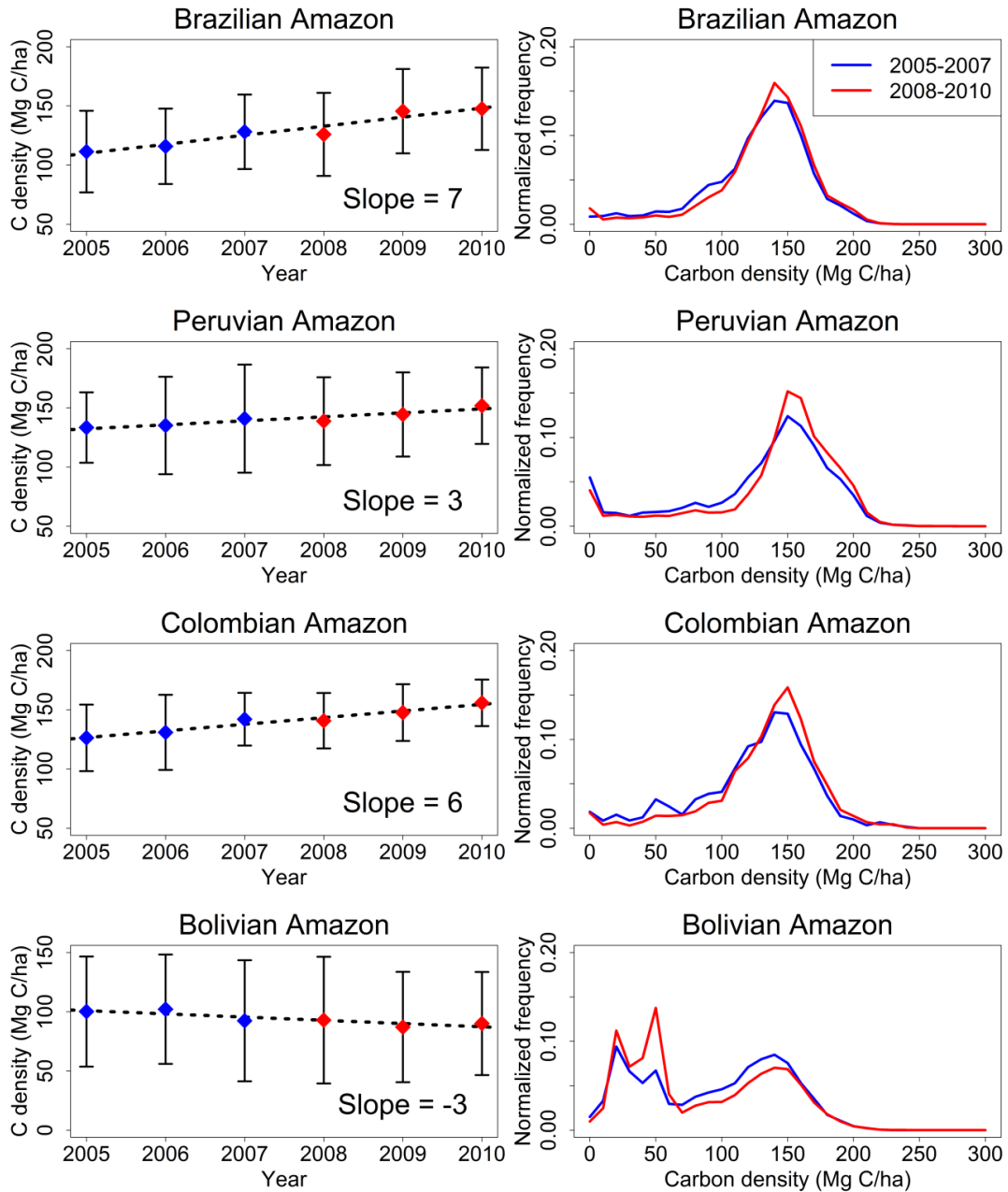


Figure 4.9 Carbon density of lost forests between 2005 and 2010. The left column shows trends in different regions over time. Blue and red diamond dots represent the mean value, with vertical bars representing \pm one standard deviation. Dotted lines represent the linear fit of mean values. The right column shows distributions of carbon density, aggregated to two time periods 2005-2007 (blue lines) and 2008-2010 (red lines).

These trends resulted from changes in the carbon density of the cleared forests. Brazil, Peru, and Colombia had slightly higher proportions of high carbon density forests that were cleared between 2008 and 2010 than those cleared before 2008, while their proportions of low carbon density forests cleared between 2008 and 2010 were lower than those cleared before 2008 (Figure 4.9). These results indicate that deforestation has been progressively encroaching into higher-biomass forests in the Amazon interior. In Brazil this was probably due to the scarcity of available forests in the “arc of deforestation” (i.e. the southeastern Amazon edge) after more than 40 years of continuous clearing (Loarie et al. 2009). The trend in Peru might be partially caused by the recent rapid expansion of gold mining in high-biomass forests in southern Peru (Asner et al. 2013). In Bolivia, the relative proportions of low carbon density forests (i.e., $< 60 \text{ Mg C}\cdot\text{ha}^{-1}$) cleared after 2007 were higher than those cleared between 2005 and 2007, indicating increasing clearing of the low-biomass Chaco forests in this country.

4.4 Discussion

4.4.1 Effectiveness of MODIS VCF products for REDD+ MRV

A key component of REDD+ is a credible system for measuring, reporting and verifying (MRV) changes in forest area and carbon stock (Herold and Skutsch 2009). In general, medium resolution data acquired by Landsat or Landsat-class satellites e.g. SPOT (Satellite Pour l'Observation de la Terre) are deemed necessary for deriving reliable estimates of forest change (Herold 2009). However, many areas have frequent cloud cover and often do not have enough cloud-free images for forest

change assessment at the required temporal intervals (e.g., annual) (Achard et al. 2014; Asner 2001; Broich et al. 2011; Ju and Roy 2008). Some developing countries currently do not even have the minimum capacity for establishing Landsat-based annual forest monitoring systems for REDD+ MRV (Herold 2009; Herold and Skutsch 2009). Since the MODIS VCF based approach for quantifying deforestation and carbon emissions can produce results that are comparable to those derived using Landsat-based approaches, it may serve as a credible alternative when a Landsat-based MRV system is not available or not feasible due to lack of adequate cloud-free Landsat images. From an operational perspective, it is suggested that a nested framework consisted of multi-resolution satellite data as well as in-situ observations should be adopted in order to effectively and accurately monitor changes in forest cover and carbon stock in developing countries (DeFries et al. 2007). The MODIS VCF approach presented in this study may be used as the top layer (i.e. global, coarse-resolution data) of the framework.

Currently, MODIS VCF is produced annually for all land areas of the globe (DiMiceli et al. 2011). However, MODIS images the entire globe on a daily basis and produces near cloud-free global datasets at monthly or seasonal intervals. Therefore, it may allow development of VCF products at sub-annual intervals. Should such sub-annual VCF products become available, the approach developed through this study may allow forest monitoring at sub-annual intervals. This approach likely will be applicable in the foreseeable future, as MODIS-like data will be acquired continuously through the Visible Infrared Imaging Radiometer Suite (VIIRS), which is onboard the Suomi National Polar-orbiting Partnership (S-NPP) satellite launched

in 2011 and will be deployed on the Joint Polar Satellite System (JPSS), NOAA's next generation polar-orbiting operational environmental satellite system.

4.4.2 Implications of annual emission estimates for REDD+ baseline setting

Being able to derive deforestation and emission estimates annually or more frequently may have a significant impact on REDD+ policy. Among numerous challenges confronting REDD+, defining the reference emission level (REL) or baseline is one of the most urgent because REL is a crucial input in determining the amount of financial credits generated from REDD+ (Angelsen 2008; Griscom et al. 2009; Herold et al. 2012; Huettner et al. 2009). A number of proposals have been submitted to UNFCCC for baseline setting, including the combined incentives approach (Strassburg et al. 2009), the compensated reductions approach (Environmental Defense and the Instituto de Pesquisa Ambiental da Amazonia 2007), the corridor approach (Joanneum Research et al. 2006), the Joint Research Centre approach (Mollicone et al. 2007), the stock flow approach (Woods Hole Research Center and Amazon Institute for Environmental Research 2008) and the Terrestrial Carbon Group approach (Terrestrial Carbon Group 2008). A common component of baseline in these proposed methods is the historical emission rate, which refers to the mean emission rate over a moderately long time period (e.g. 5-10 years). While the scientific community has yet to reach a consensus on the methods for setting REL (Griscom et al. 2009), we argue that any method selected should be flexible enough to account for the different temporal dynamics of deforestation emissions in different countries.

The temporal dynamics of emissions observed in this study indicate that determining consistent REL for REDD+ may often be difficult. A marked example being that the Brazilian Amazon and the non-Brazilian Amazon have experienced generally opposite trends over the last decade (Figure 4.10). Emissions from deforestation also present various patterns of inter-annual variability at different spatial and temporal scales (Figure 4.6). High inter-annual variability can create particular challenges in a REDD+ payment system, as funding flows would vary greatly from year to year with the REL fixed over several years. Hence, trends and inter-annual variability within a specific time frame are highly relevant metrics for a REL formula. In practice, future reduction in deforestation under specific mitigation projects should be treated differently when the reduction is within or exceeds the natural variability.

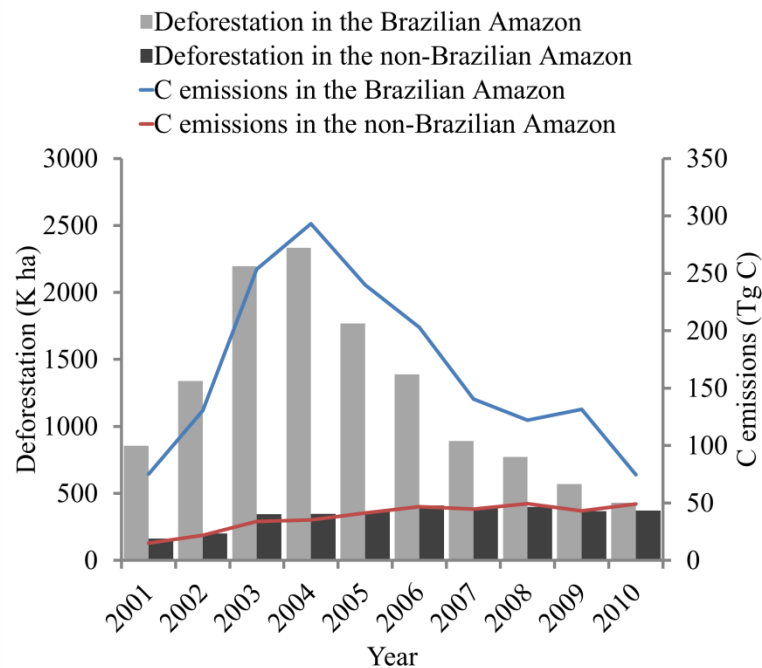


Figure 4.10 Annual deforestation and associated carbon emissions in the Brazilian and non-Brazilian Amazon.

Additional complexities to REDD+ REL setting are related to forest degradation (the second “D”) and forest regrowth (the “+”), which are not assessed in this study. It has been suggested that selective logging could contribute as much as 25% more carbon emissions in the Brazilian Amazon than accounting for deforestation alone (Asner et al. 2005). Tropical regrowth forests can offset as much as 50% of gross carbon emissions from deforestation (Houghton et al. 2012; Pan et al. 2011). However, compared with the estimation of carbon emissions from deforestation, how to accurately quantify carbon fluxes from forest degradation and forest regrowth remains an open scientific question (Aguilar et al. 2012).

4.4.3 Uncertainties in carbon emissions from deforestation

It remains a major challenge to conduct a comprehensive assessment of uncertainties in carbon emission estimation (Houghton et al. 2012; Ramankutty et al. 2007). In this study we take into account the two largest sources of uncertainty in emission estimation—uncertainties in deforestation estimates and uncertainties in biomass estimates. Discussion on the relative contribution of deforestation data and biomass data as well as the scale of analysis to emission uncertainty can be found in previous studies (Aguilar et al. 2012; Ometto et al. 2014; Pelletier et al. 2011; Tyukavina et al. 2013). Our deforestation area estimates derived from MODIS VCF and Landsat sample are proved to have $\pm 16\%$ uncertainty. Due to the combined uncertainties from both datasets, the emission rates have an uncertainty range of $\pm 38\%$. This suggests that one third of the emission uncertainties are inherited from the deforestation map and two thirds are from the biomass map. Compared with other remote sensing-based emission estimates, our uncertainty range is smaller than DeFries *et al.* (42-50%)

(DeFries et al. 2002) and Harris *et al.* (40%) (Harris et al. 2012b), but larger than Achard *et al.* (27%) (Achard et al. 2004) and Achard *et al.* (33-36%) (Achard et al. 2014).

The factor that is not explicitly considered here but may potentially increase our uncertainty estimates is errors associated with the Landsat reference data (i.e. errors in PRODES due to cloud or misclassification). If we were to estimate net carbon emissions, potential uncertainties would also include those associated with other forest dynamics such as degradation and regrowth, those associated with other significant carbon pools (i.e. dead wood, litter and soil) as well as those associated with the land cover dynamics on deforested land. Beside these factors, to reach a conceptually comprehensive estimate of carbon emissions from land cover and land use change as well as associated uncertainty, Houghton *et al.* (2012) summarize a list of land use processes that are often omitted in many or all existing studies, which includes forest management, agricultural management, fire management, land degradation, peatlands, wetlands and mangroves, human settlements and infrastructure, erosion/redeposition and woody encroachment.

4.4.4 Risks of future deforestation in the Amazon

Closed-canopy forests in the Amazon have high carbon stocks peaked around 150 Mg C·ha⁻¹ (Figure 4.11), but deforestation in tropical America is reported to have occurred in relatively lower-biomass lands between 2000 and 2005—the average carbon density of lost forests is 90 Mg C·ha⁻¹ by (Harris et al. 2012a; Harris et al. 2012b) and 88 Mg C·ha⁻¹ by (Baccini et al. 2012)). Our results reveal the same conclusion for the period of 2005-2010—the basin-wide average carbon density of

remaining forests in year 2010 is $144 \text{ Mg C}\cdot\text{ha}^{-1}$, ~11% higher than the average carbon density of cleared forests after 2005 ($130 \text{ Mg C}\cdot\text{ha}^{-1}$). Methodologically, this suggests that using a biome-level average biomass value in non-spatial carbon accounting models e.g. the bookkeeping model (Ramankutty et al. 2007) or the IPCC Tier 1 and Tier 2 approaches (IPCC 2006) may overestimate emissions by more than 10%. It is also reported that deforestation has been encroaching into higher-biomass lands between 2001 and 2007 in the Brazilian Amazon (Loarie et al. 2009). Our findings here show that the encroaching trend continues to year 2010. This trend would boost future carbon emissions from deforestation, if deforestation rates increase or even remain stable.

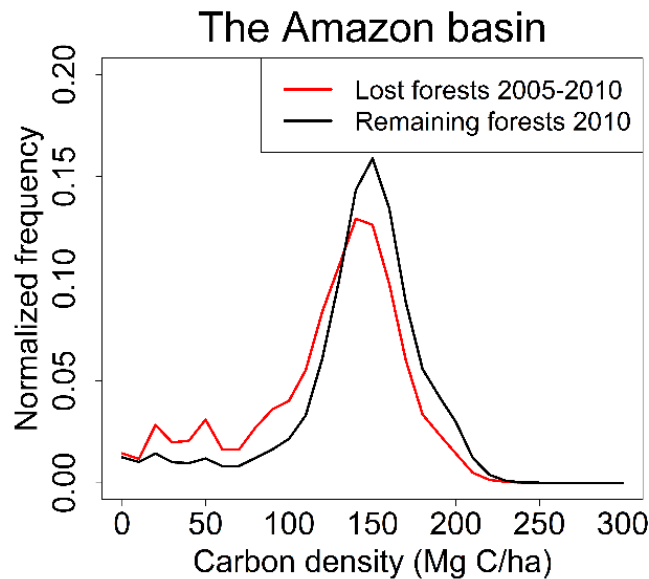


Figure 4.11 Carbon density of lost forests and remaining forests in 2010. Deforestation in the Amazon basin occurred in relatively lower biomass forests between 2005 and 2010.

Deforestation in the Brazilian Amazon has been attracting huge attention from the scientific community as well as the general public. However, ~40% of the Amazonian rainforests grow outside Brazil. Forests in western Amazon contain the highest live biomass as well as the richest biodiversity, including a large number of endemic and threatened species (Pimm et al. 2014). From 2000 to 2010, the Bolivian Amazon, the Peruvian Amazon and the Colombian Amazon all experienced an increase in deforestation when deforestation in the Brazilian Amazon plunged. Whether the low deforestation rate in Brazil can be sustained or not is yet to be determined. Questions can also be asked, for example, are these countries at different phases of forest transition (Rudel et al. 2005)? Or, will the rising deforestation in the non-Brazilian Amazon continue? Relatively higher deforestation rates were found on the Bolivia and Peru side along the Brazil/Bolivia/Peru tri-national border after 2007 when forests on the Brazil side have been either cleared or designated as protected areas (Figure 4.12). Because accessibility to a road is often closely related to deforestation (Chomitz and Gray 1996; Cropper et al. 1999), the risks that the “arc of deforestation” may expand from Brazil to the most bio-diverse, most carbon-rich, yet mostly unprotected rainforests in Northern Bolivia and Southern Peru following the recent completion of the interoceanic highway appear high (Perz et al. 2013).

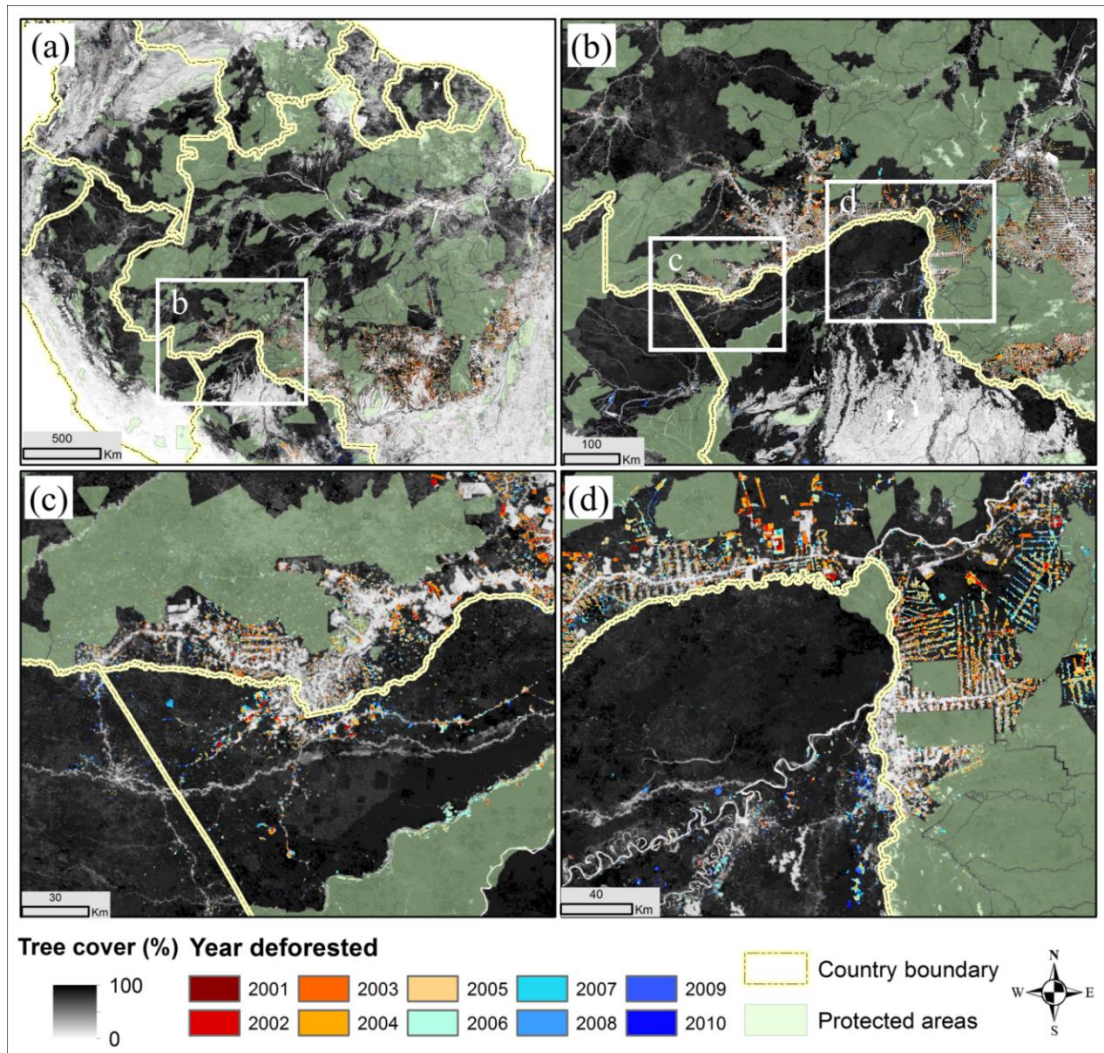


Figure 4.12 Forest, deforestation and protected areas in the Amazon basin. Four map layers are overlaying on each other in the order of (from top to bottom): country boundary, protected areas, deforestation year map and tree cover map in year 2000. (a) Overview of the entire basin. (b) A close-up in the Brazil/Bolivia/Peru tri-national border where forests on the Brazil side are either cleared or protected. (c) Further zoom-in over the city of Cobija, the capital of the Bolivian Pando Department. The inter-oceanic highway begins in this region. (d) Zoom-in over the city of Guayaramerin, where more deforestation is observed on the Bolivia side after year 2006.

4.4 Conclusions

We have demonstrated the effective use of satellite data for estimating deforestation and associated carbon emissions on a year-to-year basis. The increased temporal resolution is useful for understanding the global atmospheric CO₂ variability and also provides important information for emerging policies such as REDD+. We found that carbon emissions from deforestation varied considerably not only among different regions but also from year to year. Largely driven by Brazil's efforts to halt deforestation in recent years (Nepstad et al. 2014), deforestation rates over the Brazilian Amazon and the entire basin declined significantly in the second half of the last decade, which resulted in greatly reduced carbon emissions. An opposite emission trend was observed in the non-Brazilian Amazon; this consisted of various inter-annual variability in the Bolivian Amazon, the Colombian Amazon and the Peruvian Amazon. Furthermore, forests of higher-biomass accounted for an increasing portion of the cleared area. This trend plus the fact that remaining forests have higher biomass than previously cleared forests poses a new challenge for projecting carbon fluxes of future deforestation. Using a national or regional average carbon density value in non-spatial carbon accounting models may overestimate emissions by more than 10%. Spatially explicit and temporally consistent monitoring of forest cover and carbon stocks, like those used in this study, are needed to address this problem. Since our method essentially depends on long-term operational meteorological satellite data for deforestation monitoring, continuity of this study is expected in the foreseeable future. Ultimately, a comprehensive understanding of the complex and dynamic drivers of deforestation is needed to devise effective policies to

mitigate global deforestation.

Chapter 5: Conclusion

5.1 Summary of research

The studies presented in this dissertation addressed a range of issues related to the use of satellite data for quantifying forest cover change (FCC). Contributions to the literature include a new data-fusion method and the resulting improved global forest cover dataset, a statistical algorithm for detecting FCC at an annual frequency, and findings on the trend and inter-annual variability of deforestation and committed carbon emissions in the Amazon basin between 2000 and 2010. Although the research was focused on the impact of FCC on the carbon cycle, these results would also have significant impact on understanding the causes of changes in the hydrological cycle as well as changes in terrestrial biodiversity. In this chapter, I will briefly review each study and draw implications for future research.

Several global land cover products have been generated by different research groups using various satellite data and methods. Collectively these maps represent our current best knowledge on global land cover. However, substantial discrepancies exist in their representation of forest, with obvious overestimation by some datasets and underestimation by others. In Chapter 2 I described an analysis on the global patterns of agreement and disagreement between GLCC, UMD LC, GLC2000, MODIS LC, MODIS VCF, and GlobCover. Different products tend to agree more with each other in places with either low or high forest cover but disagree considerably in places with moderate forest cover, implying great difficulties in characterizing moderate forest cover with coarse-resolution data. Based on reference data with finer resolution and

higher accuracy, these coarse-resolution datasets were integrated to generate a more accurate forest cover map. The developed method was applied at the global scale.

With unknown error structure, independently generated land cover datasets of different times cannot be directly subtracted to quantify land cover change. Chapter 3 presented an algorithm, called VCF-based Change Analysis (VCA), for detecting annual forest cover change using the yearly MODIS VCF product. A reasonable assumption of the i.i.d. error distribution was made because annual tree cover was independently estimated from the same data source and with the same procedure. Based on this assumption, land cover change pixels were proved to be outliers of a chi-square distribution of continuous land cover estimates. Then a logistic function was designed to model per-pixel forest cover change by conceptualizing changes in forest cover as continuous processes over time. The algorithm was quantitatively evaluated in two forest biomes with distinct patterns of FCC. This simple and efficient algorithm was also applied at continental scales to derive MODIS-based forest disturbance indicators.

To understand the temporal dynamics of carbon emissions from deforestation and its implications for REDD+ policy, Chapter 4 of the dissertation presented a study that quantified annual deforestation emissions in the Amazon basin between 2000 and 2010. Annual deforestation data were derived from MODIS VCF by applying the VCA algorithm and calibrated with Landsat samples. Annual emission rates were derived by combining the deforestation data with a spatially explicit biomass dataset. Increasing the temporal resolution of the emission estimation to an annual frequency has led to the finding that carbon emissions from deforestation vary

considerably not only among different regions but also from year to year. A spatial analysis of the trend of deforestation locations and biomass distribution concluded that deforestation has been progressively encroaching into higher biomass lands in the Amazon interior. These observed dynamics may have significant implications for REDD+ policy. Satellite data at coarse spatial resolution but fine temporal resolution should play an important role in monitoring, reporting and verifying (MRV) forest cover and carbon stock change in developing countries. When setting the reference emission level (REL) for REDD+, trends and inter-annual variability of deforestation emissions within a specific time frame are greatly relevant metrics for an REL formula. Thus, future reduction in deforestation under specific mitigation projects should be treated differently when the reduction is within or exceeds the natural variability.

5.2 Implications for future research

Classifying land cover at the global scale requires comprehensive training samples to capture the complexity of land surface characteristics (Ban et al. 2015). Deriving sufficient and representative training in an automated manner is, therefore, a critical step in operational global land cover mapping (Townshend et al. 2012). For forest cover characterization and change detection, several studies have demonstrated the feasibility of using “stable pixels” of existing land cover products (e.g. MODIS VCF or Landsat VCF) as training for generating new products at different spatial resolutions or at different times (Hansen et al. 2008b; Huang et al. 2008; Kim et al. 2014; Sexton et al. 2013a). In contrast, usage of a limited human-interpreted training sample has resulted in a global land cover map with lower accuracy (Gong et al.

2013). However, forest cover is perhaps one of the easiest land cover types to characterize using remotely sensed data because of its spatial and spectral homogeneity, its relatively long growing season, and stable seasonality. Other classes, such as cropland or urban are more difficult to characterize because of their greater spectral variability, smaller field size, and various phenology.

The cross-product comparison and integration analysis presented in Chapter 2 of the dissertation suggests that the existing coarse-resolution land cover maps, although each has its unknown uncertainty, collectively can reveal to a certain degree the true land cover type on the ground, especially in highly agreed areas. Can we use the embedded knowledge in the land cover agreement/disagreement map to form an efficient strategy to guide training collection for future land cover mapping? Pixels that are classified to the same class by several independent maps may be considered reliable and directly used as training. A training sample may need to be augmented in places where different products show large disagreement. The applicability of these ideas is subject to evaluation in future research.

Error assessment of land cover maps is a time- and resource-consuming, but necessary prerequisite to realizing the value of land cover data in subsequent applications, such as area estimation. A traditional confusion matrix generated using a probabilistic sample is useful for adjusting bias and deriving confidence intervals for area statistics at the map level (Foody 2002; Olofsson et al. 2013). However, having a quality assurance (QA) layer associated with a land cover layer may enable more advanced analysis in a spatially explicit manner. For instance, knowing the error distribution or having per-pixel quality indicators are essential for some post-

classification change-detection algorithms (e.g. VCA or Sexton et al. [2015]). Per-pixel accuracy on land cover change is also crucial for analyzing the propagation of error in downstream applications, such as carbon emission estimation. The error layer associated with the current Landsat VCF product (Sexton et al. 2013) contains errors inherited from training data and errors introduced by the classification algorithm. How to incorporate other error sources, such as atmospheric contamination, terrain effect or BRDF effect, into per-pixel classification in a statistically coherent manner is also a line of future research.

Land cover conversion often exhibits a strong contrast before and after change that is detectable with multi-spectral data. However, land cover modification notably forest degradation, which does not necessarily lead to categorical cover change, poses major challenges to optical data (Lambin 1999). Processes causing forest degradation include selective logging, fragmentation, and conversion of primary forests to secondary forests (Asner et al. 2005; Laurance et al. 1997; Margono et al. 2014; Putz et al. 2014). Quantifying changes in vegetation structure and biomass caused by forest degradation may require an integrated use of optical, Radar and Lidar data coupled with ecological processes. Compared with deforestation, the extent and severity of global forest degradation, the resultant carbon dynamics, and its contribution to the uncertainty of the global carbon cycle is still largely unknown. The developed FCC method may find its use in degradation mapping.

Land change science seeks to understand the dynamics of land cover and land use change (LCLUC) as a coupled human-environment system (Turner et al. 2007). As an interdisciplinary field, land change science still lacks a comprehensive theory

for guiding land use decisions—a theory that can address the challenge of balancing trade-offs between satisfying immediate human needs and maintaining long-term ecosystem functions (DeFries et al. 2004; Foley et al. 2005). Satellite remote sensing provides an effective tool for quantifying rates and monitoring spatial patterns of LCLUC, which serve as the empirical foundation for understanding the causes, impacts and feedbacks of land change. With reliable, uninterrupted time series of forest cover change data, it may be possible to examine the idea of “forest transition”—forest area over a territory decreases with economic development until the economy industrializes, in which case forest recovers with altered composition and structure (Barbier et al. 2010; Mather 1992; Rudel et al. 2005). Future research could also investigate the diverse and dynamic drivers of deforestation (Geist and Lambin 2002). A prerequisite step would be attributing every patch/pixel of identified forest cover loss to specific causes, such as timber extraction, food production, biofuel production and urban development.

Looking forward, an inevitable trend is predicted that the global, operational retrieval of land cover and other biophysical variables, such as vegetation productivity, from satellite data will be conducted at an increasing spatial resolution. In particular, data acquired by the Landsat series of sensors, with their global coverage, more than four-decade temporal span, tens of meters resolution, and dense time series, serve as the most valuable data source for monitoring natural disturbances and human modification of land. Mining the freely available Landsat archive is the easiest way to reconstruct the most comprehensive land use change history such as deforestation, cropland expansion and urbanization over the past half century. In

doing so, new knowledge on human-environment interaction will be gained. Research presented in this dissertation also points out ways to move forward in this direction.

Glossary

AVHRR	Advanced Very High Resolution Radiometer
BFAST	Breaks for Additive Seasonal and Trend
BRDF	Bidirectional reflectance distribution function
CO ₂	Carbon Dioxide
CONUS	Conterminous United States
D&FD	Deforestation and forest degradation
DBH	Diameter at breast height
DCW	Digital Chart of the World
Df	Degrees of freedom
EOSD	Earth Observation for Sustainable Development of Forests
ETM+	Enhanced Thematic Mapper Plus
FAO	Food and Agriculture Organization of the United Nations
FCC	Forest cover change
FIA	Forest Inventory Analysis
GFCL	Global forest cover loss
GIS	Geographic Information System
GLC2000	Global Land Cover 2000
GLCC	Global Land Cover Characterization
GlobCover	GlobCover land cover product
GLS	Global Land Survey
GOFC-GOLD	Global Observations of Forest Cover and Land Cover Dynamics
I.I.D.	Independent and identical distribution
IGBP	International Geosphere-Biosphere Programme
IPCC	Intergovernmental Panel on Climate Change
IPFC	Integrated percent forest cover
JPSS	Joint Polar Satellite System
JRC	Joint Research Center
LCCS	Land Cover Classification System
LCLUC	land cover and land use change
LEDAPS	Landsat Ecosystem Disturbance Adaptive Processing System
Lidar	Light detection and ranging
MAE	Mean absolute error
MBE	Mean bias error
MLE	Maximum likelihood estimation
MODIS	Moderate Resolution Imaging Spectroradiometer
MRV	Measurement, Reporting and Verification
MSS	Multispectral Scanner
MT	Mato Grosso
NDVI	Normalized Difference Vegetation Index
NLCD	National Land Cover Database
NOAA	National Oceanic and Atmospheric Administration
PRODES	Deforestation Monitoring in the Brazilian Amazon

QA	Quality assurance
Q-Q	Quantile-Quantile
REDD+	Reducing emissions from deforestation and forest degradation
REL	Reference emission level
RMSE	Root mean square error
SAR	Synthetic Aperture Radar
SiB	Simple Biosphere model
S-NPP	Suomi National Polar-orbiting Partnership
SPOT	Satellite Pour l'Observation de la Terre
SR	Surface reflectance
TDA-SVM	Training data automation-support vector machine
TM	Thematic Mapper
TOA	Top-of-atmosphere
UMD LC	University of Maryland land cover product
UNFCCC	United Nations Framework Convention on Climate Change
USGS	United States Geological Survey
VCA	VCF-based Change Analysis
VCF	Vegetation Continuous Fields
VCT	Vegetation change tracker
VIIRS	Visible Infrared Imaging Radiometer Suite
WA	Washington State

Bibliography

- Achard, F., Beuchle, R., Mayaux, P., Stibig, H.J., Bodart, C., Brink, A., Carboni, S., Desclee, B., Donnay, F., Eva, H.D., Lupi, A., Rasi, R., Seliger, R., & Simonetti, D. (2014). Determination of tropical deforestation rates and related carbon losses from 1990 to 2010. *Glob Chang Biol*, In press
- Achard, F., DeFries, R., Eva, H., Hansen, M., Mayaux, P., & Stibig, H.J. (2007). Pan-tropical monitoring of deforestation. *Environmental Research Letters*, 2, 045022
- Achard, F., Eva, H.D., Mayaux, P., Stibig, H.-J., & Belward, A. (2004). Improved estimates of net carbon emissions from land cover change in the tropics for the 1990s. *Global Biogeochemical Cycles*, 18, GB2008
- Aguiar, A.P.D., Ometto, J.P., Nobre, C., Lapola, D.M., Almeida, C., Vieira, I.C., Soares, J.V., Alvala, R., Saatchi, S., Valeriano, D., & Castilla-Rubio, J.C. (2012). Modeling the spatial and temporal heterogeneity of deforestation-driven carbon emissions: the INPE-EM framework applied to the Brazilian Amazon. *Global Change Biology*, 18, 3346-3366
- Angelsen, A. (2008). REDD models and baselines. *International Forestry Review*, 10, 465-475
- Asner, G.P. (2001). Cloud cover in Landsat observations of the Brazilian Amazon. *International Journal of Remote Sensing*, 22, 3855-3862
- Asner, G.P., Clark, J.K., Mascaró, J., Galindo García, G.A., Chadwick, K.D., Navarrete Encinales, D.A., Paez-Acosta, G., Cabrera Montenegro, E., Kennedy-Bowdoin, T., Duque, Á., Balaji, A., von Hildebrand, P., Maatoug, L., Phillips Bernal, J.F., Yepes Quintero, A.P., Knapp, D.E., García Dávila, M.C., Jacobson, J., & Ordóñez, M.F. (2012). High-resolution mapping of forest carbon stocks in the Colombian Amazon. *Biogeosciences*, 9, 2683-2696
- Asner, G.P., Knapp, D.E., Broadbent, E.N., Oliveira, P.J., Keller, M., & Silva, J.N. (2005). Selective logging in the Brazilian Amazon. *Science*, 310, 480-482
- Asner, G.P., Llactayo, W., Tupayachi, R., & Luna, E.R.e. (2013). Elevated rates of gold mining in the Amazon revealed through high-resolution monitoring. *Proc Natl Acad Sci USA*, 110, 18454-18459
- Baccini, A., Goetz, S.J., Walker, W.S., Laporte, N.T., Sun, M., Sulla-Menashe, D., Hackler, J., Beck, P.S.A., Dubayah, R., Friedl, M.A., Samanta, S., & Houghton, R.A. (2012). Estimated carbon dioxide emissions from tropical deforestation improved by carbon-density maps. *Nature Climate Change*, 2, 182-185

- Ban, Y., Gong, P., & Giri, C. (2015). Global land cover mapping using Earth observation satellite data: Recent progresses and challenges. *ISPRS Journal of Photogrammetry and Remote Sensing*
- Barbier, E.B., Burgess, J.C., & Grainger, A. (2010). The forest transition: Towards a more comprehensive theoretical framework. *Land Use Policy*, 27, 98-107
- Bartholomé, E., & Belward, A.S. (2005). GLC2000: a new approach to global land cover mapping from Earth observation data. *International Journal of Remote Sensing*, 26, 1959-1977
- Belward, A.S. (1996). The IGBP-DIS global 1 km land cover data set "DISCover": Proposal and implementation plans. In, *Report of the Land Cover Working Group of IGBP-DIS*. Toulouse, France: IGBP-DIS Office
- Bicheron, P., Defourny, P., Brockmann, C., Schouten, L., Vancutsem, C., Huc, M., Bontemps, S., Leroy, M., Achard, F., Herold, M., Ranera, F., & Arino, O. (2008). GlobCover: Products Description and Validation Report. In. Toulouse Cedex, France
- Bonan, G.B. (2008). Forests and climate change: forcings, feedbacks, and the climate benefits of forests. *Science*, 320, 1444-1449
- Bonan, G.B., Levis, S., Kergoat, L., & Oleson, K.W. (2002a). Landscapes as patches of plant functional types: An integrating concept for climate and ecosystem models. *Global Biogeochemical Cycles*, 16, 1021
- Bonan, G.B., Oleson, K.W., Vertenstein, M., Levis, S., Zeng, X., Dai, Y., Dickinson, R.E., & Yang, Z.-L. (2002b). The Land Surface Climatology of the Community Land Model Coupled to the NCAR Community Climate Model*. *Journal of Climate*, 15, 3123-3149
- Bousquet, P., Peylin, P., Ciais, P., Le Quere, C., Friedlingstein, P., & Tans, P.P. (2000). Regional Changes in Carbon Dioxide Fluxes of Land and Oceans Since 1980. *Science*, 290, 1342-1346
- Brando, P.M., Balch, J.K., Nepstad, D.C., Morton, D.C., Putz, F.E., Coe, M.T., Silverio, D., Macedo, M.N., Davidson, E.A., Nobrega, C.C., Alencar, A., & Soares-Filho, B.S. (2014). Abrupt increases in Amazonian tree mortality due to drought-fire interactions. *Proc Natl Acad Sci USA*, 111, 6347-6352
- Breiman, L., Friedman, J.H., Olshen, R.A., & Stone, C.J. (1984). *Classification and regression trees*. Boca Raton, Florida: Chapman & Hall/CRC
- Broich, M., Hansen, M.C., Potapov, P., Adusei, B., Lindquist, E., & Stehman, S.V. (2011). Time-series analysis of multi-resolution optical imagery for quantifying forest cover loss in Sumatra and Kalimantan, Indonesia. *International Journal of Applied Earth Observation and Geoinformation*, 13, 277-291

- Brown, S. (1997). *Estimating biomass and biomass change of tropical forests: A primer. FAO Forestry Paper 134*. Rome: Food and Agriculture Organization of the United Nations
- Brown, S., & Zarin, D. (2013). What does zero deforestation mean? *Science*, *342*, 805-807
- Canadell, J.G., Le Quere, C., Raupach, M.R., Field, C.B., Buitenhuis, E.T., Ciais, P., Conway, T.J., Gillett, N.P., Houghton, R.A., & Marland, G. (2007). Contributions to accelerating atmospheric CO₂ growth from economic activity, carbon intensity, and efficiency of natural sinks. *Proceedings of the National Academy of Sciences of the United States of America*, *104*, 18866-18870
- Channan, S., Feng, M., Kim, D.-H., Sexton, J.O., Song, X.-P., Song, D.-X., Noojipady, P., Collins, K., Anand, A., & Townshend, J.R. (2015). The GLS+: An Enhancement of the Global Land Survey Datasets. *Photogrammetric Engineering & Remote Sensing*
- Chave, J., Andalo, C., Brown, S., Cairns, M.A., Chambers, J.Q., Eamus, D., Fölster, H., Fromard, F., Higuchi, N., Kira, T., Lescure, J.-P., Nelson, B.W., Ogawa, H., Puig, H., Riera, B., & Yamakura, T. (2005). Tree allometry and improved estimation of carbon stocks and balance in tropical forests. *Oecologia*, *145*, 87-99
- Chen, J., Chen, J., Liao, A., Cao, X., Chen, L., Chen, X., He, C., Han, G., Peng, S., Lu, M., Zhang, W., Tong, X., & Mills, J. (2014). Global land cover mapping at 30m resolution: A POK-based operational approach. *ISPRS Journal of Photogrammetry and Remote Sensing*
- Chomitz, K.M., & Gray, D.A. (1996). Roads, Land Use, and Deforestation: A Spatial Model Applied to Belize. *The World Bank Economic Review*, *10*, 487-512
- Ciais, P., Sabine, G., Bala, G., Bopp, L., Brovkin, V., Canadell, J., Chhabra, A., Defries, R., Galloway, J., Heimann, M., Jones, C., Le Quere, C., Myneni, R.B., Piao, S., & Thornton, P. (2013). Carbon and Other Biogeochemical Cycles. In T.F. Stocker, D. Qin, G.-K. Plattner, M. Tignor, S.K. Allen, J. Boschung, A. Nauels, Y. Xia, V. Bex & P.M. Midgley (Eds.), *Climate Change 2013: The Physical Science Basis. Contribution of Working Group I to the Fifth Assessment Report of the Intergovernmental Panel on Climate Change*. Cambridge, United Kingdom and New York, NY, USA: Cambridge University Press. Available: http://www.climatechange2013.org/images/report/WG1AR5_Chapter06_FINAL.pdf. Accessed 10 July 2014.
- Clark, M.L., Aide, T.M., Grau, H.R., & Riner, G. (2010). A scalable approach to mapping annual land cover at 250 m using MODIS time series data: A case study in the Dry Chaco ecoregion of South America. *Remote Sensing of Environment*, *114*, 2816-2832

Cohen, W.B., Yang, Z., & Kennedy, R. (2010). Detecting trends in forest disturbance and recovery using yearly Landsat time series: 2. TimeSync — Tools for calibration and validation. *Remote Sensing of Environment*, 114, 2911-2924

Colwell, J.E. (1974). Vegetation Canopy Reflectance. *Remote Sensing of Environment*, 3, 175-183

Coppin, P., Jonckheere, I., Nackaerts, K., Muys, B., & Lambin, E. (2004). Digital change detection methods in ecosystem monitoring: a review. *International Journal of Remote Sensing*, 25, 1565-1596

Cropper, M., Griffiths, C., & Mani, M. (1999). Roads, Population Pressures, and Deforestation in Thailand, 1976-1989. *Land Economics*, 75, 58-73

Danko, D.M. (1992). The digital chart of the world project. *Photogrammetric engineering and remote sensing*, 58, 1125-1128

DeFries, R., Achard, F., Brown, S., Herold, M., Murdiyarso, D., Schlamadinger, B., & de Souza, C. (2007). Earth observations for estimating greenhouse gas emissions from deforestation in developing countries. *Environmental Science & Policy*, 10, 385-394

DeFries, R.S., & Chan, J.C.-W. (2000). Multiple Criteria for Evaluating Machine Learning Algorithms for Land Cover Classification from Satellite Data. *Remote Sensing of Environment*, 74, 503-515

DeFries, R.S., Foley, J.A., & Asner, G.P. (2004). Land-use choices: balancing human needs and ecosystem function. *Frontiers in Ecology and the Environment*, 2, 249-257

DeFries, R.S., Hansen, M., Townshend, J.R.G., & Sohlberg, R. (1998). Global land cover classifications at 8 km spatial resolution: the use of training data derived from Landsat imagery in decision tree classifiers. *International Journal of Remote Sensing*, 19, 3141-3168

DeFries, R.S., Houghton, R.A., Hansen, M.C., Field, C.B., Skole, D., & Townshend, J. (2002). Carbon emissions from tropical deforestation and regrowth based on satellite observations for the 1980s and 1990s. *Proc. Natl. Acad. Sci. USA*, 99, 14256-14261

DeFries, R.S., & Townshend, J.R.G. (1994a). Global land cover: comparison of ground-based data sets to classifications with AVHRR data. In G.M. Foody (Ed.), *Environmental Remote Sensing from Regional to Global Scales* (pp. 84-110). New York: Wiley

Defries, R.S., & Townshend, J.R.G. (1994b). NDVI-Derived Land-Cover Classifications at a Global-Scale. *International Journal of Remote Sensing*, 15, 3567-3586

Di Gregorio, A. (2005). *Land cover classification system: classification concepts and user manual: LCCS*: Food & Agriculture Org.

DiMiceli, C.M., Carroll, M.L., Sohlberg, R.A., Huang, C., Hansen, M.C., & Townshend, J.R.G. (2011). Annual Global Automated MODIS Vegetation Continuous Fields (MOD44B) at 250 m Spatial Resolution for Data Years Beginning Day 65, 2000 - 2010, Collection 5 Percent Tree Cover. In. University of Maryland: The Global Land Cover Facility. Available: <http://glcf.umd.edu/data/vcf/>. Accessed 12 December 2013.

Dubayah, R.O., & Drake, J.B. (2000). Lidar remote sensing for forestry. *Journal of Forestry*, 98, 44-46

Environmental Defense, & the Instituto de Pesquisa Ambiental da Amazonia (2007). Reducing Emissions from Deforestation in Developing Countries: Policy Approaches to Stimulate Action. Submission to the XXVI Session of the Subsidiary Body on Scientific and Technological Advice of the UNFCCC. In

Espirito-Santo, F.D., Gloor, M., Keller, M., Malhi, Y., Saatchi, S., Nelson, B., Junior, R.C., Pereira, C., Lloyd, J., Froking, S., Palace, M., Shimabukuro, Y.E., Duarte, V., Mendoza, A.M., Lopez-Gonzalez, G., Baker, T.R., Feldpausch, T.R., Brienen, R.J., Asner, G.P., Boyd, D.S., & Phillips, O.L. (2014). Size and frequency of natural forest disturbances and the Amazon forest carbon balance. *Nat Commun*, 5, 3434

Fairbanks, D., Thompson, M., Vink, D., Newby, T., Van den Berg, H., & Everard, D. (2000). South African land-cover characteristics database: a synopsis of the landscape. *South African Journal of Science*, 96, 69-82

FAO (2012). *Global Forest Resources Assessment 2010*. Rome: United Nations Food and Agriculture Organization. Available: <http://www.fao.org/forestry/fra/fra2010/en/>. Accessed 23 September 2013.

Ferraz, G., Russell, G.J., Stouffer, P.C., Bierregaard, R.O., Jr., Pimm, S.L., & Lovejoy, T.E. (2003). Rates of species loss from Amazonian forest fragments. *Proc Natl Acad Sci USA*, 100, 14069-14073

Filzmoser, P., Garrett, R.G., & Reimann, C. (2005). Multivariate outlier detection in exploration geochemistry. *Computers & Geosciences*, 31, 579-587

Foley, J.A., Defries, R., Asner, G.P., Barford, C., Bonan, G., Carpenter, S.R., Chapin, F.S., Coe, M.T., Daily, G.C., Gibbs, H.K., Helkowski, J.H., Holloway, T., Howard, E.A., Kucharik, C.J., Monfreda, C., Patz, J.A., Prentice, I.C., Ramankutty, N., & Snyder, P.K. (2005). Global consequences of land use. *Science*, 309, 570-574

Foody, G.M. (2002). Status of land cover classification accuracy assessment. *Remote Sensing of Environment*, 80, 185-201

- Friedl, M.A., McIver, D.K., Hodges, J.C.F., Zhang, X.Y., Muchoney, D., Strahler, A.H., Woodcock, C.E., Gopal, S., Schneider, A., Cooper, A., Baccini, A., Gao, F., & Schaaf, C. (2002). Global land cover mapping from MODIS: algorithms and early results. *Remote Sensing of Environment*, 83, 287-302
- Friedl, M.A., Sulla-Menashe, D., Tan, B., Schneider, A., Ramankutty, N., Sibley, A., & Huang, X. (2010). MODIS Collection 5 global land cover: Algorithm refinements and characterization of new datasets. *Remote Sensing of Environment*, 114, 168-182
- Friedlingstein, P., Houghton, R.A., Marland, G., Hackler, J., Boden, T.A., Conway, T.J., Canadell, J.G., Raupach, M.R., Ciais, P., & Le Quéré, C. (2010). Update on CO₂ emissions. *Nature Geoscience*, 3, 811-812
- Fritz, S., & See, L. (2008). Identifying and quantifying uncertainty and spatial disagreement in the comparison of Global Land Cover for different applications. *Global Change Biology*, 14, 1057-1075
- Fritz, S., See, L., McCallum, I., You, L., Bun, A., Moltchanova, E., Duerauer, M., Albrecht, F., Schill, C., Perger, C., Havlik, P., Mosnier, A., Thornton, P., Wood-Sichra, U., Herrero, M., Becker-Reshef, I., Justice, C., Hansen, M., Gong, P., Abdel Aziz, S., Cipriani, A., Cumani, R., Cecchi, G., Conchedda, G., Ferreira, S., Gomez, A., Haffani, M., Kayitakire, F., Malanding, J., Mueller, R., Newby, T., Nonguierma, A., Olusegun, A., Ortner, S., Rajak, D.R., Rocha, J., Schepaschenko, D., Schepaschenko, M., Terekhov, A., Tiangwa, A., Vancutsem, C., Vintrou, E., Wenbin, W., van der Velde, M., Dunwoody, A., Kraxner, F., & Obersteiner, M. (2015). Mapping global cropland and field size. *Glob Chang Biol*
- Fritz, S., See, L., & Rembold, F. (2010). Comparison of global and regional land cover maps with statistical information for the agricultural domain in Africa. *International Journal of Remote Sensing*, 31, 2237-2256
- Fritz, S., You, L., Bun, A., See, L., McCallum, I., Schill, C., Perger, C., Liu, J., Hansen, M., & Obersteiner, M. (2011). Cropland for sub-Saharan Africa: A synergistic approach using five land cover data sets. *Geophysical Research Letters*, 38, L04404
- Garrett, R.G. (1989). The chi-square plot: a tool for multivariate outlier recognition. *Journal of Geochemical Exploration*, 32, 319-341
- Garson, G.D. (2012). Testing statistical assumptions. In: Statistical Associates Publishing
- Ge, Y., Avitabile, V., Heuvelink, G.B.M., Wang, J., & Herold, M. (2014). Fusion of pan-tropical biomass maps using weighted averaging and regional calibration data. *International Journal of Applied Earth Observation and Geoinformation*, 31, 13-24
- Geist, H.J., & Lambin, E.F. (2002). Proximate Causes and Underlying Driving Forces of Tropical Deforestation. *Bioscience*, 52, 143-150

- Gibbs, H.K., Brown, S., Niles, J.O., & Foley, J.A. (2007). Monitoring and estimating tropical forest carbon stocks: making REDD a reality. *Environmental Research Letters*, 2, 045023
- Giri, C., Pengra, B., Long, J., & Loveland, T.R. (2013). Next generation of global land cover characterization, mapping, and monitoring. *International Journal of Applied Earth Observation and Geoinformation*, 25, 30-37
- Giri, C., Zhu, Z., & Reed, B. (2005). A comparative analysis of the Global Land Cover 2000 and MODIS land cover data sets. *Remote Sensing of Environment*, 94, 123-132
- Goetz, S.J., Baccini, A., Laporte, N.T., Johns, T., Walker, W., Kellndorfer, J., Houghton, R.A., & Sun, M. (2009). Mapping and monitoring carbon stocks with satellite observations: a comparison of methods. *Carbon Balance Manag*, 4, 2
- GOFC-GOLD (2012). A sourcebook of methods and procedures for monitoring and reporting anthropogenic greenhouse gas emissions and removals associated with deforestation, gains and losses of carbon stocks in forests remaining forests, and forestation. In. GOFC-GOLD Land Cover Project Office, Wageningen University, The Netherlands. Available: <http://www.gofcgold.wur.nl/redd/>. Accessed 23 September 2013
- Gong, P., Wang, J., Yu, L., Zhao, Y., Zhao, Y., Liang, L., Niu, Z., Huang, X., Fu, H., Liu, S., Li, C., Li, X., Fu, W., Liu, C., Xu, Y., Wang, X., Cheng, Q., Hu, L., Yao, W., Zhang, H., Zhu, P., Zhao, Z., Zhang, H., Zheng, Y., Ji, L., Zhang, Y., Chen, H., Yan, A., Guo, J., Yu, L., Wang, L., Liu, X., Shi, T., Zhu, M., Chen, Y., Yang, G., Tang, P., Xu, B., Giri, C., Clinton, N., Zhu, Z., Chen, J., & Chen, J. (2013). Finer resolution observation and monitoring of global land cover: first mapping results with Landsat TM and ETM+ data. *International Journal of Remote Sensing*, 34, 2607-2654
- Goward, S., Arvidson, T., Williams, D., Faundeen, J., Irons, J., & Franks, S. (2006). Historical Record of Landsat Global Coverage: Mission Operations, NSLRSDA, and International Cooperator Stations. *Photogrammetric Engineering & Remote Sensing*, 72, 1155-1169
- Grainger, A. (2008). Difficulties in tracking the long-term global trend in tropical forest area. *Proc Natl Acad Sci USA*, 105, 818-823
- Griscom, B., Shoch, D., Stanley, B., Cortez, R., & Virgilio, N. (2009). Sensitivity of amounts and distribution of tropical forest carbon credits depending on baseline rules. *Environmental Science & Policy*, 12, 897-911
- Gutman, G., Huang, C., Chander, G., Noojipady, P., & Masek, J.G. (2013). Assessment of the NASA–USGS Global Land Survey (GLS) datasets. *Remote Sensing of Environment*, 134, 249-265

Hansen, M., Shimabukuro, Y., Potapov, P., & Pittman, K. (2008a). Comparing annual MODIS and PRODES forest cover change data for advancing monitoring of Brazilian forest cover. *Remote Sensing of Environment*, *112*, 3784-3793

Hansen, M.C., & DeFries, R.S. (2004). Detecting Long-term Global Forest Change Using Continuous Fields of Tree-Cover Maps from 8-km Advanced Very High Resolution Radiometer (AVHRR) Data for the Years 1982-99. *Ecosystems*, *7*, 695-716

Hansen, M.C., DeFries, R.S., Townshend, J.R.G., Carroll, M., Dimiceli, C., & Sohlberg, R.A. (2003). Global percent tree cover at a spatial resolution of 500 meters: First results of the MODIS vegetation continuous fields algorithm. *Earth Interactions*, *7*, 1-15

Hansen, M.C., DeFries, R.S., Townshend, J.R.G., Marufu, L., & Sohlberg, R. (2002). Development of a MODIS tree cover validation data set for Western Province, Zambia. *Remote Sensing of Environment*, *83*, 320-335

Hansen, M.C., DeFries, R.S., Townshend, J.R.G., & Sohlberg, R.A. (2000). Global land cover classification at 1 km spatial resolution using a classification tree approach. *International Journal of Remote Sensing*, *21*, 1331-1364

Hansen, M.C., Egorov, A., Potapov, P.V., Stehman, S.V., Tyukavina, A., Turubanova, S.A., Roy, D.P., Goetz, S.J., Loveland, T.R., Ju, J., Kommareddy, A., Kovalskyy, V., Forsyth, C., & Bents, T. (2014). Monitoring conterminous United States (CONUS) land cover change with Web-Enabled Landsat Data (WELD). *Remote Sensing of Environment*, *140*, 466-484

Hansen, M.C., Potapov, P.V., Moore, R., Hancher, M., Turubanova, S.A., Tyukavina, A., Thau, D., Stehman, S.V., Goetz, S.J., Loveland, T.R., Kommareddy, A., Egorov, A., Chini, L., Justice, C.O., & Townshend, J.R.G. (2013). High-resolution global maps of 21st-century forest cover change. *Science*, *342*, 850-853

Hansen, M.C., & Reed, B.C. (2000). A comparison of the IGBP DISCover and University of Maryland 1 km global land cover products. *International Journal of Remote Sensing*, *21*, 1365-1373

Hansen, M.C., Roy, D.P., Lindquist, E., Adusei, B., Justice, C.O., & Altstatt, A. (2008b). A method for integrating MODIS and Landsat data for systematic monitoring of forest cover and change in the Congo Basin. *Remote Sensing of Environment*, *112*, 2495-2513

Hansen, M.C., Stehman, S.V., & Potapov, P.V. (2010). Quantification of global gross forest cover loss. *Proc. Natl. Acad. Sci. USA*, *107*, 8650-8655

Hansen, M.C., Stehman, S.V., Potapov, P.V., Loveland, T.R., Townshend, J.R., DeFries, R.S., Pittman, K.W., Arunarwati, B., Stolle, F., Steininger, M.K., Carroll, M., & Dimiceli, C. (2008c). Humid tropical forest clearing from 2000 to 2005

- quantified by using multitemporal and multiresolution remotely sensed data. *Proc. Natl. Acad. Sci. USA*, 105, 9439-9444
- Harding, D.J., & Carabajal, C.C. (2005). ICESat waveform measurements of within-footprint topographic relief and vegetation vertical structure. *Geophysical Research Letters*, 32, L21S10
- Harris, N.L., Brown, S., Hagen, S.C., Baccini, A., & Houghton, R. (2012a). *Progress towards a Consensus on Carbon Emissions from Tropical Deforestation*. Washington DC: Meridian Institute
- Harris, N.L., Brown, S., Hagen, S.C., Saatchi, S.S., Petrova, S., Salas, W., Hansen, M.C., Potapov, P.V., & Lotsch, A. (2012b). Baseline map of carbon emissions from deforestation in tropical regions. *Science*, 336, 1573-1576
- Healey, S., Cohen, W., Zhiqiang, Y., & Krankina, O. (2005). Comparison of Tasseled Cap-based Landsat data structures for use in forest disturbance detection. *Remote Sensing of Environment*, 97, 301-310
- Heiskanen, J. (2008). Evaluation of global land cover data sets over the tundra-taiga transition zone in northernmost Finland. *International Journal of Remote Sensing*, 29, 3727-3751
- Herold, M. (2009). An assessment of national forest monitoring capabilities in tropical non-Annex I countries: recommendations for capacity building Report for The Prince's Rainforests Project and The Government of Norway. In: GOFCC-GOLD Land Cover Project Office and Friedrich Schiller University Jena
- Herold, M., Angelsen, A., Verchot, L.V., Wijaya, A., & Ainembabazi, J.H. (2012). A stepwise framework for developing REDD+ reference levels. In A. Angelsen, M. Brockhaus, W.D. Sunderlin & L.V. Verchot (Eds.), *Analysing REDD+: Challenges and choices* (pp. 279-300). Bogor, Indonesia: Center for International Forestry Research
- Herold, M., Mayaux, P., Woodcock, C.E., Baccini, A., & Schmillius, C. (2008). Some challenges in global land cover mapping: An assessment of agreement and accuracy in existing 1 km datasets. *Remote Sensing of Environment*, 112, 2538-2556
- Herold, M., & Skutsch, M.M. (2009). Measurement, reporting and verification for REDD+: objectives, capacities and institutions. In A. Angelsen (Ed.), *Realising REDD+: National Strategy and Policy Options* (pp. 85-100). Bogor, Indonesia: Center for International Forestry Research
- Homer, C., Huang, C., Yang, L., Wylie, B., & Coan, M. (2004). Development of a 2001 National Land-Cover Database for the United States. *Photogrammetric Engineering & Remote Sensing*, 70, 829-840

- Houghton, R.A. (1999). The annual net flux of carbon to the atmosphere from changes in land use 1850–1990. *Tellus B*, 51, 298-313
- Houghton, R.A. (2000). Interannual variability in the global carbon cycle. *Journal of Geophysical Research*, 105, 20121-20130
- Houghton, R.A. (2003). Revised estimates of the annual net flux of carbon to the atmosphere from changes in land use and land management 1850–2000. *Tellus B*, 55, 378-390
- Houghton, R.A. (2005). Aboveground Forest Biomass and the Global Carbon Balance. *Global Change Biology*, 11, 945-958
- Houghton, R.A., Boone, R.D., Fruci, J.R., Hobbie, J.E., Melillo, J.M., Palm, C.A., Peterson, B.J., Shaver, G.R., Woodwell, G.M., Moore, B., Skole, D.L., & Myers, N. (1987). The flux of carbon from terrestrial ecosystems to the atmosphere in 1980 due to changes in land use: geographic distribution of the global flux. *Tellus B*, 39B, 122-139
- Houghton, R.A., House, J.I., Pongratz, J., van der Werf, G.R., DeFries, R.S., Hansen, M.C., Le Quéré, C., & Ramankutty, N. (2012). Carbon emissions from land use and land-cover change. *Biogeosciences*, 9, 5125-5142
- Huang, C., Goward, S.N., Masek, J., Gao, F., Vermote, E., Thomas, N., Schleeweis, K., Kennedy, R., Zhu, Z., Eidenshink, J.C., & Townshend, J.R.G. (2009a). Development of time series stacks of Landsat images for reconstructing forest disturbance history. *International Journal of Digital Earth*, 2, 195-218
- Huang, C., Goward, S.N., Masek, J.G., Thomas, N., Zhu, Z., & Vogelmann, J.E. (2010a). An automated approach for reconstructing recent forest disturbance history using dense Landsat time series stacks. *Remote Sensing of Environment*, 114, 183-198
- Huang, C., Goward, S.N., Schleeweis, K., Thomas, N., Masek, J.G., & Zhu, Z. (2009b). Dynamics of national forests assessed using the Landsat record: Case studies in eastern United States. *Remote Sensing of Environment*, 113, 1430-1442
- Huang, C., Kim, S., Song, K., Townshend, J.R.G., Davis, P., Altstatt, A., Rodas, O., Yanosky, A., Clay, R., Tucker, C.J., & Musinsky, J. (2009c). Assessment of Paraguay's forest cover change using Landsat observations. *Global and Planetary Change*, 67, 1-12
- Huang, C., Schleeweis, K., Thomas, N., & Goward, S. (2011). Forest dynamics within and around the Olympic National Park assessed using time series Landsat observations. In Y. Wang (Ed.), *Remote Sensing of Protected Lands* (pp. 71-93). London: Talyor & Francis

Huang, C., Song, K., Kim, S., Townshend, J.R.G., Davis, P., Masek, J.G., & Goward, S.N. (2008). Use of a dark object concept and support vector machines to automate forest cover change analysis. *Remote Sensing of Environment*, 112, 970-985

Huang, C., Thomas, N., Goward, S.N., Masek, J.G., Zhu, Z., Townshend, J.R.G., & Vogelmann, J.E. (2010b). Automated masking of cloud and cloud shadow for forest change analysis using Landsat images. *International Journal of Remote Sensing*, 31, 5449-5464

Huang, C., Wylie, B., Yang, L., Homer, C., & Zylstra, G. (2002). Derivation of a tasseled cap transformation based on Landsat 7 at-satellite reflectance. *International Journal of Remote Sensing*, 23, 1741-1748

Huettner, M., Leemans, R., Kok, K., & Ebeling, J. (2009). A comparison of baseline methodologies for 'Reducing Emissions from Deforestation and Degradation'. *Carbon Balance Manag*, 4, 1-12

INPE (2013). Available: <http://www.obt.inpe.br/prodes/index.php>. Accessed 23 September 2013. In

IPCC (2006). IPCC Guidelines for National Greenhouse Gas Inventories, Prepared by the National Greenhouse Gas Inventories Programme. In S. Eggleston, L. Buendia, K. Miwa, T. Ngara & K. Tanabe (Eds.). Hayama, Kanagawa, Japan: Institute for Global Environmental Strategies. Available: <http://www.ipcc-nggip.iges.or.jp/public/2006gl/>. Accessed 23 September 2013.

Jain, A.K., & Yang, X. (2005). Modeling the effects of two different land cover change data sets on the carbon stocks of plants and soils in concert with CO₂ and climate change. *Global Biogeochemical Cycles*, 19, GB2015

Jin, S., & Sader, S.A. (2005). Comparison of time series tasseled cap wetness and the normalized difference moisture index in detecting forest disturbances. *Remote Sensing of Environment*, 94, 364-372

Joanneum Research, Union of Concerned Scientists, Woods Hole Research Center, & Instituto de Pesquisa Ambiental da Amazonia (2006). Reducing Emissions from Deforestation in Developing Countries: potential policy approaches and positive incentives. In

Ju, J., & Roy, D.P. (2008). The availability of cloud-free Landsat ETM+ data over the conterminous United States and globally. *Remote Sensing of Environment*, 112, 1196-1211

Jung, M., Henkel, K., Herold, M., & Churkina, G. (2006). Exploiting synergies of global land cover products for carbon cycle modeling. *Remote Sensing of Environment*, 101, 534-553

- Justice, C.O., Townshend, J.R.G., Holben, B.N., & Tucker, C.J. (1985). Analysis of the phenology of global vegetation using meteorological satellite data. *International Journal of Remote Sensing*, 6, 1271-1318
- Kaimowitz, D., & Angelsen, A. (1998). *Economic Models of Tropical Deforestation: A Review*. Bogor, Indonesia: Center for International Forestry Research
- Karstensen, J., Peters, G.P., & Andrew, R.M. (2013). Attribution of CO₂ emissions from Brazilian deforestation to consumers between 1990 and 2010. *Environmental Research Letters*, 8, 024005
- Kauth, R.J., & Thomas, G. (1976). The tasselled cap--a graphic description of the spectral-temporal development of agricultural crops as seen by Landsat. In, *Proceedings of the Symposium on Machine Processing of Remotely Sensed Data* (pp. 41-51). West Lafayette, Indiana
- Keeling, C.D., Whorf, T.P., Wahlen, M., & van der Plicht, J. (1995). Interannual extremes in the rate of rise of atmospheric carbon dioxide since 1980. *Nature*, 375, 666-670
- Kennedy, R.E., Cohen, W.B., & Schroeder, T.A. (2007). Trajectory-based change detection for automated characterization of forest disturbance dynamics. *Remote Sensing of Environment*, 110, 370-386
- Kennedy, R.E., Yang, Z., & Cohen, W.B. (2010). Detecting trends in forest disturbance and recovery using yearly Landsat time series: 1. LandTrendr — Temporal segmentation algorithms. *Remote Sensing of Environment*, 114, 2897-2910
- Kicklighter, D.W., Bruno, M., Dönges, S., Esser, G., Heimann, M., Helfrich, J., Ift, F., Joos, F., Kaduk, J., Kohlmaier, G.H., McGuire, A.D., Melillo, J.M., Meyer, R., Moore III, B., Nadler, A., Prentice, I.C., Sauf, W., Schloss, A.L., Sitch, S., Wittenberg, U., & Würth, G. (1999). A first-order analysis of the potential rôle of CO₂ fertilization to affect the global carbon budget: a comparison of four terrestrial biosphere models. *Tellus B*, 51, 343-366
- Kim, D.-H., Narashiman, R., Sexton, J.O., Huang, C., & Townshend, J.R. (2011). Methodology to select phenologically suitable Landsat scenes for forest change detection. In, *IEEE International Geoscience and Remote Sensing Symposium (IGARSS)* (pp. 2613 - 2616). Vancouver
- Kim, D.-H., Sexton, J.O., Noojipady, P., Huang, C., Anand, A., Channan, S., Feng, M., & Townshend, J.R. (2014). Global, Landsat-based forest-cover change from 1990 to 2000. *Remote Sensing of Environment*, 155, 178-193
- Kim, D.-H., Sexton, J.O., & Townshend, J.R. (2015). Accelerated Deforestation in the Humid Tropics from the 1990s to the 2000s. *Geophysical Research Letters*, 2014GL062777

- Kindermann, G.E., McCallum, I., Fritz, S., & Obersteiner, M. (2008). A global forest growing stock, biomass and carbon map based on FAO statistics. *Silva Fennica*, 42, 387-396
- Kindermann, J., Würth, G., Kohlmaier, G.H., & Badeck, F.-W. (1996). Interannual variation of carbon exchange fluxes in terrestrial ecosystems. *Global Biogeochemical Cycles*, 10, 737-755
- Kleynhans, W., Olivier, J.C., Wessels, K.J., Salmon, B.P., Van den Bergh, F., & Steenkamp, K. (2011). Detecting land cover change using an extended Kalman filter on MODIS NDVI time-series data. *IEEE Geoscience and Remote Sensing Letters*, 8, 507-511
- Lambin, E.F. (1999). Monitoring forest degradation in tropical regions by remote sensing: some methodological issues. *Global Ecology and Biogeography*, 8, 191-198
- Lancaster, H.O., & Seneta, E. (2005). Chi-Square Distribution. *Encyclopedia of Biostatistics*: John Wiley & Sons, Ltd
- Laurance, W.F., Laurance, S.G., Ferreira, L.V., Merona, J.M.R.-d., Gascon, C., & Lovejoy, T.E. (1997). Biomass Collapse in Amazonian Forest Fragments. *Science*, 278, 1117-1118
- Lawrence, P.J., & Chase, T.N. (2007). Representing a new MODIS consistent land surface in the Community Land Model (CLM 3.0). *Journal of Geophysical Research*, 112, G01023
- Le Quéré, C., Moriarty, R., Andrew, R.M., Peters, G.P., Ciais, P., Friedlingstein, P., Jones, S.D., Sitch, S., Tans, P., Arneeth, A., Boden, T.A., Bopp, L., Bozec, Y., Canadell, J.G., Chevallier, F., Cosca, C.E., Harris, I., Hoppema, M., Houghton, R.A., House, J.I., Jain, A., Johannessen, T., Kato, E., Keeling, R.F., Kitidis, V., Klein Goldewijk, K., Koven, C., Landa, C.S., Landschützer, P., Lenton, A., Lima, I.D., Marland, G., Mathis, J.T., Metzl, N., Nojiri, Y., Olsen, A., Ono, T., Peters, W., Pfeil, B., Poulter, B., Raupach, M.R., Regnier, P., Rödenbeck, C., Saito, S., Salisbury, J.E., Schuster, U., Schwinger, J., Séférian, R., Segschneider, J., Steinhoff, T., Stocker, B.D., Sutton, A.J., Takahashi, T., Tilbrook, B., van der Werf, G.R., Viovy, N., Wang, Y.P., Wanninkhof, R., Wiltshire, A., & Zeng, N. (2014). Global carbon budget 2014. *Earth System Science Data Discussions*, 7, 521-610
- Le Quéré, C., Raupach, M.R., Canadell, J.G., & Marland, G. (2009). Trends in the sources and sinks of carbon dioxide. *Nature Geoscience*, 2, 831-836
- Lechner, A.M., Stein, A., Jones, S.D., & Ferwerda, J.G. (2009). Remote sensing of small and linear features: Quantifying the effects of patch size and length, grid position and detectability on land cover mapping. *Remote Sensing of Environment*, 113, 2194-2204

- Lefsky, M.A. (2010). A global forest canopy height map from the Moderate Resolution Imaging Spectroradiometer and the Geoscience Laser Altimeter System. *Geophysical Research Letters*, *37*, n/a-n/a
- Liu, J., Liu, M., Deng, X., Zhuang, D., Zhang, Z., & Luo, D. (2002). The land use and land cover change database and its relative studies in China. *Journal of Geographical Sciences*, *12*, 275-282
- Loarie, S.R., Asner, G.P., & Field, C.B. (2009). Boosted carbon emissions from Amazon deforestation. *Geophysical Research Letters*, *36*, L14810
- Loveland, T.R., Reed, B.C., Brown, J.F., Ohlen, D.O., Zhu, Z., Yang, L., & Merchant, J.W. (2000). Development of a global land cover characteristics database and IGBP DISCover from 1 km AVHRR data. *International Journal of Remote Sensing*, *21*, 1303-1330
- Lu, D., Mausel, P., Brondízio, E., & Moran, E. (2004). Change detection techniques. *International Journal of Remote Sensing*, *25*, 2365-2401
- Lund, H.G. (2014). Definitions of Forest, Deforestation, Afforestation, and Reforestation. In Gainesville, VA: Forest Information Services. Available: <http://home.comcast.net/~gyde/DEFpaper.htm>. Accessed 22 September 2014.
- Lunetta, R.S., Knight, J.F., Ediriwickrema, J., Lyon, J.G., & Worthy, L.D. (2006). Land-cover change detection using multi-temporal MODIS NDVI data. *Remote Sensing of Environment*, *105*, 142-154
- Macedo, M.N., DeFries, R.S., Morton, D.C., Stickler, C.M., Galford, G.L., & Shimabukuro, Y.E. (2012). Decoupling of deforestation and soy production in the southern Amazon during the late 2000s. *Proc. Natl. Acad. Sci. USA*, *109*, 1341-1346
- Mackey, B., Prentice, I.C., Steffen, W., House, J.I., Lindenmayer, D., Keith, H., & Berry, S. (2013). Untangling the confusion around land carbon science and climate change mitigation policy. *Nature Climate Change*, *3*, 552-557
- Malhi, Y., & Grace, J. (2000). Tropical forests and atmospheric carbon dioxide. *Trends in Ecology & Evolution*, *15*, 332
- Margono, B.A., Potapov, P.V., Turubanova, S., Stolle, F., & Hansen, M.C. (2014). Primary forest cover loss in Indonesia over 2000–2012. *Nature Climate Change*, *4*, 730-735
- Markwardt, C.B. (2009). Non-linear Least Squares Fitting in IDL with MPFIT. In D. Bohlender, P. Dowler & D. Durand (Eds.), *Astronomical Data Analysis Software and Systems XVIII* (pp. 251-254). Quebec, Canada: Astronomical Society of the Pacific

- Martin-Lopez, B., Montes, C., & Benayas, J. (2007). Influence of user characteristics on valuation of ecosystem services in Do(n)over-tildeana Natural Protected Area (south-west Spain). *Environmental Conservation*, 34, 215-224
- Masek, J.G., Goward, S.N., Kennedy, R.E., Cohen, W.B., Moisen, G.G., Schleeweis, K., & Huang, C. (2013). United States Forest Disturbance Trends Observed Using Landsat Time Series. *Ecosystems*, 16, 1087-1104
- Masek, J.G., Huang, C., Wolfe, R., Cohen, W., Hall, F., Kutler, J., & Nelson, P. (2008). North American forest disturbance mapped from a decadal Landsat record. *Remote Sensing of Environment*, 112, 2914-2926
- Masek, J.G., Vermote, E.F., Saleous, N.E., Wolfe, R.E., Hall, F.G., Huemmrich, K.F., Gao, F., Kutler, J., & Lim, T.-K. (2006). A Landsat Surface Reflectance Dataset for North America, 1990-2000. *IEEE Geoscience and Remote Sensing Letters*, 3, 68-72
- Mather, A.S. (1992). The forest transition. *Area*, 24, 367-379
- Mather, P.M., & Koch, M. (2011). *Computer Processing of Remotely-Sensed Images: An Introduction*. West Sussex, UK: John Wiley & Sons
- Matthews, E., & Grainger, A. (2002). Evaluation of FAO's Global Forest Resources Assessment from the user perspective. *Unasylva* 210, 53, 42-50
- Mayaux, P., Eva, H., Gallego, J., Strahler, A.H., Herold, M., Agrawal, S., Naumov, S., De Miranda, E.E., Di Bella, C.M., Ordoyne, C., Kopin, Y., & Roy, P.S. (2006). Validation of the global land cover 2000 map. *Geoscience and Remote Sensing, IEEE Transactions on*, 44, 1728-1739
- Mayaux, P., Holmgren, P., Achard, F., Eva, H., Stibig, H.J., & Branthomme, A. (2005). Tropical forest cover change in the 1990s and options for future monitoring. *Philosophical Transactions of the Royal Society of London B Biological Sciences*, 360, 373-384
- Mayaux, P., & Lambin, E.F. (1995). Estimation of tropical forest area from coarse spatial resolution data: A two-step correction function for proportional errors due to spatial aggregation. *Remote Sensing of Environment*, 53, 1-15
- Mayaux, P., Pekel, J.F., Desclee, B., Donnay, F., Lupi, A., Achard, F., Clerici, M., Bodart, C., Brink, A., Nasi, R., & Belward, A. (2013). State and evolution of the African rainforests between 1990 and 2010. *Philosophical Transactions of the Royal Society of London B Biological Sciences*, 368, 20120300
- McGuire, A.D., Sitch, S., Clein, J.S., Dargaville, R., Esser, G., Foley, J., Heimann, M., Joos, F., Kaplan, J., Kicklighter, D.W., Meier, R.A., Melillo, J.M., Moore, B., Prentice, I.C., Ramankutty, N., Reichenau, T., Schloss, A., Tian, H., Williams, L.J., & Wittenberg, U. (2001). Carbon balance of the terrestrial biosphere in the Twentieth

Century: Analyses of CO₂, climate and land use effects with four process-based ecosystem models. *Global Biogeochemical Cycles*, 15, 183-206

Mildrexler, D.J., Zhao, M., & Running, S.W. (2009). Testing a MODIS Global Disturbance Index across North America. *Remote Sensing of Environment*, 113, 2103-2117

Miles, L., Newton, A.C., DeFries, R.S., Ravilious, C., May, I., Blyth, S., Kapos, V., & Gordon, J.E. (2006). A global overview of the conservation status of tropical dry forests. *Journal of Biogeography*, 33, 491-505

Mitchard, E.T.A., Feldpausch, T.R., Brienen, R.J.W., Lopez-Gonzalez, G., Monteagudo, A., Baker, T.R., Lewis, S.L., Lloyd, J., Quesada, C.A., Gloor, M., ter Steege, H., Meir, P., Alvarez, E., Araujo-Murakami, A., Aragão, L.E.O.C., Arroyo, L., Aymard, G., Banki, O., Bonal, D., Brown, S., Brown, F.I., Cerón, C.E., Chama Moscoso, V., Chave, J., Comiskey, J.A., Cornejo, F., Corrales Medina, M., Da Costa, L., Costa, F.R.C., Di Fiore, A., Domingues, T.F., Erwin, T.L., Frederickson, T., Higuchi, N., Honorio Coronado, E.N., Killeen, T.J., Laurance, W.F., Levis, C., Magnusson, W.E., Marimon, B.S., Marimon Junior, B.H., Mendoza Polo, I., Mishra, P., Nascimento, M.T., Neill, D., Núñez Vargas, M.P., Palacios, W.A., Parada, A., Pardo Molina, G., Peña-Claros, M., Pitman, N., Peres, C.A., Poorter, L., Prieto, A., Ramirez-Angulo, H., Restrepo Correa, Z., Roopsind, A., Roucoux, K.H., Rudas, A., Salomão, R.P., Schiatti, J., Silveira, M., de Souza, P.F., Steininger, M.K., Stropp, J., Terborgh, J., Thomas, R., Toledo, M., Torres-Lezama, A., van Andel, T.R., van der Heijden, G.M.F., Vieira, I.C.G., Vieira, S., Vilanova-Torre, E., Vos, V.A., Wang, O., Zartman, C.E., Malhi, Y., & Phillips, O.L. (2014). Markedly divergent estimates of Amazon forest carbon density from ground plots and satellites. *Global Ecology and Biogeography*, 23, 935-946

Mitchard, E.T.A., Saatchi, S.S., Baccini, A., Asner, G.P., Goetz, S.J., Harris, N.L., & Brown, S. (2013). Uncertainty in the spatial distribution of tropical forest biomass: a comparison of pan-tropical maps. *Carbon Balance Manag*, 8, 10

Mollicone, D., Achard, F., Federici, S., Eva, H.D., Grassi, G., Belward, A., Raes, F., Seufert, G., Stibig, H.-J., Matteucci, G., & Schulze, E.-D. (2007). An incentive mechanism for reducing emissions from conversion of intact and non-intact forests. *Climatic Change*, 83, 477-493

Montesano, P.M., Nelson, R., Sun, G., Margolis, H., Kerber, A., & Ranson, K.J. (2009). MODIS tree cover validation for the circumpolar taiga-tundra transition zone. *Remote Sensing of Environment*, 113, 2130-2141

Moore, B., Boone, R.D., Hobbie, J.E., Houghton, R.A., Melillo, J.M., Peterson, B.J., Shaver, G.R., Vorosmarty, C.J., & Woodwell, G.M. (1983). A simple model for analysis of the role of terrestrial ecosystems in the global carbon budget. *Modelling the Global Carbon Cycle, SCOPE Report No. 16*, 365-385

- Moré, J. (1978). The Levenberg-Marquardt algorithm: Implementation and theory. In G.A. Watson (Ed.), *Numerical Analysis* (pp. 105-116): Springer Berlin Heidelberg
- Morton, D.C., DeFries, R.S., Shimabukuro, Y.E., Anderson, L.O., Arai, E., del Bon Espirito-Santo, F., Freitas, R., & Morisette, J. (2006). Cropland expansion changes deforestation dynamics in the southern Brazilian Amazon. *Proc. Natl. Acad. Sci. USA*, *103*, 14637-14641
- Myneni, R.B., Hoffman, S., Knyazikhin, Y., Privette, J.L., Glassy, J., Tian, Y., Wang, Y., Song, X., Zhang, Y., Smith, G.R., Lotsch, A., Friedl, M., Morisette, J.T., Votava, P., Nemani, R.R., & Running, S.W. (2002). Global products of vegetation leaf area and fraction absorbed PAR from year one of MODIS data. *Remote Sensing of Environment*, *83*, 214-231
- Neigh, C., Bolton, D., Diabate, M., Williams, J., & Carvalhais, N. (2014). An Automated Approach to Map the History of Forest Disturbance from Insect Mortality and Harvest with Landsat Time-Series Data. *Remote Sensing*, *6*, 2782-2808
- Nepstad, D., McGrath, D., Stickler, C., Alencar, A., Azevedo, A., Swette, B., Bezerra, T., DiGiano, M., Shimada, J., Seroa da Motta, R., Armijo, E., Castello, L., Brando, P., Hansen, M.C., McGrath-Horn, M., Carvalho, O., & Hess, L. (2014). Slowing Amazon deforestation through public policy and interventions in beef and soy supply chains. *Science*, *344*, 1118-1123
- Olofsson, P., Foody, G.M., Stehman, S.V., & Woodcock, C.E. (2013). Making better use of accuracy data in land change studies: Estimating accuracy and area and quantifying uncertainty using stratified estimation. *Remote Sensing of Environment*, *129*, 122-131
- Olson, J. (1994). Global ecosystem framework-definitions. In, *USGS EROS Data Center Internal Report*. Sioux Falls, SD
- Ometto, J.P., Aguiar, A.P., Assis, T., Soler, L., Valle, P., Tejada, G., Lapola, D.M., & Meir, P. (2014). Amazon forest biomass density maps: tackling the uncertainty in carbon emission estimates. *Climatic Change*, *124*, 545-560
- Pan, Y., Birdsey, R.A., Fang, J., Houghton, R., Kauppi, P.E., Kurz, W.A., Phillips, O.L., Shvidenko, A., Lewis, S.L., Canadell, J.G., Ciais, P., Jackson, R.B., Pacala, S.W., McGuire, A.D., Piao, S., Rautiainen, A., Sitch, S., & Hayes, D. (2011). A large and persistent carbon sink in the world's forests. *Science*, *333*, 988-993
- Pedely, J., Devadiga, S., Masuoka, E., Brown, M., Pinzon, J., Tucker, C., Roy, D., J., J., Vermote, E., Prince, S., Nagol, J., Justice, C., Schaaf, C., Liu, J., Privette, J., & Pinheiro, A. (2007). Generating a long-term land data record from the AVHRR and MODIS Instruments. In, *IEEE International Geoscience and Remote Sensing Symposium (IGARSS)* (pp. 1021-1025). Barcelona

- Pelletier, J., Ramankutty, N., & Potvin, C. (2011). Diagnosing the uncertainty and detectability of emission reductions for REDD + under current capabilities: an example for Panama. *Environmental Research Letters*, *6*, 024005
- Perz, S.G., Qiu, Y., Xia, Y., Southworth, J., Sun, J., Marsik, M., Rocha, K., Passos, V., Rojas, D., Alarcón, G., Barnes, G., & Baraloto, C. (2013). Trans-boundary infrastructure and land cover change: Highway paving and community-level deforestation in a tri-national frontier in the Amazon. *Land Use Policy*, *34*, 27-41
- Peters, G.P., Marland, G., Le Quéré, C., Boden, T., Canadell, J.G., & Raupach, M.R. (2011). Rapid growth in CO₂ emissions after the 2008–2009 global financial crisis. *Nature Climate Change*, *2*, 2-4
- Pflugmacher, D., Krankina, O.N., Cohen, W.B., Friedl, M.A., Sulla-Menashe, D., Kennedy, R.E., Nelson, P., Loboda, T.V., Kuemmerle, T., Dyukarev, E., Elsakov, V., & Kharuk, V.I. (2011). Comparison and assessment of coarse resolution land cover maps for Northern Eurasia. *Remote Sensing of Environment*, *115*, 3539-3553
- Pimm, S.L., Jenkins, C.N., Abell, R., Brooks, T.M., Gittleman, J.L., Joppa, L.N., Raven, P.H., Roberts, C.M., & Sexton, J.O. (2014). The biodiversity of species and their rates of extinction, distribution, and protection. *Science*, *344*, 1246752
- Posso, D.G.I. (2000). Coca, deforestation and food security in the Colombian Amazon region. *Unasylva*, *51*, 32-35
- Potapov, P., Turubanova, S., & Hansen, M.C. (2011). Regional-scale boreal forest cover and change mapping using Landsat data composites for European Russia. *Remote Sensing of Environment*, *115*, 548-561
- Potapov, P.V., Turubanova, S.A., Hansen, M.C., Adusei, B., Broich, M., Altstatt, A., Mane, L., & Justice, C.O. (2012). Quantifying forest cover loss in Democratic Republic of the Congo, 2000–2010, with Landsat ETM+ data. *Remote Sensing of Environment*, *122*, 106-116
- Poulter, B., Frank, D., Ciais, P., Myneni, R.B., Andela, N., Bi, J., Broquet, G., Canadell, J.G., Chevallier, F., Liu, Y.Y., Running, S.W., Sitch, S., & van der Werf, G.R. (2014). Contribution of semi-arid ecosystems to interannual variability of the global carbon cycle. *Nature*, *509*, 600-603
- Putz, S., Groeneveld, J., Henle, K., Knogge, C., Martensen, A.C., Metz, M., Metzger, J.P., Ribeiro, M.C., de Paula, M.D., & Huth, A. (2014). Long-term carbon loss in fragmented Neotropical forests. *Nat Commun*, *5*, 5037
- Ramankutty, N., Gibbs, H.K., Achard, F., Defries, R., Foley, J.A., & Houghton, R.A. (2007). Challenges to estimating carbon emissions from tropical deforestation. *Global Change Biology*, *13*, 51-66

- Rayner, P.J., Law, R.M., Allison, C.E., Francey, R.J., Trudinger, C.M., & Pickett-Heaps, C. (2008). Interannual variability of the global carbon cycle (1992-2005) inferred by inversion of atmospheric CO₂ and δ¹³CO₂ measurements. *Global Biogeochemical Cycles*, 22, GB3008
- Reed, B.C., Brown, J.F., VanderZee, D., Loveland, T.R., Merchant, J.W., & Ohlen, D.O. (1994). Measuring phenological variability from satellite imagery. *Journal of Vegetation Science*, 5, 703-714
- Roy, D.P., Ju, J., Kline, K., Scaramuzza, P.L., Kovalskyy, V., Hansen, M., Loveland, T.R., Vermote, E., & Zhang, C. (2010). Web-enabled Landsat Data (WELD): Landsat ETM+ composited mosaics of the conterminous United States. *Remote Sensing of Environment*, 114, 35-49
- Rudel, T.K., Coomes, O.T., Moran, E., Achard, F., Angelsen, A., Xu, J., & Lambin, E. (2005). Forest transitions: towards a global understanding of land use change. *Global Environmental Change*, 15, 23-31
- Running, S.W., Loveland, T.R., Pierce, L.L., Nemani, R.R., & Hunt Jr, E.R. (1995). A remote sensing based vegetation classification logic for global land cover analysis. *Remote Sensing of Environment*, 51, 39-48
- Saatchi, S., Asefi-Najafabady, S., Malhi, Y., Aragao, L.E., Anderson, L.O., Myneni, R.B., & Nemani, R. (2013). Persistent effects of a severe drought on Amazonian forest canopy. *Proc Natl Acad Sci USA*, 110, 565-570
- Saatchi, S., Ulander, L., Williams, M., Quegan, S., LeToan, T., Shugart, H., & Chave, J. (2012). Forest biomass and the science of inventory from space. *Nature Climate Change*, 2, 826-827
- Saatchi, S.S., Harris, N.L., Brown, S., Lefsky, M., Mitchard, E.T., Salas, W., Zutta, B.R., Buermann, W., Lewis, S.L., Hagen, S., Petrova, S., White, L., Silman, M., & Morel, A. (2011). Benchmark map of forest carbon stocks in tropical regions across three continents. *Proc. Natl. Acad. Sci. USA*, 108, 9899-9904
- Schepaschenko, D., McCallum, I., Shvidenko, A., Fritz, S., Kraxner, F., & Obersteiner, M. (2011). A new hybrid land cover dataset for Russia: a methodology for integrating statistics, remote sensing and in situ information. *Journal of Land Use Science*, 6, 245-259
- Schimel, D.S., House, J.I., Hibbard, K.A., Bousquet, P., Ciais, P., Peylin, P., Braswell, B.H., Apps, M.J., Baker, D., Bondeau, A., Canadell, J., Churkina, G., Cramer, W., Denning, A.S., Field, C.B., Friedlingstein, P., Goodale, C., Heimann, M., Houghton, R.A., Melillo, J.M., Moore III, B., Murdiyarso, D., Noble, I., Pacala, S.W., Prentice, I.C., Raupach, M.R., Rayner, P.J., Scholes, R.J., Steffen, W.L., & Wirth, C. (2001). Recent patterns and mechanisms of carbon exchange by terrestrial ecosystems. *Nature*, 414, 169-172

- See, L., Fritz, S., You, L., Ramankutty, N., Herrero, M., Justice, C., Becker-Reshef, I., Thornton, P., Erb, K., Gong, P., Tang, H., Velde, M.v.d., Ericksen, P., McCallum, I., Kraxner, F., & Obersteiner, M. (2014). Improved global cropland data as an essential ingredient for food security. *Global Food Security*, 4, 37-45
- Sellers, P.J., Mintz, Y., Sud, Y.C., & Dalcher, A. (1986). A Simple Biosphere Model (SIB) for Use within General Circulation Models. *Journal of the Atmospheric Sciences*, 43, 505-531
- Sexton, J.O., Noojipady, P., Anand, A., Song, X.-P., McMahon, S., Huang, C., Feng, M., Channan, S., & Townshend, J.R. (2014). A model for the propagation of uncertainty from continuous estimates of tree cover to categorical forest cover and change. *Remote Sensing of Environment*, In review
- Sexton, J.O., Noojipady, P., Anand, A., Song, X.-P., McMahon, S., Huang, C., Feng, M., Channan, S., & Townshend, J.R. (2015). A model for the propagation of uncertainty from continuous estimates of tree cover to categorical forest cover and change. *Remote Sensing of Environment*, 156, 418-425
- Sexton, J.O., Song, X.-P., Feng, M., Noojipady, P., Anand, A., Huang, C., Kim, D.-H., Collins, K.M., Channan, S., DiMiceli, C., & Townshend, J.R. (2013a). Global, 30-m resolution continuous fields of tree cover: Landsat-based rescaling of MODIS vegetation continuous fields with lidar-based estimates of error. *International Journal of Digital Earth*, 6, 427-448
- Sexton, J.O., Song, X.-P., Huang, C., Channan, S., Baker, M.E., & Townshend, J.R. (2013b). Urban growth of the Washington, D.C.–Baltimore, MD metropolitan region from 1984 to 2010 by annual, Landsat-based estimates of impervious cover. *Remote Sensing of Environment*, 129, 42-53
- Shimabukuro, Y.E., dos Santos, J.R., Formaggio, A.R., Duarte, V., & Rudorff, B.F.T. (2012). The Brazilian Amazon monitoring program: PRODES and DETER projects In F. Achard & M.C. Hansen (Eds.), *Global Forest Monitoring from Earth Observation* (pp. 153-169). Boca Raton, FL: CRC Press/Taylor & Francis Group.
- Shimada, M., Itoh, T., Motooka, T., Watanabe, M., Shiraishi, T., Thapa, R., & Lucas, R. (2014). New global forest/non-forest maps from ALOS PALSAR data (2007–2010). *Remote Sensing of Environment*, In press
- Simard, M., Pinto, N., Fisher, J.B., & Baccini, A. (2011). Mapping forest canopy height globally with spaceborne lidar. *Journal of Geophysical Research*, 116, G04021
- Song, X.-P., Huang, C., Feng, M., Sexton, J.O., Channan, S., & Townshend, J.R. (2014a). Integrating global land cover products for improved forest cover characterization: an application in North America. *International Journal of Digital Earth*, 7, 709-724

- Song, X.-P., Huang, C., Sexton, J.O., Channan, S., & Townshend, J.R. (2014b). Annual Detection of Forest Cover Loss Using Time Series Satellite Measurements of Percent Tree Cover. *Remote Sensing*, 6, 8878-8903
- Song, X.-P., Huang, C., Sexton, J.O., Feng, M., Narasimhan, R., Channan, S., & Townshend, J.R. (2011). An assessment of global forest cover maps using regional higher-resolution reference data sets. In, *IEEE International Geoscience and Remote Sensing Symposium (IGARSS)* (pp. 752-755). Vancouver
- Souza, C.M., Siqueira, J., Sales, M., Fonseca, A., Ribeiro, J., Numata, I., Cochrane, M., Barber, C., Roberts, D., & Barlow, J. (2013). Ten-Year Landsat Classification of Deforestation and Forest Degradation in the Brazilian Amazon. *Remote Sensing*, 5, 5493-5513
- Steininger, M.K. (2000). Satellite estimation of tropical secondary forest above-ground biomass: Data from Brazil and Bolivia. *International Journal of Remote Sensing*, 21, 1139-1157
- Strahler, A.H., Boschetti, L., Foody, G.M., Friedl, M.A., Hansen, M.C., Herold, M., Mayaux, P., Morisette, J.T., Stehman, S.V., & Woodcock, C.E. (2006). Global land cover validation: recommendations for evaluation and accuracy assessment of global land cover maps. In. Luxembourg: Office for Official Publications of the European Communities
- Strassburg, B., Turner, R.K., Fisher, B., Schaeffer, R., & Lovett, A. (2009). Reducing emissions from deforestation—The “combined incentives” mechanism and empirical simulations. *Global Environmental Change*, 19, 265-278
- Tans, P.P., Fung, I.Y., & Takahashi, T. (1990). Observational constraints on the global atmospheric CO₂ budget. *Science*, 247, 1431-1438
- Terrestrial Carbon Group (2008). How to Include Terrestrial Carbon in Developing Nations in the Overall Climate Change Solution. Available: www.terrestrialcarbon.org. Accessed 23 September 2013. In
- Thomas, R.Q., Canham, C.D., Weathers, K.C., & Goodale, C.L. (2010). Increased tree carbon storage in response to nitrogen deposition in the US. *Nature Geoscience*, 3, 13-17
- Tian, H., Melillo, J.M., Kicklighter, D.W., McGuire, A.D., Helfrich, J.V., Moore, B., & Vögeli-Smart, C.J. (1998). Effect of interannual climate variability on carbon storage in Amazonian ecosystems. *Nature*, 396, 664-667
- Townshend, J.R., Masek, J.G., Huang, C., Vermote, E.F., Gao, F., Channan, S., Sexton, J.O., Feng, M., Narasimhan, R., Kim, D., Song, K., Song, D., Song, X.-P., Noojipady, P., Tan, B., Hansen, M.C., Li, M., & Wolfe, R.E. (2012). Global characterization and monitoring of forest cover using Landsat data: opportunities and challenges. *International Journal of Digital Earth*, 5, 373-397

- Townshend, J.R.G., & Justice, C.O. (1988). Selecting the spatial resolution of satellite sensors required for global monitoring of land transformations. *International Journal of Remote Sensing*, 9, 187-236
- Townshend, J.R.G., Justice, C.O., Gurney, C., & McManus, J. (1992). The impact of misregistration on change detection. *IEEE Transactions on Geoscience and Remote Sensing*, 30, 1054-1060
- Tucker, C.J. (1979). Red and Photographic Infrared Linear Combinations for Monitoring Vegetation. *Remote Sensing of Environment*, 8, 127-150
- Tucker, C.J., Grant, D.M., & Dykstra, J.D. (2004). NASA's Global Orthorectified Landsat Data Set. *Photogrammetric Engineering & Remote Sensing*, 70, 313-322
- Tucker, C.J., & Townshend, J.R.G. (2000). Strategies for monitoring tropical deforestation using satellite data. *International Journal of Remote Sensing*, 21, 1461-1471
- Turner, B.L., Lambin, E.F., & Reenberg, A. (2007). The emergence of land change science for global environmental change and sustainability. *Proceedings of the National Academy of Sciences of the United States of America*, 104, 20666-20671
- Tyukavina, A., Stehman, S.V., Potapov, P.V., Turubanova, S.A., Baccini, A., Goetz, S.J., Laporte, N.T., Houghton, R.A., & Hansen, M.C. (2013). National-scale estimation of gross forest aboveground carbon loss: a case study of the Democratic Republic of the Congo. *Environmental Research Letters*, 8, 044039
- UNFCCC (2002). Report of the Conference of the Parties on its Seventh Session: the Marrakesh Accords & the Marrakesh Declaration. In. Marrakesh, Morocco
- van der Werf, G.R., Morton, D.C., DeFries, R.S., Olivier, J.G.J., Kasibhatla, P.S., Jackson, R.B., Collatz, G.J., & Randerson, J.T. (2009). CO₂ emissions from forest loss. *Nature Geoscience*, 2, 737-738
- Verbesselt, J., Hyndman, R., Newnham, G., & Culvenor, D. (2010). Detecting trend and seasonal changes in satellite image time series. *Remote Sensing of Environment*, 114, 106-115
- Werth, D., & Avissar, R. (2002). The local and global effects of Amazon deforestation. *Journal of Geophysical Research*, 107, 8087
- White, M.A., Shaw, J.D., & Ramsey, R.D. (2005). Accuracy assessment of the vegetation continuous field tree cover product using 3954 ground plots in the southwestern USA. *International Journal of Remote Sensing*, 26, 2699-2704
- Wickham, J.D., Stehman, S.V., Fry, J.A., Smith, J.H., & Homer, C.G. (2010). Thematic accuracy of the NLCD 2001 land cover for the conterminous United States. *Remote Sensing of Environment*, 114, 1286-1296

- Wilkinson, G.G. (2005). Results and implications of a study of fifteen years of satellite image classification experiments. *IEEE Transactions on Geoscience and Remote Sensing*, 43, 433-440
- Willmott, C.J. (1982). Some Comments on the Evaluation of Model Performance. *Bulletin of the American Meteorological Society*, 63, 1309-1313
- Wolfe, R.E., Nishihama, M., Fleig, A.J., Kuyper, J.A., Roy, D.P., Storey, J.C., & Patt, F.S. (2002). Achieving sub-pixel geolocation accuracy in support of MODIS land science. *Remote Sensing of Environment*, 83, 31-49
- Woodhouse, I.H., Mitchard, E.T.A., Brolly, M., Maniatis, D., & Ryan, C.M. (2012). Radar backscatter is not a 'direct measure' of forest biomass. *Nature Climate Change*, 2, 556-557
- Woods Hole Research Center, & Amazon Institute for Environmental Research (2008). How to distribute REDD funds across countries? A stock flow mechanism. Submission to the United Nations Framework Convention on Climate Change regarding AWG-LCA (FCCC/AWGLCA/ 2008/L.7). In
- Wulder, M.A., Masek, J.G., Cohen, W.B., Loveland, T.R., & Woodcock, C.E. (2012). Opening the archive: How free data has enabled the science and monitoring promise of Landsat. *Remote Sensing of Environment*, 122, 2-10
- Wulder, M.A., White, J.C., Cranny, M., Hall, R.J., Luther, J.E., Beaudoin, A., Goodenough, D.G., & Dechka, J.A. (2008). Monitoring Canada's forests. Part 1: Completion of the EOSD land cover project. *Canadian Journal of Remote Sensing*, 34, 549-562
- Xian, G., & Crane, M. (2005). Assessments of urban growth in the Tampa Bay watershed using remote sensing data. *Remote Sensing of Environment*, 97, 203-215
- Xin, Q., Olofsson, P., Zhu, Z., Tan, B., & Woodcock, C.E. (2013). Toward near real-time monitoring of forest disturbance by fusion of MODIS and Landsat data. *Remote Sensing of Environment*, 135, 234-247
- Yu, L., Liang, L., Wang, J., Zhao, Y., Cheng, Q., Hu, L., Liu, S., Yu, L., Wang, X., Zhu, P., Li, X., Xu, Y., Li, C., Fu, W., Li, X., Li, W., Liu, C., Cong, N., Zhang, H., Sun, F., Bi, X., Xin, Q., Li, D., Yan, D., Zhu, Z., Goodchild, M.F., & Gong, P. (2014). Meta-discoveries from a synthesis of satellite-based land-cover mapping research. *International Journal of Remote Sensing*, 35, 4573-4588
- Yu, L., Wang, J., Clinton, N., Xin, Q., Zhong, L., Chen, Y., & Gong, P. (2013). FROM-GC: 30 m global cropland extent derived through multisource data integration. *International Journal of Digital Earth*, 6, 521-533

Zhang, X., Friedl, M.A., Schaaf, C.B., Strahler, A.H., Hodges, J.C.F., Gao, F., Reed, B.C., & Huete, A. (2003). Monitoring vegetation phenology using MODIS. *Remote Sensing of Environment*, 84, 471-475

Zhu, Z., Woodcock, C.E., & Olofsson, P. (2012). Continuous monitoring of forest disturbance using all available Landsat imagery. *Remote Sensing of Environment*, 122, 75-91